THE UNIVERSITY

OF BIRMINGHAM

MICROMACHINED MICROWAVE FILTERS

by

Ignacio Llamas Garro

A thesis submitted to the School of Engineering of
The University of Birmingham
for the degree of
DOCTOR OF PHILOSOPHY

School of Engineering
Department of Electronic, Electrical and Computer Engineering
The University of Birmingham
April 2003

Abstract

Microwave circuits in the millimetre wave region demand low loss, and low dispersion transmission lines. The work carried out in this thesis is on low loss transmission lines and filters, based on a square coaxial transmission line which is made only of metal, avoiding dielectric and radiation losses. The metal structure inside the square coaxial transmission line is supported by stubs, which provide the mechanical support for the centre conductor for the coaxial transmission lines and filters.

The coaxial structure is made by stacking thick planar layers of material to suit microfabrication, providing the means to design high Q Microwave and RF passive devices, this transmission line structure is compact compared with a microstrip or a stripline, and gives better loss performance.

Through this thesis, the way of optimising the square coaxial transmission line to provide a low loss will be presented, which will end in the presentation of one dielectric supported coaxial structure and three self supported filters, three of them were designed for the X-band, and one of them was designed for the Ka band. The application of the coaxial transmission line is demonstrated with wideband and narrow band designs.

To my family,

Ignacio, Nora and Maria Elena

Acknowledgments

I am very grateful to Professor Michael J. Lancaster for supervising this thesis, for sharing his knowledge and enthusiasm for microwaves, and for his support and encouragement during this period of work. I would also like to thank Professor Peter S. Hall for getting me started in this PhD, for providing a nice working place to carry out this work, and for his useful discussions.

Many thanks to Dr. Benjamin Carrión, Dr. Alonso Corona, Dr. Demian Hinojosa and Rosana Marques for all the great moments that we had together, from the very beginning to the end of this project. This would have not been the same without them.

I would like to thank my colleagues and members of the EDT and CE groups, for their companionship and useful discussions. Thanks to Peng Jin and Dr. Kyle Jiang in Mechanical Engineering for the fabrication of the SU8 pieces. Thanks to the outstanding work of Warren Hay responsible for the fabrication of the X band filters, thanks to Clifford Ansell for the fabrication of the brass box and for helping me ensemble the Ka band filter, and thanks to Adnam Zentani for machining the resonators.

Finally I would like to thank the National Council for Science and Technology (CONACYT) in Mexico for partially funding this PhD, along with my dear parents Dr. Ignacio Llamas Huitrón and Dr. Nora Garro Bordonaro for always being so generous.

Index

Glossary of abbreviations

BCB - Benzocyclobutene

CAD – Computer Aided Design

ECPW – Elevated Coplanar transmission line

IC – Integrated Circuit

IMSL – Inverted Microstrip Line

LIGA – German acronym with an English translation of Lithography, Electroforming and Moulding

LMDS – Local Multipoint Distribution System

MEMS – Micro Electro-Mechanical Systems

MMIC – Monolithic Microwave Integrated Circuit

MOPA – Master Oscillator Power Amplifier

OCPW – Overlay Coplanar transmission line

SU8 – Organic Photosensitive Resin

TEM – Transverse Electromagnetic Mode

Approximate Band designations

X- Band 8-12 GHz

Ka- Band 26-40 GHz

U- Band 40-60 GHz

W- Band 60-100 GHz

List of Figures

CHAPTER FOUR: MICROWAVE RESONATORS

CHAPTER FIVE: GENERAL FILTER DESIGN

CHAPTER SIX: MICROMACHINED TRANSMISSION LINES AND RESONATORS

CHAPTER SEVEN: SQUARE COAXIAL MICROWAVE BANDPASS FILTERS

CHAPTER EIGHT: CONCLUSIONS AND FURTHER WORK

List of Tables

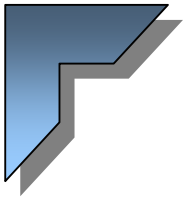

CHAPTER ONE
INTRODUCTION

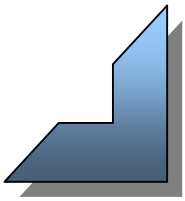

1.1. CONTENTS OF THE THESIS

The objective of this Chapter is to introduce each chapter of this thesis, as well discuss the potential application of the Ka band dual mode filter discussed further in Chapter 7, section 7.5.

Chapter 2 contains a literature review on micromachined transmission lines, resonators and filters, followed by Chapters 3, 4 and 5 which describe the theory used in the development of the resonators and filters discussed in Chapters 6 and 7; the notation in Table 1-1 will be used throughout the theory chapters. Chapter 8 contains the overall conclusions of this research and some proposals for further work. In the following paragraphs there will be a description of the contents by chapter to give an overview of the contents of this thesis.

QUANTITY	NOTATION			SI UNITS
	Time varying field	Static field	Sinusoidal steady state variation of the field vectors	
Electric field intensity	$\overline{E}$	E	$\hat{E}$	V/m
Electric flux density	$\overline{D}$	D	$\hat{D}$	C/m^2
Magnetic field intensity	$\overline{H}$	H	$\hat{H}$	A/m
Magnetic flux density	$\overline{B}$	B	$\hat{B}$	Wb/m^2 or T
Current density	$\overline{J}$	J	$\hat{J}$	A/m^2

QUANTITY	NOTATION	SI UNITS
Volume charge density	ρ	C/m^3
Conductivity	σ	S/m
Skin depth	δ_s	m
Surface resistance	R_s	Ω/square
Attenuation constant	α	Np/m
Propagation constant	β	Rad/m

PHYSICAL CONSTANT	NOTATION	VALUE
Permittivity of free space	ε_o	8.854×10^{-12} F/m
Permeability of free space	μ_o	$4\pi \times 10^{-7}$ H/m
Intrinsic impedance of free space	η_o	376.73 Ω

Table 1-1 Notation used in this thesis

Chapter 2 starts with the review of a square coaxial transmission line proposed for the operation in the millimetre wave region, up to the terahertz frequency range. In section 2.2, a table of several low loss micromachined transmission lines is presented, summarising their respective loss performance. And finally in section 2.3, several micromachined filters are presented.

Chapter 3 focuses on transmission line theory, where the first section deals with the lumped element model of a transmission line, out of which the telegrapher's

equations will be derived. These equations are general and relate voltages and currents on the transmission line to any point in time and space. Section 3.3, treats standing waves, and ends with the input impedance of a low loss, half wavelength transmission line terminated in an open circuit, which will be a useful result for the calculation of the unloaded quality factor of a half wavelength transmission line resonator in Chapter 4. In section 3.4, wave propagation is discussed, followed by the definition of the TEM (Transverse Electromagnetic Mode) mode, and dispersion problems in transmission lines. Finally, at the end of the chapter, basic transmission lines used in microwave engineering will be presented.

In Chapter 4, resonator theory is reviewed; resonators are used in frequency selective devices, like filters, oscillators or frequency measurement devices. Section 4.2 contains a description of lumped element resonant circuits. In section 4.3, the formula to calculate the unloaded quality factor for a half wavelength distributed element resonator will be derived. Section 4.4 treats material losses, especially the conductor loss, since the main structures used in this thesis are conductor loss limited transmission lines. Section 4.5 contains a practical way of extracting the unloaded quality factor directly from experimental measurements, and finally in section 4.6, the unloaded quality factor for a square coaxial resonator is discussed.

Chapter 5 contains the theory used to design the bandpass filters presented in Chapter 7. Section 5.2 contains a discussion of the low pass filter prototype, which will be converted to give a bandpass response in section 5.3; where narrowband coupled resonator filters will be addressed. The rest of section 5.3 contains the theory on how to develop a practical Chebyschev bandpass filter with the aid of a CAD simulator. Section 5.4, contains the design formulae for a wideband bandpass filter using quarter wavelength stubs as resonators, with quarter wavelength transmission lines connecting the resonators. Finally in section 5.5, a method of extracting the unloaded quality factor from experimental filter measurements will be presented; as well as a formula to calculate the insertion loss of a practical filter assuming that the resonator's unloaded quality factor is known.

Chapter 6 contains the first experiments that were carried out in order to define a good transmission line to make the filters discussed in Chapter 7. These experiments start with a shielded microstrip line, followed by a parallel plate waveguide, and a deep coplanar waveguide, and finally the square coaxial transmission line, as shown in Figure 1-1. Section 6.3 contains an analytical loss comparison of four different transmission lines, which include the microstrip, the stripline, the round coaxial line and the square coaxial line.

Chapter 7 is divided into two parts, Part I contains filters which were designed using a coaxial structure, with its centre conductor supported with a bar of dielectric, and Part II contains filters, which were designed using all metal structures that have an air propagation media, enhancing filter performance by avoiding substrate losses. The link between Chapters 6 and 7 is shown in Figure 1-1.

Finally Chapter 8 contains the overall conclusions on this research, as well as some proposed further work, which is mainly focused on different ways of producing the square coaxial filters of Chapter 7, and the possibilities of creating new filters or transmission line architectures using self supported metals.

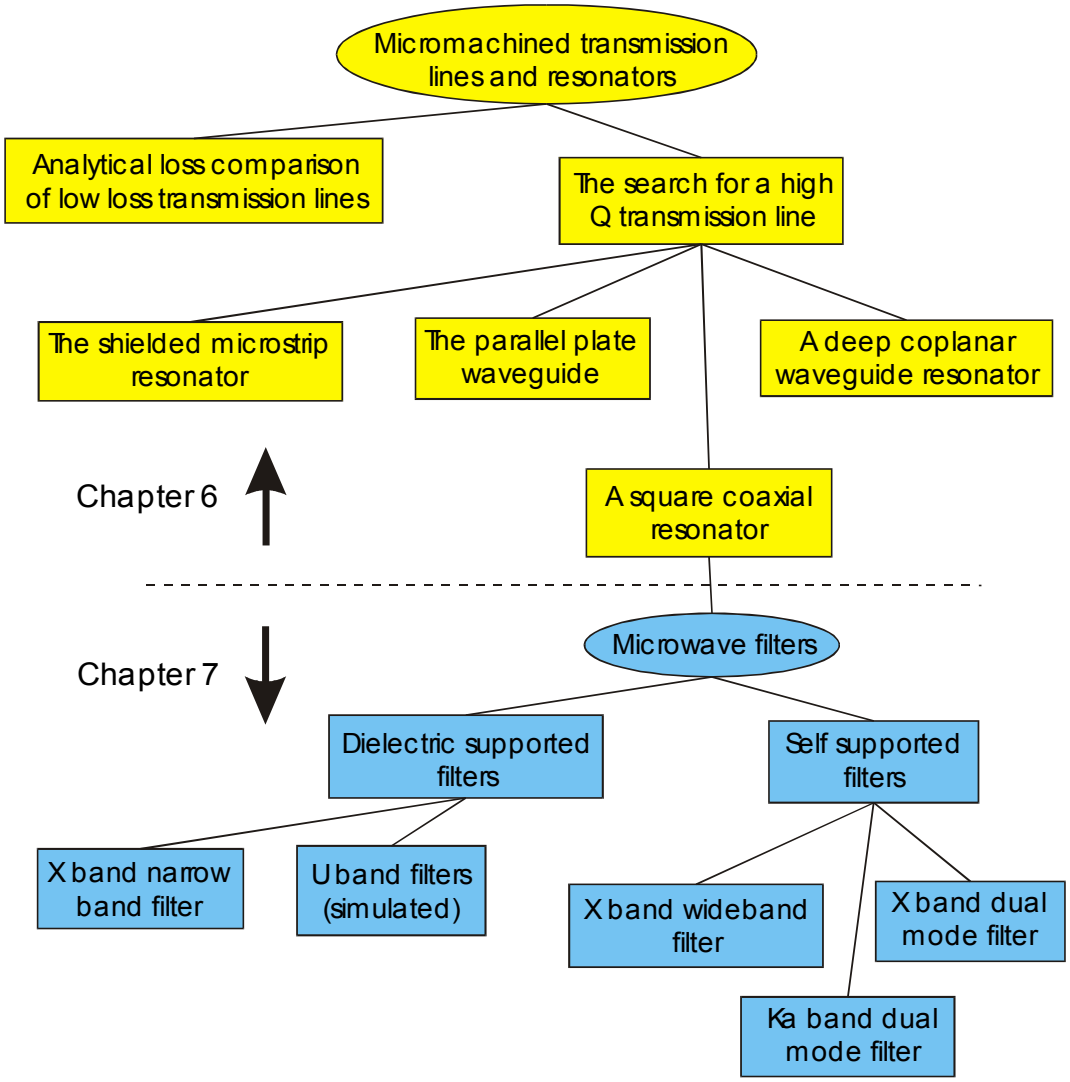

Figure 1-1 Diagram of the experiments in this research

1.2. LMDS

The objective of this section is to illustrate the potential application of the Ka band, dual mode filter discussed in Chapter 7, section 7.5. The filter was designed to meet an LMDS (Local Multipoint Distribution System) specification, provided by Alps Electric UK Ltd., the specification is shown in Table 1-2. The background presented in this section has been taken from [1-1].

LMDS filter specification	
Pass Band	29.5 - 30GHz
Ins. Loss	2dB max
Selectivity	-30dB at 27GHz
Temperature	-40 to + 90 deg C

Table 1-2 Specification of the Ka band dual mode filter

LMDS is a broadband fixed wireless technology, which can compete with wired local loop services, but it has been held back in many countries by slow licensing procedures.

LMDS is the highest capacity technology multipoint technology yet devised. It uses high frequencies and small cells, and it can provide all the fully integrated communication services. It has a peak data rate of around 155 Mbps, which includes plenty of capacity to spare even if providing telephone, internet, interactive television and other services. LMDS uses frequencies around 30 GHz, which makes its signal vulnerable to many weather phenomena effects, specifically rain.

LMDS requires exact line of sight. This makes the cell size dependent on the climate, 8Km is possible in ideal conditions, but many operators in Northern Europe and many U.S. cities cannot make them much larger than 1 or 2 Km.

Each LMDS cell uses between four and six directional transmitters, each of which can provide a shared capacity of many megabits per second. The exact figure depends on how much spectrum the operator has been licensed. Figure 1-2 shows an example of a typical cell, with a total capacity of 150 Mbps.

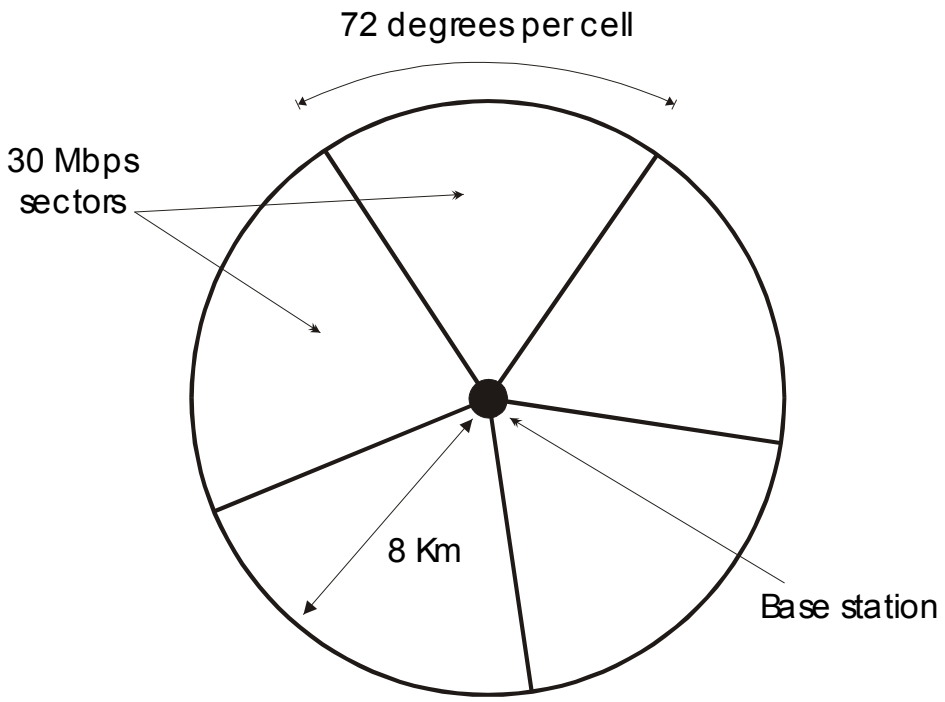

Figure 1-2 A five sectored LMDS cell

1.3. REFERENCES

[1-1] A. Dornan, "The essential guide to wireless communications applications", *Prentice Hall PTR, 2001.*

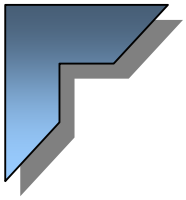

CHAPTER TWO
LITERATURE REVIEW

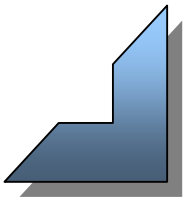

2.1. INTRODUCTION

The study of low loss and low dispersion transmission lines is the first step towards developing a high performance millimetre wave filter. As the design frequency gets higher, the circuit dimensions shrink inversely proportional to frequency, and the skin effect resistance increases approximately proportional to the square root of frequency.

This chapter starts with the presentation of a square coaxial transmission line proposed for millimetre wave integrated circuits, followed by a table in section 2.3, containing several transmission lines and resonators, each with its respective attenuation constant and unloaded quality factor for a half wavelength resonator made out of its respective structure. Finally in section 2.4 there is a review on micromachined filters.

2.2. A SQUARE COAXIAL TRANMSMISSION LINE

A square coaxial transmission line, which is integrable and compatible with existing MMIC technology has been reported in [2-1]. The structure is shown in Figure 2-1.

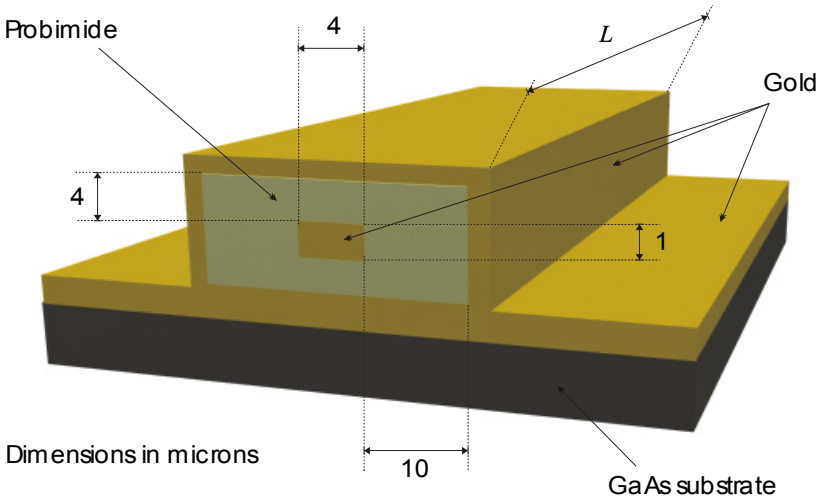

Figure 2-1 A square coaxial transmission line, taken from [2-1]

This coaxial line has potential operation in the terahertz region, and as it is MMIC compatible, it presents the possibility of having no crosstalk between adjacent lines, which enables denser IC design.

The square coaxial transmission line had a measured loss of 1.5 dB/mm at 35 GHz, and a predicted loss of 6.4 dB/mm at 1 THz using a 4 micron width centre conductor, and a predicted loss of 3 dB/mm at 1 THz using a 10 micron width centre conductor.

2.3. MICROMACHINED TRANSMISSION LINES AND RESONATORS

Several transmission lines and resonators taken from several publications are shown in Table 2-1. The experimental results for each reference is resumed as the total loss, and the Q_O for a half wavelength resonator made out of its respective transmission line architecture.

Structure	Loss	Q_O	Reference
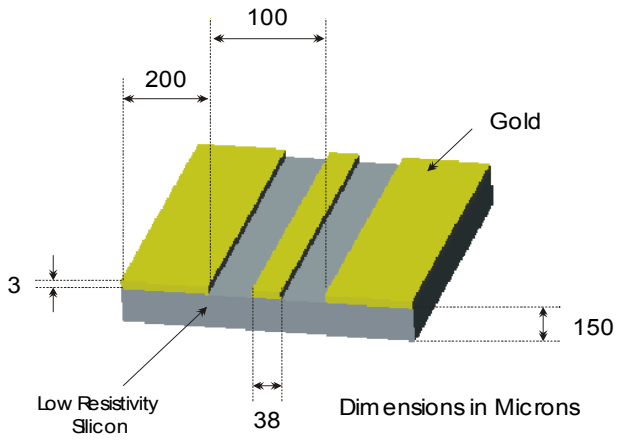 (a)	3.4 dB/mm at 50 GHz	1.34 at 50GHz	[2-2]
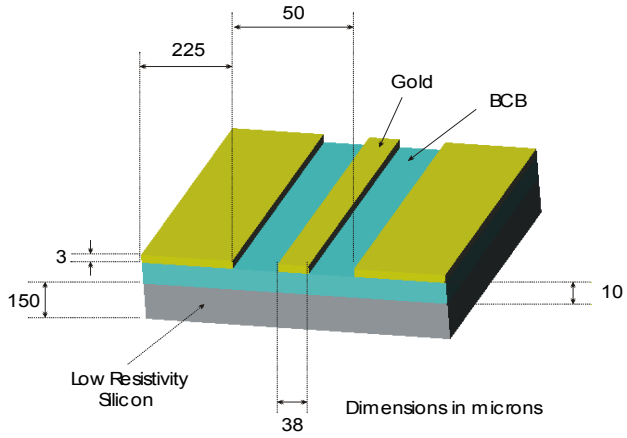 (b)	0.6 dB/mm at 50 GHz	7.58 at 50 GHz	[2-2]
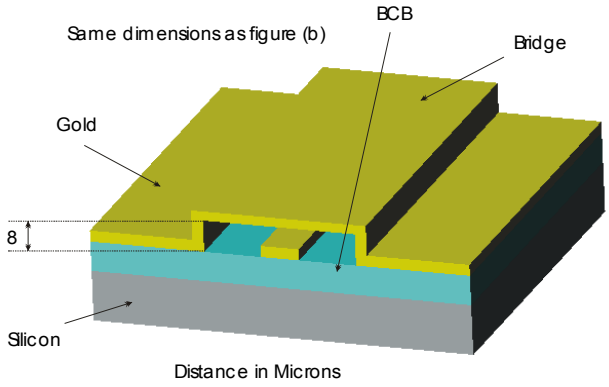 (c)	0.55 dB/mm at 50 GHz	8.26 at 50 GHz	[2-2]

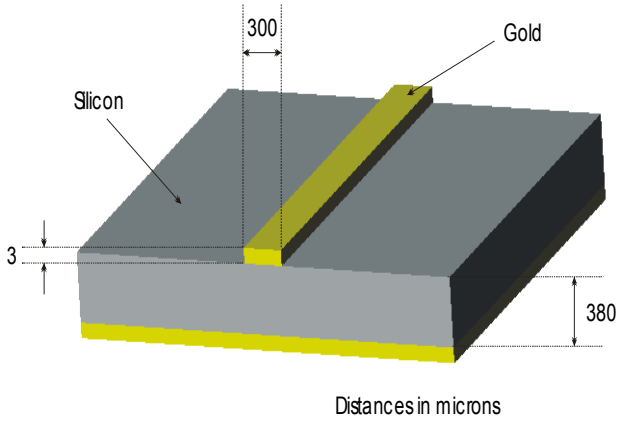 (d)	0.15 dB/mm at 40 GHz	24 at 40 GHz	[2-3]
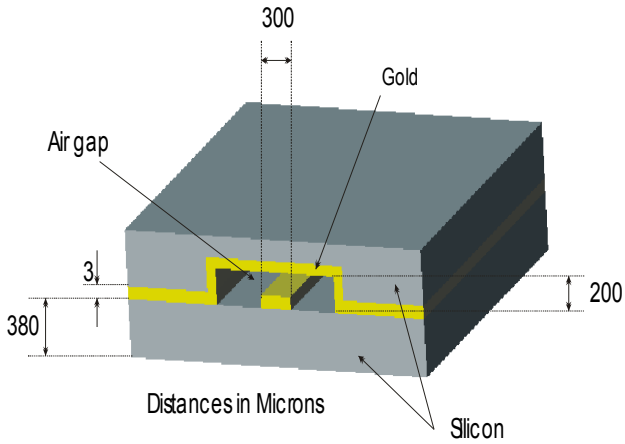 (e)	0.12 dB/mm at 40 GHz	30 at 40 GHz	[2-3]
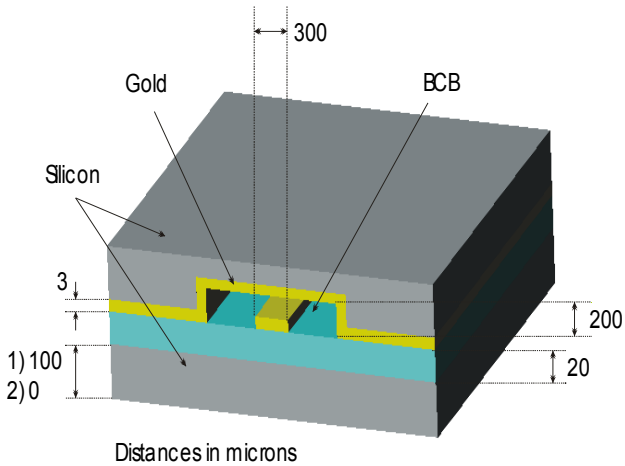 (f)	1) 0.06 dB/mm at 40 GHz 2) 0.033 dB/mm at 40 GHz	1) 60 at 40 GHz 2) 110 at 40 GHz	[2-3]

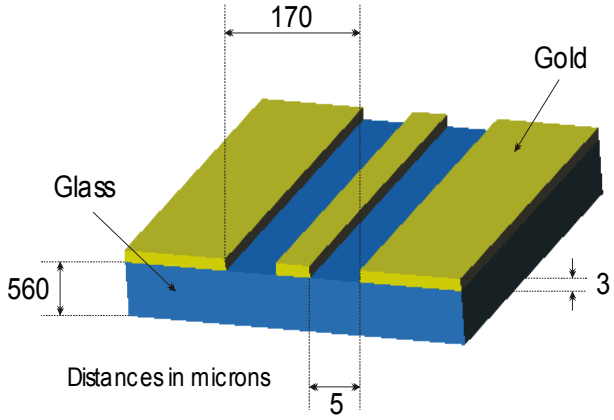 (g)	0.265 dB/mm at 50 GHz	17 at 50 GHz	[2-4]
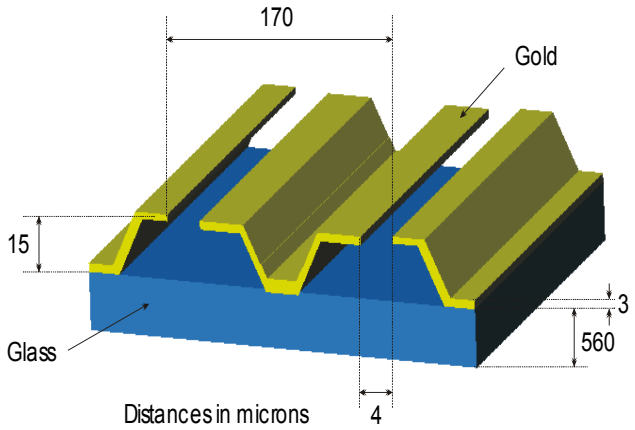 (h)	0.19 dB/mm at 50 GHz	23 at 50 GHz	[2-4]
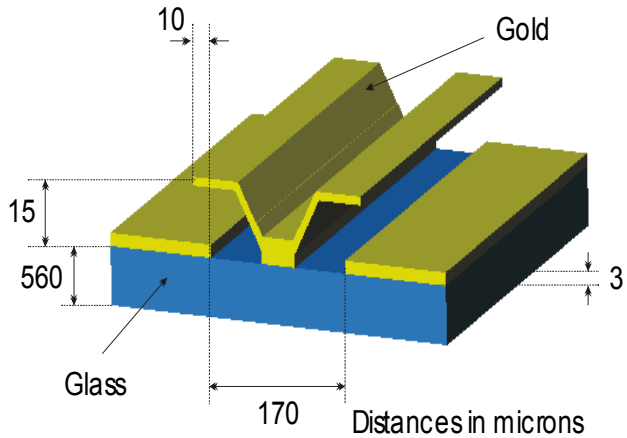 (i)	0.125 dB/mm at 50 GHz	36 at 50 GHz	[2-4]

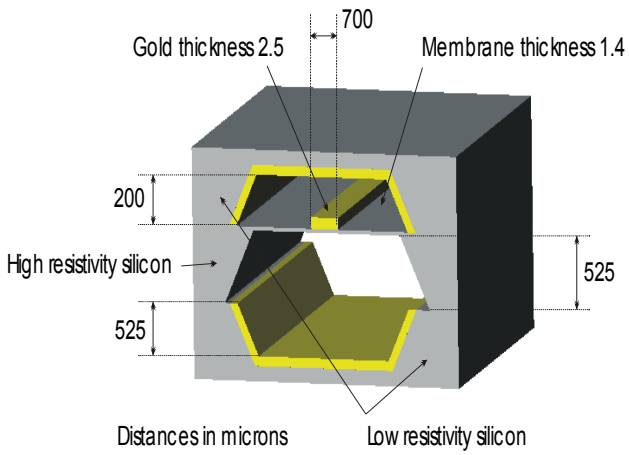 (j)	0.008 dB/mm at 37 GHz	420 at 37 GHz	[2-5]
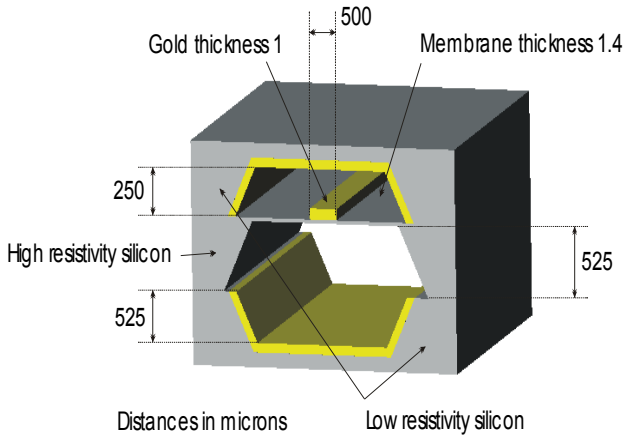 (k)	0.012 dB/mm at 60 GHz	450 at 60 GHz	[2-5]
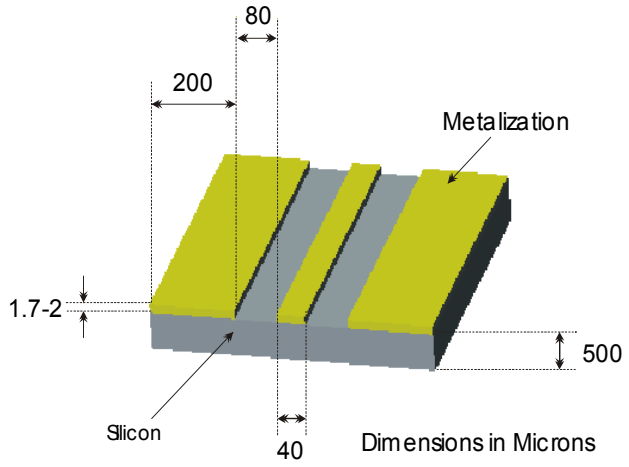 (l)	0.162 dB/mm at 60 GHz	33 at 60 GHz	[2-6]

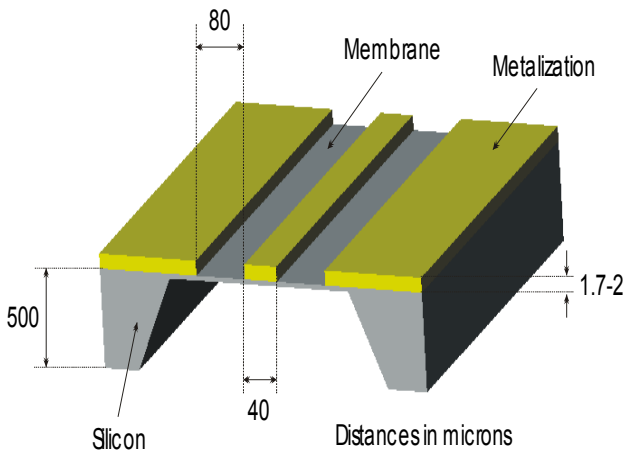 (m)	0.069 dB/mm at 60 GHz	79 at 60 GHz	[2-6]
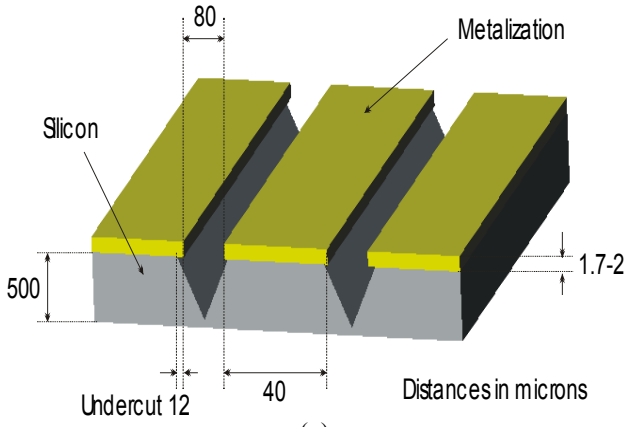 (n)	0.115 dB/mm at 60 GHz	47 at 60 GHz	[2-6]
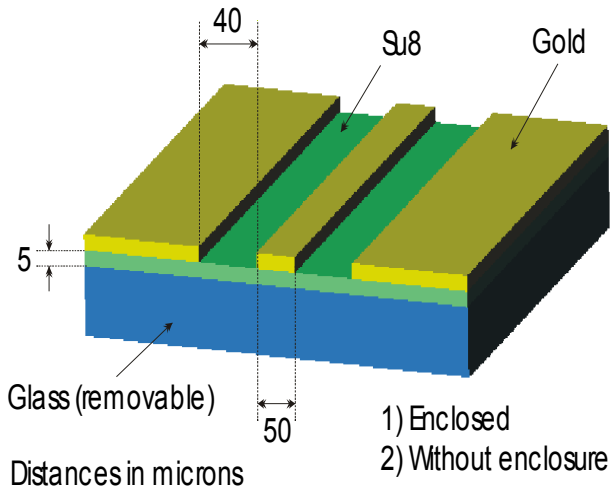 (o)	1) 0.07 dB/mm across W band 2) 0.14 dB/mm across W band	1) 120 at 93 GHz 2) 60 at 93 GHz	[2-7]

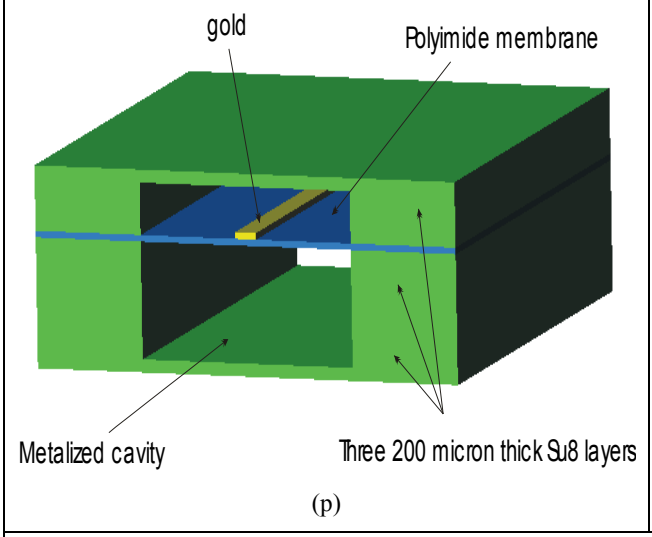 (p)	0.02 dB/mm at 29 GHz	130 at 29 GHz	[2-8]

Table 2-1 Micromachined transmission lines

In the next paragraphs a brief overview of the structures in Table 2-1 will be given. The main point of interest here is the overall loss performance of the structure along with some of its physical structural advantages.

Low cost, low resistivity silicon transmission lines cannot yet be applied effectively to microwave circuits, mainly due to the significant transmission line losses. The loss of a coplanar line with a low resistivity silicon substrate (ρ=10 Ω cm) as shown on Table 2-1a, has a loss of 3.4 dB/mm at 50 GHz. The losses of these lines can be significantly reduced by inserting a thick dielectric layer of 10μm of benzocyclobutene BCB between the substrate and the transmission line, giving a loss of 0.6 dB/mm at 50 GHz, shown on Table 2-1b. The losses of the semi-coaxial structure in Table 2-1c improved slightly compared to the structure in Table 2-1b to 0.55 dB/mm at 50 GHz, but in this structure the dielectric bridge can be used to achieve lower characteristic impedances by optimising the dielectric bridge height. The structure in Table 2-1b having a low characteristic impedance will imply that the electric field will penetrate further into the substrate giving increased losses. Note all transmission lines presented in [2-2] have a characteristic impedance of 50 Ohms.

The microstrip structure in Table 2-1d, is compared to the inverted microstrip line (IMSL) of Table 2-1e in [2-3], where the simulated results gave a loss of 0.15 dB/mm at 40 GHz for the microstrip structure. By reducing the loss using the IMSL which consists of two substrates bonded together and using the air gap formed between the line and cavity to obtain a low loss transmission, the simulated result gave 0.12 dB/mm at 40 GHz. Finally the IMSL was modified to give additional low loss characteristics by incorporating a membrane layer of BCB as shown on Table 2-1f. Here the results gave a loss of 0.06 dB/mm at 40 GHz when using a 100 micron thick silicon substrate below the membrane, and a loss of 0.033 dB/mm at 40 GHz when using BCB only as a substrate.

The structures in reference [2-4] are all coplanar transmission lines on a glass substrate. The first one, which is a conventional coplanar transmission line shown in Table 2-1g, has a loss of 0.265 dB/mm at 50 GHz. The transmission line in Table 2-1h is introduced as the elevated coplanar transmission line ECPW, this structure has a loss of 0.19 dB/mm at 50 GHz, and finally the figure in Table 2-1i is introduced as the overlay coplanar transmission line OCPW and has a loss of 0.125 dB/mm at 50 GHz. These transmission lines use micromachining technology to elevate the metal lines from the substrate reducing conductor and dielectric loss. The transmission lines compared here have a characteristic impedance of 40 Ohms.

The use of membrane technology as in [2-5] allows a significant reduction of loss. These circuits have a very good overall performance due to the thin membrane that permits an air propagation media in a completely shielded structure. This structure also allows the reduction of ohmic losses in the circuit, since it is possible to use wide microstrips. A half wavelength resonator at 37 GHz made out of the structure in Table 2-1j has a loss of 0.008 dB/mm at 37 GHz, and a loss of 0.012 dB/mm at 60 GHz as shown in Table 2-1k.

In the coplanar transmission lines exposed in [2-6] (Table 2-1m), the idea is to use silicon micromachining to remove the dielectric material from the gap regions to reduce dispersion and minimize the propagation loss. In coplanar lines, the field is

tightly concentrated in the gaps between the conductors. When the material in this area is removed, the line capacitance is reduced, leading to less current flow in the conductors [2-6]. As a result, the line exhibits lower ohmic and dielectric loss. Here three types of coplanar lines are compared: the first one on Table 2-1l shows a conventional coplanar line on a high resistivity silicon wafer that has a loss of 0.162 dB/mm at 60 GHz, the next coplanar line is suspended by membrane technology and has a loss of 0.069 dB/mm at 60 GHz, shown in Table 2-1m. Finally, the coplanar line in Table 2-1n which has the material removed between conductors, with an undercut below them, in this case 12 μm, has a loss of 0.115 dB/mm at 60 GHz.

A low cost membrane supported structure to realize planar printed circuits compared to the membrane technology in [2-5] is demonstrated in [2-7]. Here the membrane is made from a thin organic photosensitive resin SU8, this structure is illustrated in Table 2-1o. This process allows active devices to be mounted on a membrane of controllable thickness before removing the glass membrane backing. The mechanical strength provided by the glass substrate minimizes mechanical damage to the membrane when the active device is mounted. The coplanar structure has a loss of 0.07 dB/mm across W band under an enclosed environment, and a loss of 0.14 dB/mm across W band without the enclosure, here a ≈500 nm gold metalization is used. On [2-9], a method is reported that allows the use of higher conductivity metals like copper or silver; with this technique a finline resonator was realized, having a loss of 0.074 dB/mm at 81.5 Ghz.

The structure in Table 2-1p has a similar form as the one in Table 2-1j or k. The difference here is that SU8 is employed instead of silicon, the metalization is gold with a thickness of 2-3 μm, and the polyimide membrane is 2-3 mil thick, and the entire cavity walls are coated with gold. SU8 is very attractive for micromachining structures with significant thickness and with high aspect ratios [2-8]. A half wavelength resonator at 29 GHz has a loss of 0.02 dB/mm. The *Qo* value can be increased by having a higher cavity. The process used to make this structure is considerably simpler than silicon processing and presents a creative way to form more complicated shapes than those achievable in silicon.

The structure proposed in reference [2-5], is the one that presents the best overall loss performance, regardless of its complex processing compared to other structures like the ones presented in references [2-7], [2-8] and [2-9]. Transmission lines with the lowest dispersion are the ones that have a uniform air propagation media, compared to those that have one or more propagation medias, the dispersion of a particular transmission line will depend on the field distribution of the particular line and the propagation media used, the transmission lines with most dispersion are the ones that have their fields confined through different materials with different dielectric constants.

2.4. MICROMACHINED MIRCOWAVE FILTERS

2.4.1 INTRODUCTION

In this section there is a review of micromachined filters, with the objective of showing different micromachined microwave filters designed by different technologies.

2.4.2 MICROMACHINED CAVITY RESONATORS AND FILTERS

Figure 2-2 shows a micromachined cavity presented in [2-10], which is coupled by two microstrip lines through two slots, this structure can be used as a microwave high Q resonator for the development of narrowband low loss filters in a planar environment.

The microstrip lines are gold electroplated with a total thickness of 7.5 microns in order to minimize losses, the cavity is also metalized with a thickness of 2 microns.

The cavity had a measured Q of 506 ± 55, which is very close to the theoretical value of 526 for a metallic cavity with the same dimensions.

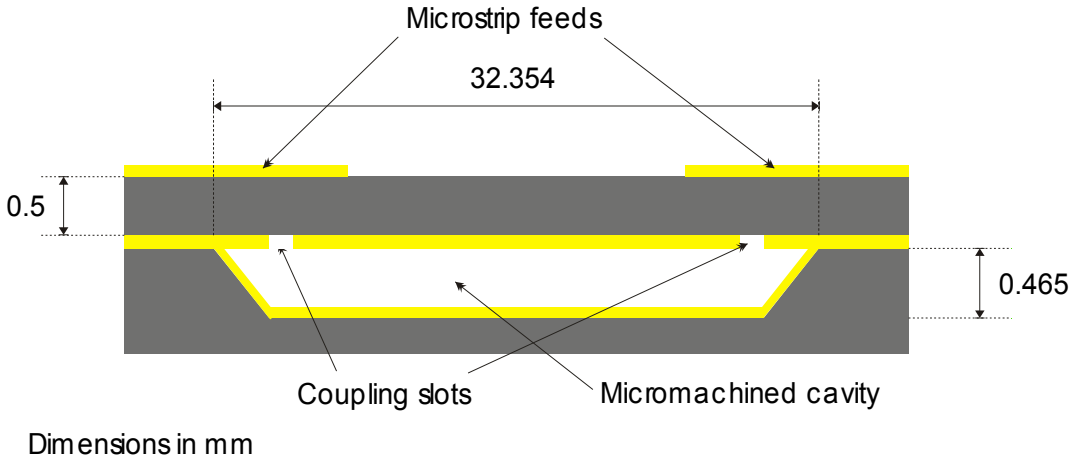

Figure 2-2 Side view of the X band micromachined resonator, taken from [2-10]

A 10 GHz filter constructed of slot coupled micromachined cavities in silicon is presented in [2-11]. The simulated model has a bandwidth of 4% with an insertion loss of 0.9 dB at 10.02 GHz. The measured filter yields a 3.7% bandwidth with a deembedded insertion loss of 2 dB at 10.01 GHz. The difference of loss is due to in part to the CPW-microstrip transition and line lengths; also an equipment malfunction during the bonding process caused an unexpected rapid raise in temperature, which created a gold-silicon eutectic, which resulted in a reduction in conductivity of the gold. The three cavity filter that consists of three slot-coupled vertically integrated resonators is shown in Figure 2-3.

Micromachined cavity resonators can be the building blocks for a filter that is low loss, narrow in bandwidth and small in size, and that can be integrated with monolithic circuit design.

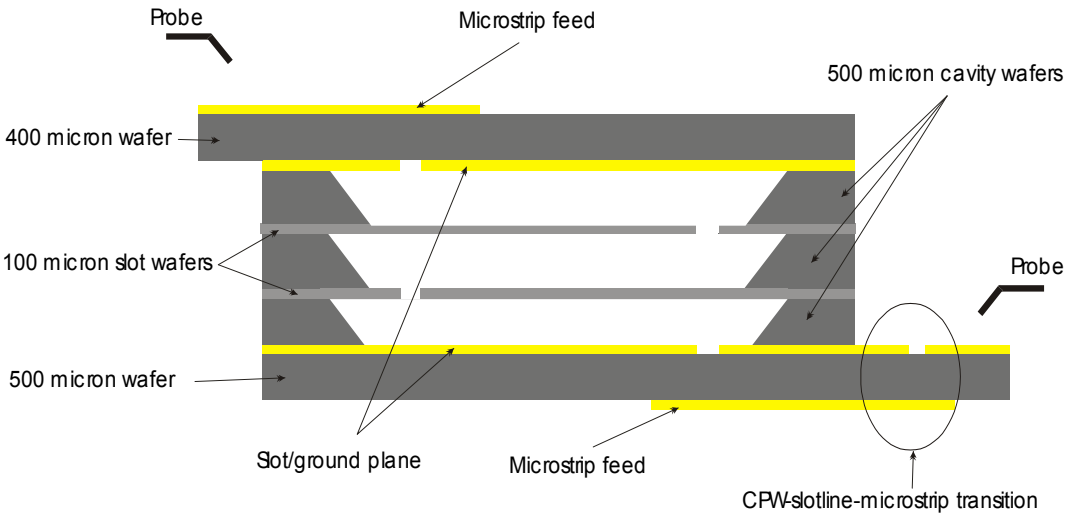

Figure 2-3 Side view of the three-cavity filter, taken from [2-11]

A high Q filter constructed of these resonators yields high power handling capabilities as the surface currents are distributed over a large conductor area. The microstrip lines, CPW lines, and top and bottom wafer ground/slot planes are gold electroplated to approximately 3 microns, and all surfaces of the etched slot and cavity wafers are gold electroplated to a similar depth. The overall dimensions of the finished filter are approximately 5 cm long x 3cm wide x 2600 micron high. The deembedded measured and simulated response for the filter is shown in Figure 2-4.

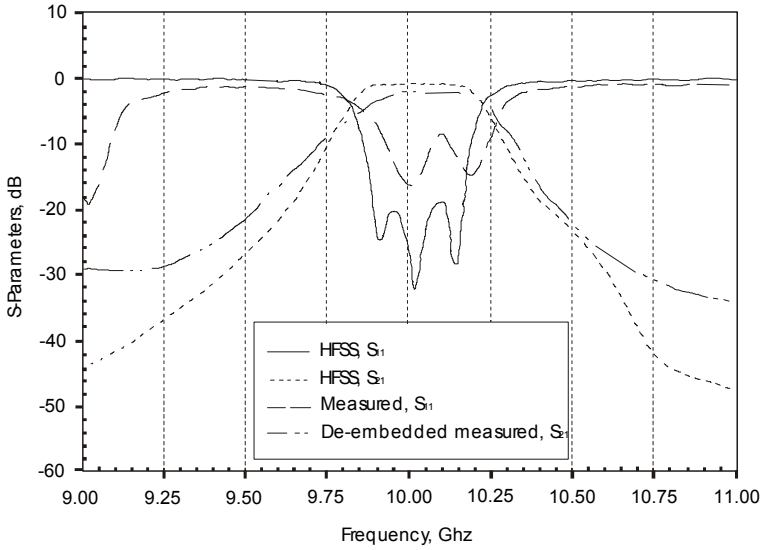

Figure 2-4 Measured and simulated response for the three cavity filter, taken from [2-11]

2.4.3 LIGA PLANAR TRANSMISSION LINES AND FILTERS

The LIGA fabrication process (a German acronym with an English translation of lithography, electroforming, and molding), allows the production of tall metal structures (10 microns – 1mm) with steep sidewalls, which can be precisely formed on an arbitrary substrate material using deep X-ray lithography and plated metal.

To exemplify the fabrication capabilities of LIGA, X band microstrip stepped impedance lowpass and broadband bandpass filters were designed in [2-12]. The microstrip structure used in the filter designs is shown in Figure 2-5.

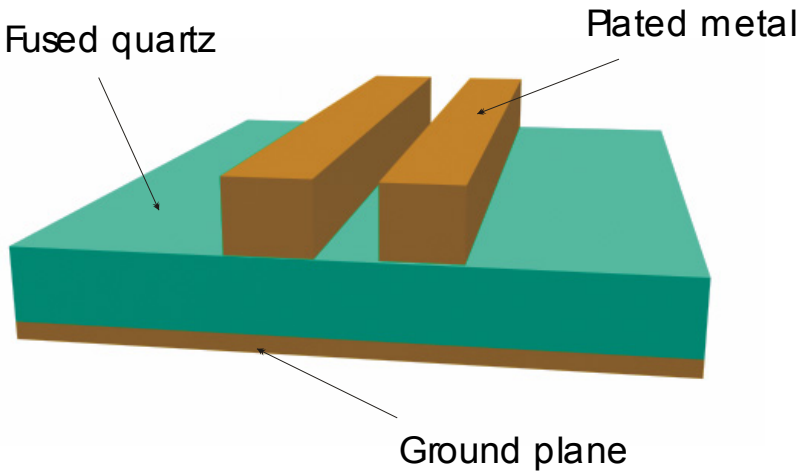

Figure 2-5 Two coupled LIGA microstrip lines

Lowpass and bandpass LIGA microstrip filters with design frequencies of 10 and 14 GHz, were fabricated and the results are summarized as follows. A 14 GHz stepped impedance low pass filter with 200 micron thick conductors was designed with a 3 dB cutoff frequency of 13.4 GHz, and an attenuation of 20 dB at 17.1 GHz, the layout, design parameters and response are summarized in Figure 2-6. The minimum insertion loss for the filter is –0.15 dB at 8.07 GHz, the filter has a flat response from 7.1 to its corner frequency.

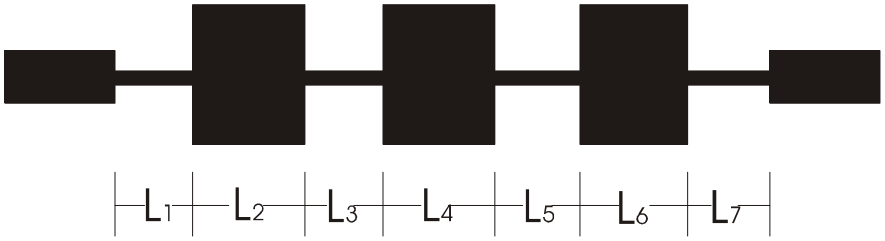

(a)

Section	Width	Z_O	Lengths
1 and 7	100 microns	106	L_1= L_7=1.8 mm
2 and 6	1.5 mm	35	L_2= L_6=1.929 mm
3 and 5	100 microns	106	L_3= L_5=2.732 mm
4	1.5 mm	35	L_4 =2.061 mm

(b)

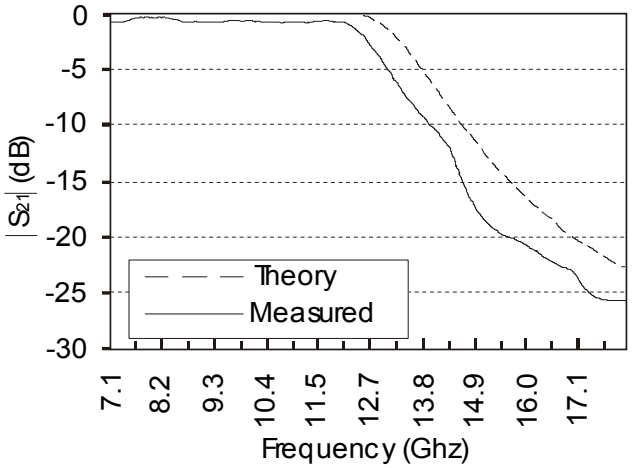

(c)

Figure 2-6 The LIGA 14 GHz low pass filter
(a) layout of the filter (b) design parameters for the filter (c) response, taken from [2-12]

A coupled line Butterworth bandpass filter was also designed with the LIGA 200 micron thick geometry, in which quarter wavelength parallel-line sections with two open circuits ports were used as coupling elements. A 10 GHz bandpass filter design was implemented with four coupling elements for a fractional bandwidth of 40%, the layout, design parameters and response are summarized in Figure 2-7. The minimum insertion loss for the filter is –0.45 dB at 10.12 GHz.

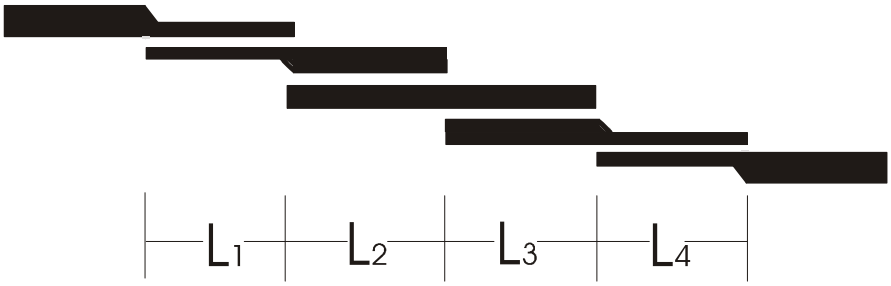

(a)

Section	Width	Gap	Z_{Oe}	Z_{Oo}	Lengths
1 and 4	200 micron	200 micron	123	43	$L_1 = L_4 = 5.063$ mm
2 and 3	400 micron	400 micron	90	41	$L_2 = L_3 = 4.845$ mm

(b)

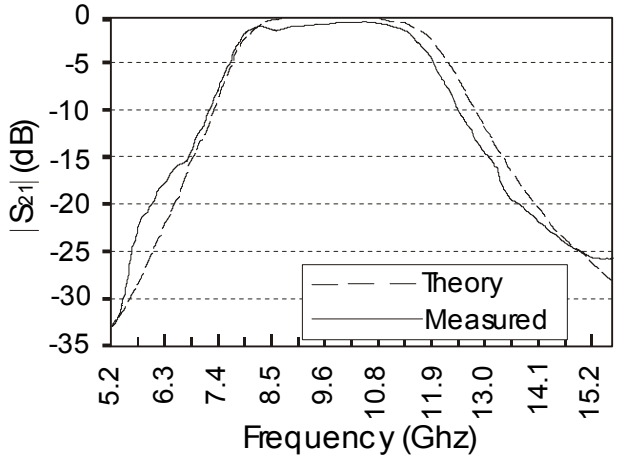

(c)

Figure 2-7 The LIGA 10 GHz bandpass filter
(a) layout of the filter (b) design parameters for the filter (c) response, taken from [2-12]

For these filters, the 200 micron thick LIGA microstrips were fabricated on a 420 micron thick, 3 in double sided polished fused-quartz. Nickel was chosen as the strip conductor metal for the first fabrication runs, although gold or copper may be also plated.

2.4.4 MEMBRANE SUPPORTED FILTERS

Membrane supported striplines [2-13] and microstrips [2-14],[2-15] have become a way of producing high performance millimetre wave circuits. High performance planar micromachined filters at 37 and 60 GHz are presented in [2-14], the filters consist of a 3.5% fractional bandwidth two pole Chebyshev filter with transmission zeros at 37 GHz, which had a 2.3 dB port to port insertion loss. A 2.7% and 4.3% fractional bandwidth four and five pole Chebyshev filters at 60 GHz, which had an insertion loss of 2.8 and 3.4 dB respectively. And shown here is the layout of an 8% fractional bandwidth quasi elliptic filter at 60 GHz exhibiting an insertion loss 1.5 dB which is shown in Figure 2-8.

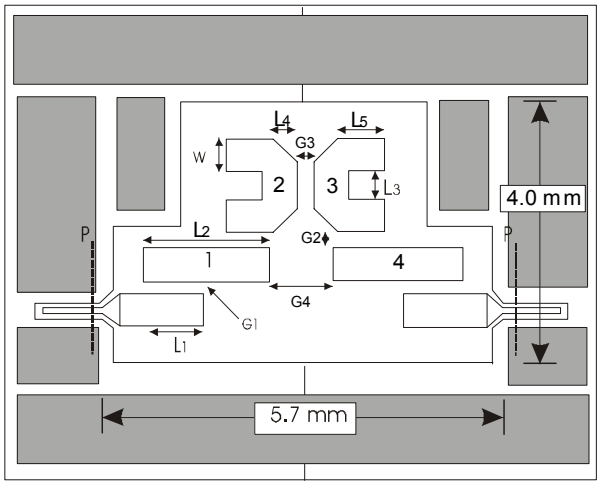

Figure 2-8 Layout of the 4 pole membrane quasi elliptic filter
L1=820, L2=2180, L3=645, L4=300, L5=675, w=500, G1=15, G2=200, G3=175, G4=625
(Dimensions in microns), taken from [2-14]

All measurements of the filters presented in [2-14] include the losses of the coplanar to microstrip transitions. These resonators are known to have Q's in the range of 400 to 500 at millimetre waves, from 30 GHz to 60 GHz. The measured response of the 8% fractional bandwidth filter is presented in Figure 2-9, the conductor width used is 500 microns and the ground to conductor spacing is 250 microns, a single resonator exhibits a Q of 454 and the metalization used is 1 micron of evaporated gold. The

shielding is made using via groves surrounding the filter. The insertion loss is 1.5 dB including the transition and the whole filter is smaller than 4 mm x 6 mm.

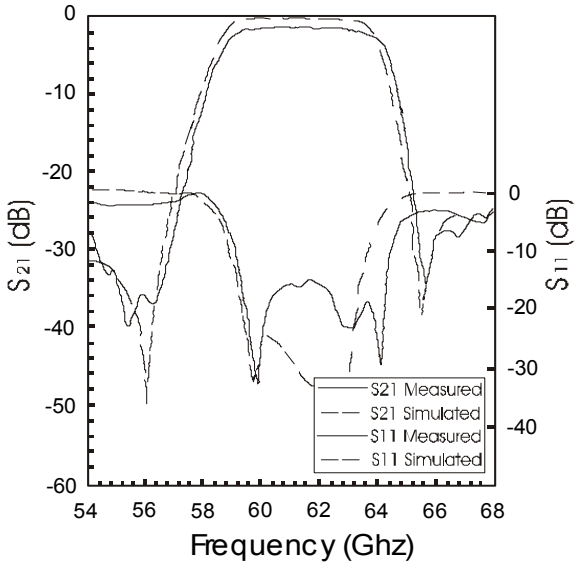

Figure 2-9 Measured response of the 4 pole membrane quasi elliptic filter, taken from [2-14]

A planar diplexer integrated on a single silicon substrate is presented in [2-15], the diplexer channels have a Chebyshev response and have a 5% and 6.5% relative bandwidth at 28 and 31 GHz, respectively. The layout of the diplexer is shown in Figure 2-10, the diplexer consists of two capacitively coupled bandpass filters with one port shared between the filters.

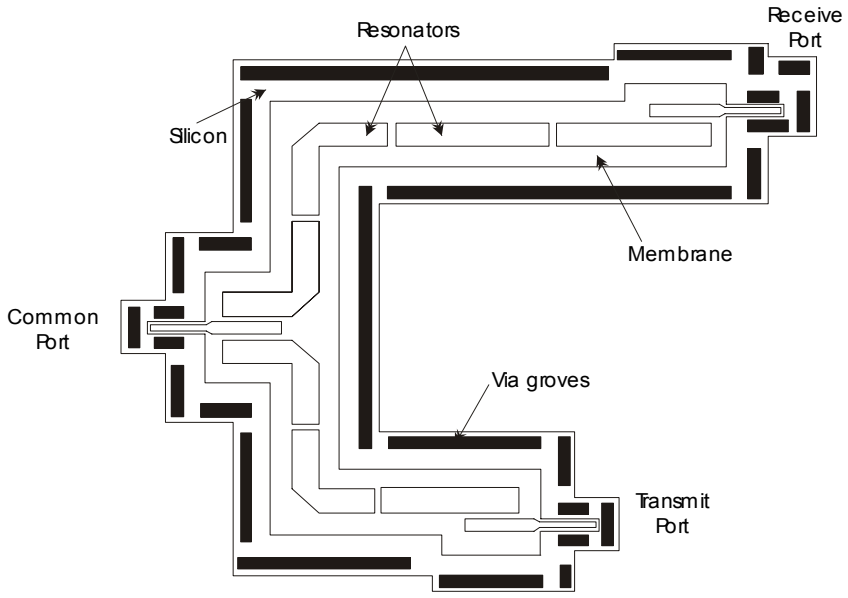

Figure 2-10 Layout of the K-band diplexer, taken from [2-15]

The receive band filter is designed using a four pole Chebyshev prototype with a centre frequency of 28 GHz, a relative bandwidth of 5.5%, and a ripple of 0.1 dB. The transmit band filter is a three pole Chebyshev filter with a centre frequency of 31.75 GHz, and a relative bandwidth of 5.5%, and a ripple of 0.1 dB.

The bent diplexer structure has a better performance than one having straight sections, because it helps to disturb any possible parasitic modes of the micromachined structure. These may result in an increase of coupling due to evanescent modes in the cavity structure, and also in propagating modes in the silicon surrounding the cavity.

The resonators used in the diplexer consist of 800 micron wide lines with a ground plane height of 250 microns, and a shielding cavity height of 800 microns. The distance from the edge of the conductors to the sidewalls of the micromachined channel is 700 microns. The conductors are 2 micron thick electroplated gold. A half wavelength resonator constructed of this geometry has an unloaded quality factor of 460 at 29 GHz. The filter response of the diplexer is shown in Figure 2-11.

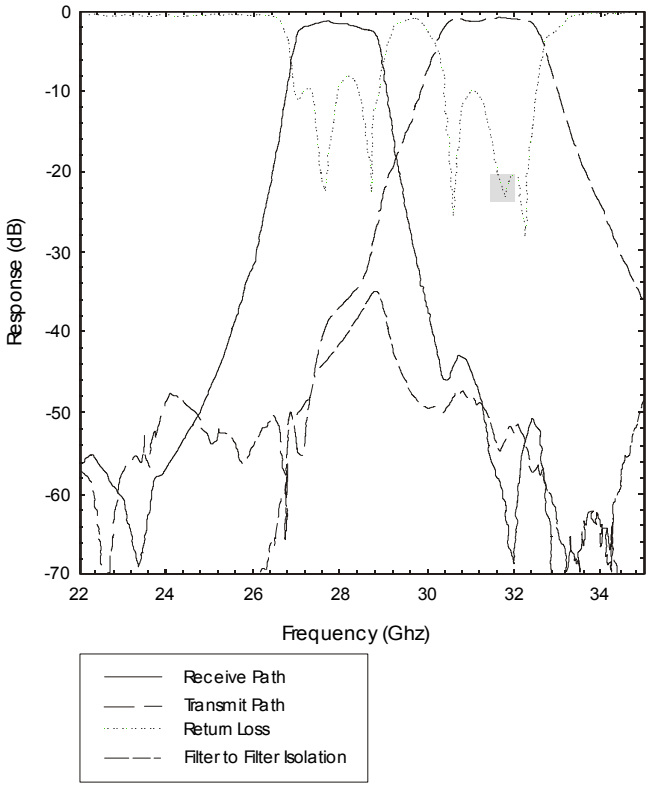

Figure 2-11 Response of the K band diplexer, taken from [2-15]

The diplexer outer dimensions are 1.5 cm x 1.6 cm x 1.4 mm thick. The insertion loss is 1.4 dB for the 28 GHz band and 0.9 dB for the 31 GHz band, including all transition effects. The measured isolation is better than –35 dB across the receive band, and better than –50 dB in the transmit band.

2.4.5 A HIGH Q MILLIMETRE WAVE DILECTRIC RESONATOR

A high performance micromachined millimetre wave passive circuit on silicon has been demonstrated in [2-16], in which an appropriate coupling between two coplanar lines and a dielectric resonator have allowed the achievement of loaded quality factors ranging from 400 to 2400 at 35 GHz, with transmission levels ranging from –5 to –14 dB. The structure is shown in Figure 2-12.

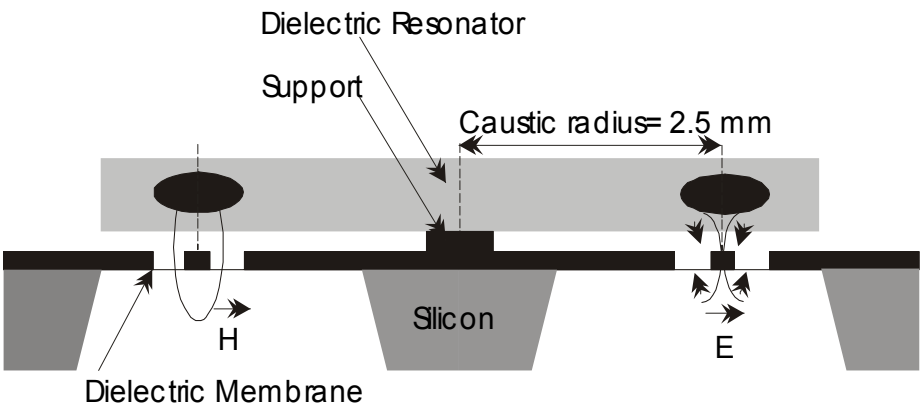

Figure 2-12 A dielectric resonator at millimetre waves, taken from [2-16]

These results were obtained with a commercial dielectric resonator featuring a relative permittivity of 30, with a thickness of 700 microns and a diameter of 6.5mm. The proposal of using high resistivity silicon as a dielectric resonator is also proposed in [2-16], having a relative permittivity of 11.5 and a loss tangent of $5x10^{-4}$ for frequencies ranging from 70 to 100 GHz, which is presumed to have a Q of 2000.

2.4.6 MICROMACHINED FILTERS ON SYNTHESIZED SUBSTRATES

[2-17] shows the use of silicon micromachining for the development of synthesised substrates, which, when utilized appropriately, can further reduce the low impedance value or increase the high impedance value of microstrip transmission lines. Good planar filter designs use equivalent transmission line representation for inductive or capacitive filter elements that result in large high to low impedance ratios. Although high dielectric constant semiconductor materials offer compactness, some designs, such as the stepped impedance filter, can suffer from shallow rolloff and poor attenuation in the stopband due to impedance range limitations that preclude achieving large high to low impedance ratios.

A silicon wafer is micromachined to form a synthesised substrate that can minimize low impedance and maximize high impedance values. Two approaches have been investigated for the development of high performance micromachined low pass

filters. The first approach attempts to further decrease the low impedance value of the microstrip line by thinning the substrate locally, shown in Figure 2-13a; whereas, the second one aims at further increasing the high impedance values by micromachining an air cavity locally to reduce the effective dielectric constant, as in Figure 2-13b.

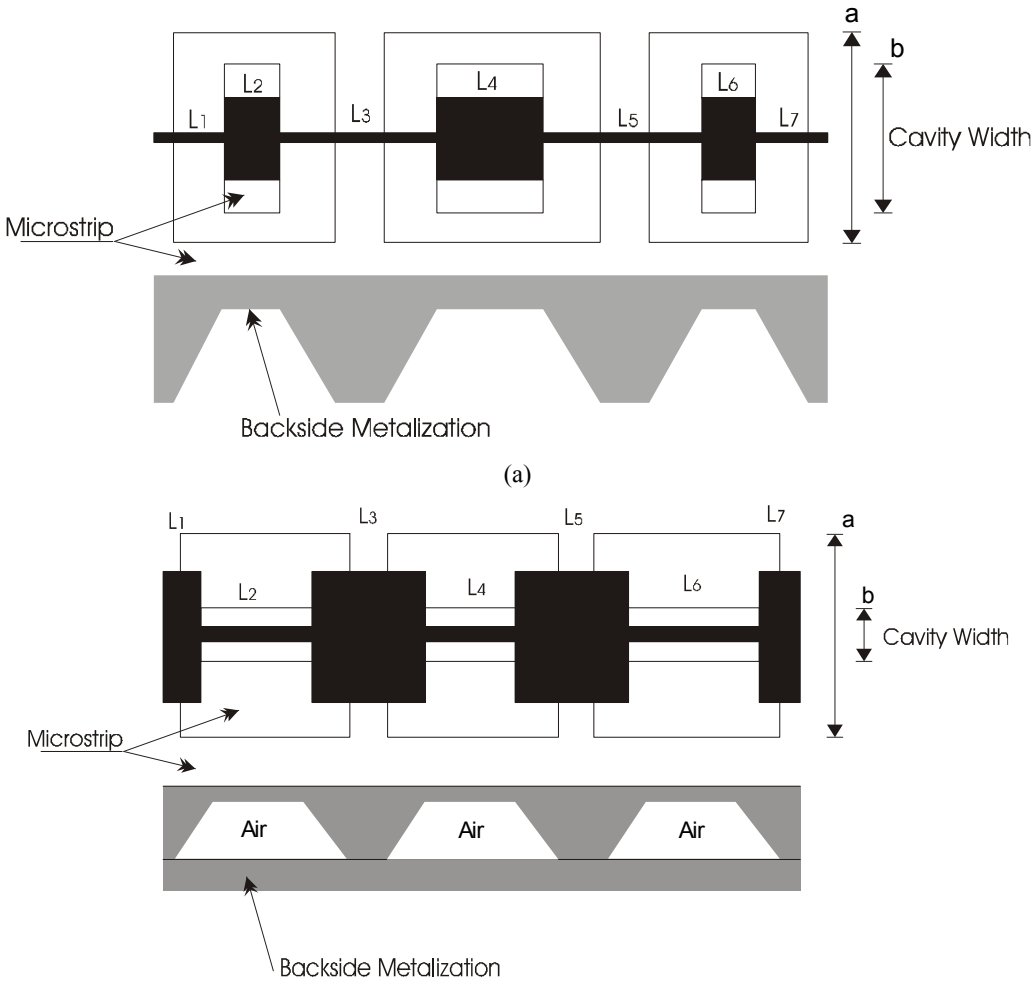

Figure 2-13 Micromachined filters on synthesized substrates, taken from [2-17]

(a) filter on synthesized low impedance substrate

(b) filter on synthesized high impedance substrate

The micromachined approach for reducing the low impedance value has been validated, and best impedance improvements occur when the full thickness conductor width is maintained over the micromachined substrate. Furthermore, in the filter

response, sharper rejection band edges have been achieved for increased high to low impedance ratios by a factor of 1.5. In the micromachined approach for increasing the high impedance value, two primary advantages are observed: 1) a reduction in fabrication and design tolerances, which allow for practical realization, and 2) a reduction of ohmic losses as a result of wider conducting lines. The measured response for a seven section Chebyshev synthesized high impedance filter on a 250 micron thick silicon substrate is shown in Figure 2-14.

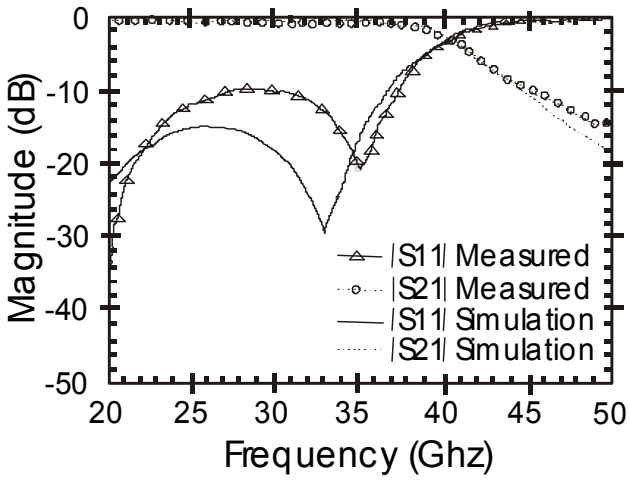

Figure 2-14 Seven section Chebyshev filter on a synthesized substrate, taken from [2-17]

The dimensions of the seven section Chebyshev filter are shown in Table 2-2, and correspond to Figure 2-13b.

Filter Section	Impedance (Ohms)	FT Width (h=250 Microns)	FT Length (Microns)	HI Width (10:90), (Microns)	HI Length (Microns)
L_1	30	500	268	500	268
L_2	150	1.2	271	70	498
L_3	30	500	500	500	500
L_4	150	1.2	327	70	600
L_5	30	500	500	500	500
L_6	150	1.2	271	70	498
L_7	30	500	268	500	268

Table 2-2 synthesized High-Impedance (HI) design parameters on full thickness silicon and micromachined high-impedance sections based on a 10%:90% ratio of Si – air regions, where FT is full-thickness substrate and h is the full thickness height, taken from [2-17]

2.4.7 MICROMACHINED TUNABLE FILTERS

A micromachined, electronically tunable filter at X band is presented in [2-18]. The filter uses membrane technology as in [2-14] and [2-15] to produce a stripline filter. The filter is tuned via varactors at the end of the resonators as in Figure 2-15.

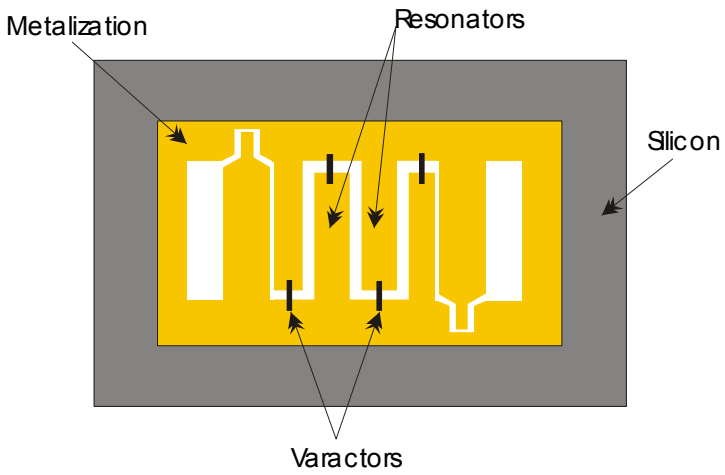

Figure 2-15 Varactor tuned X band filter, taken from [2-18]

The varactors were measured to have a capacitance variation of 1.8 pF to 1.1 pF. The tuning range was approximately from 5.5 GHz to 10.5 GHz, with an insertion loss of about 5dB. The tuning range was limited by varactor capacitance not tuning below 0.18 pF. The insertion loss and the out of band rejection were also degraded. This is due to the upper cavity not having direct contact with the ground and the ground plane being split (necessary to bias the varactors in this design). In future designs, MMIC capacitors should be used for biasing the varactors allowing for better grounding of the top and bottom ground planes of the stripline structure. The measured response for the varactor tuned X band filter is shown in Figure 2-16.

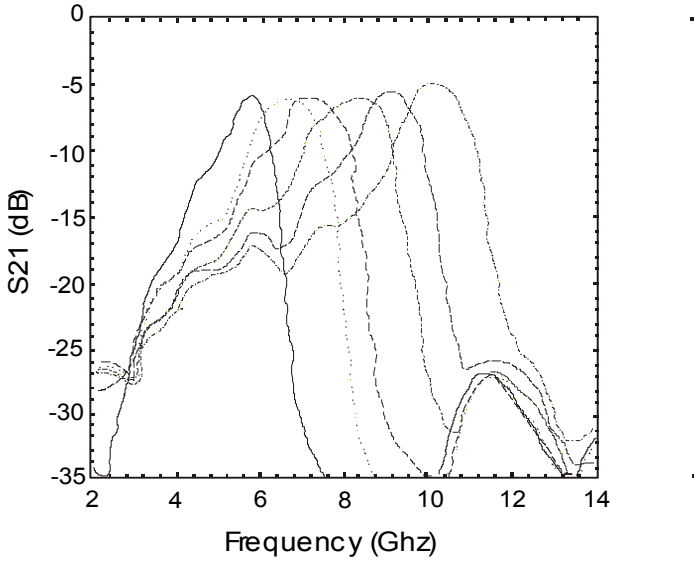

Figure 2-16 Measured response of the varactor tuned X band filter, taken from [2-18]

Another micromachined tunable filter is reported in [2-19], where micromachined variable capacitors are presented to tune the filters. Two bandpass filters are presented, one with 2 poles made with lumped elements and one with two poles made with distributed elements. Both are designed at the Ka band and are fabricated using MEMS (Micro Electro-Mechanical Systems) technology. With applied bias, the centre frequency shift is of the range of 1.1 GHz (4.2%) for the lumped element filter, and 0.8 GHz (2.5%) for the distributed element filter.

These tunable filters use the cantilever type of variable capacitors. With the application of a DC bias voltage on the cantilevers, the electrostatic force between the two plates reduces, resulting in a capacitance increase. These micromachined capacitors were employed in the Ka band filters as a part of the resonators, to demonstrate frequency tunability. A photo of the filters is shown in Figure 2-17.

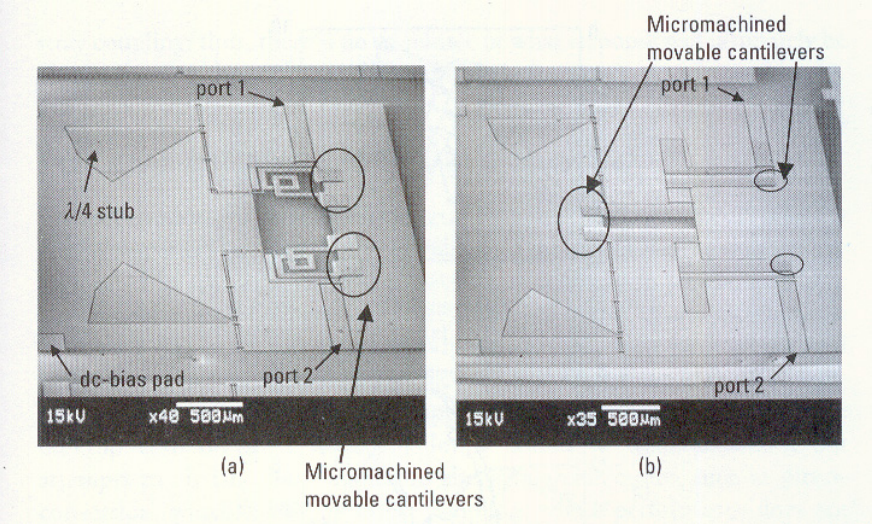

Figure 2-17 Micrograph of the two micromachined tunable filters, taken from [2-19]

(a) two pole lumped element filter (3.4 x 2.9 mm)

(b) two pole distributed resonator filter (4.1 x 3.4 mm)

The lumped element filter was designed to have a 4.7% fractional bandwidth, a 0.5 dB ripple and a centre frequency of 26.8 GHz. The distributed element filter was designed to have a 8.5% bandwidth, a 0.5 dB ripple and a centre frequency of 30.6 GHz. These circuits were patterned on a 560 micron thick glass substrate, using 2 micron thick electroplated gold. The cantilevers are suspended 6 microns above the common coplanar ground plane with an area of 200 x 200 microns. To avoid DC voltage short, a 1 micron SiO_2 dielectric layer was deposited on the coplanar top ground plane. RF choke for DC voltage bias was realized using a quarter wavelength radial stub and a quarter wavelength high impedance line. Application of a DC voltage between the cantilever and the top coplanar ground plane causes the cantilever to deflect downwards.

The measured responses for the tunable filters is shown in Figure 2-18, the passband insertion losses did not change appreciably throughout the tuning range of the filters. The minimum measured insertion losses were 4.9 dB and 3.8 dB for the lumped element and resonator filter, respectively. The losses can be improved by using thicker metals and by shielding the structure to avoid radiation losses.

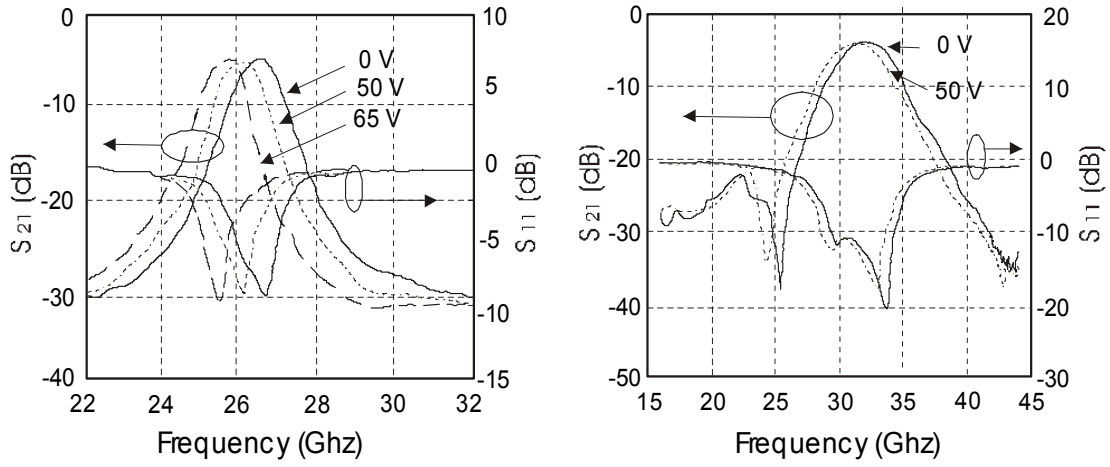

(a) (b)

Figure 2-18 Measured responses of the two micromachined tunable filters
(a) 2 pole lumped element filter (b) 2 pole distributed resonator filter, taken from [2-19]

2.5. REFERENCES

[2-1] Jennifer A. Bishop, Majid M. Hashemi, Kursad Kiziloglu, Lawrence Larson, Nadir Dagli, Umesh Mishra, "Monolithic coaxial transmission lines for mm-wave ICs", *High speed semiconductor devices and circuits, Proceedings IEEE/Cornell conference on advanced concepts,* 5-7 August 1991, pp 252-260.

[2-2] Happy Henri, Six Gonzague, Vanmackelberg Matthieu, Cappy Alain and Dambrine Gilles, "Ultra low loss transmission lines on low resistivity silicon substrate", *IEEE MTT-S Digest*, pp. 1809-1812, 2000.

[2-3] Kazuaki Takahashi, Ushio Sangawa, Suguru Fujita, Michiaki Matsuo, Takeharu Urabe, Hiroshi Ogura and Hiroyuki Yabuki, "Packaging using

microelectromechanical technologies and planar components" *IEEE Transactions on microwave theory and techniques,* Vol. 49, No. 11, pp. 2099-2104, November 2001.

[2-4] Jae-Hyoung Park, Chang-Wook Baek, Sanghwa Jung, Hong-Teuk Kim, Youngwoo Kwon and Yong-Kweon Kim, "Novel micromachined coplanar waveguide transmission lines for application in millimetre-wave circuits" *Jpn. J. Appl. Phys.* Vol. 39, Part 1, No. 12B, pp. 7120-7124, December 2000.

[2-5] Pierre Blondy, Andrew R. Brown, Dominique Cross and Gabriel M. Rebeiz, "Low loss micromachined filters for millimetre-wave telecommunication systems" *IEEE MTT-S Digest,* pp. 1181-1184, 1998.

[2-6] Katherine Juliet Herrick, Thomas A. Schwartz and Linda P. B. Katehi, "Si-micromachined coplanar waveguides for use in high-frequency circuits" *IEEE Transactions on microwave theory and techniques*, Vol. 46, No. 6, pp 762-768, June 1998.

[2-7] Wai Y. Liu, D. Paul Steenson and Michael B. Steer, "Membrane-supported CPW with mounted active devices" *IEEE Microwave and wireless components letters,* Vol. 11, No. 4, April 2001.

[2-8] J.E. Harriss, L.W. Pearson, X. Wang, C.H. Barron and A.V. Pham, "Membrane-supported Ka band resonator employing organic micromachined packaging" *IEEE MTT-S Digest,* pp. 1225-1228, 2000.

[2-9] W.Y. Liu, D.P. Steenson, M.B. Steer, "Membrane-supported e-plane circuits", *IEEE MTT-S Digest,* pp. 539-542, 2001

[2-10] John Papapolymerou, Jui-Ching Cheng, Jack East and Linda P.B. Katehi, "A Micromachined High-Q X-band resonator", *IEEE Microwave and guided letters,* Vol 7, No 6, June 1997.

[2-11] Lee Harle and Linda P.B. Katehi, "A vertically integrated micromachined filter", *IEEE transactions on theory and techniques,* Vol 50, No 9, September 2002.

[2-12] Theodore L. Willke and Steven S. Gearhart, "LIGA micromachined planar transmission lines and filters", *IEEE transactions on microwave theory and techniques,* Vol 45, No 10, October 1997.

[2-13] Chen-Yu Chi and Gabriel Rebeiz, "Conductor loss limited stripline resonator and filters", *IEEE transactions on microwave theory and techniques,* Vol 44, No 4, April 1996.

[2-14] Pierre Blondy, Andrew R. Brown, Dominique Cros and Gabriel M. Rebeiz, "Low loss micromachined filters for millimetre wave communication systems", *IEEE transactions on microwave theory and techniques,* Vol 46, No 12, December 1998.

[2-15] Andrew R. Brown and Gabriel M. Rebeiz, "A high performance integrated K-band diplexer", *IEEE transactions on microwave theory and techniques,* Vol 47, No 8, August 1999.

[2-16] B. Guillon, D. Cros, P. Pons, K.Grenier, T. Parra, J.L. Cazaux, J.C. Lalaurie, J. Graffeuil and R. Plana, "Design and realization of high Q millimetre wave structures through micromachining techniques", *IEEE MTT-S Digest,* pp. 1519-1522, 1999.

[2-17] Rhonda Franklin Drayton, Sergio Palma Pacheco, Jianei Wang, Jong-Gwan Yook, Linda P.B. Katehi, "Micromachined filters on synthesized substrates", *IEEE transactions on microwave theory and techniques,* Vol 49, No 2, February 2001.

[2-18] Andrew R. Brown and Gabriel M. Rebeiz, "Micromachined micropackaged filter banks and tunable bandpass filters", *IEEE wireless communications conference,* Proceedings 11-13, August 1997, pp 193-197.

[2-19] Hong-Teuk Kim, Jae-Hyoung Park, Yong-Kweon Kim and Youngwoo Kwon, "Millimeter wave micromachined tunable filters", *IEEE MTT-S Digest,* pp. 1235-1238, 1999.

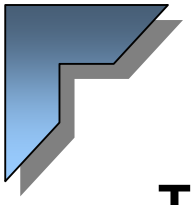

CHAPTER THREE
TRANSMISSION LINE THEORY

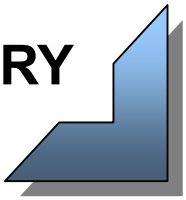

3.1 INTRODUCTION

In this Chapter a review of basic transmission line theory will be presented, the theory used in this Chapter can be found in [3-1] to [3-9]. The first section deals with the lumped element model of a transmission line, out of which the telegrapher's equations will be derived. These equations are general and relate voltages and currents on the transmission line to any point in time and space.

In section 3.3, standing waves will be introduced by the example of a lossless transmission line terminated in a mismatched load, which will produce reflected waves on the transmission line that combine with the generated wave leading to standing waves. The input impedance of a low loss, half wavelength transmission line terminated

in an open circuit will also be reviewed in this section, this result will be used later in Chapter 4, section 4.3.

In Section 3.4 wave propagation will be introduced and the wave equations derived, followed by the definition of the TEM (Transverse Electromagnetic Mode) mode, also in this section dispersion problems in transmission lines will be addressed. Finally at the end of the chapter, basic transmission lines used in microwave engineering will be presented.

3.2 THE TELEGRAPHER EQUATIONS

Microwave transmission lines may differ significantly in physical form, which leads to different electromagnetic field patterns. The objective of this section will be to describe the impedance and propagation characteristics of a transmission line; the method is general, based on ac circuit theory, and it is valid regardless of the electromagnetic field pattern of the transmission line.

In 1855 the studies made by William Thomson (Lord Kevin) led to the first distributed circuit analysis of a transmission line. His model consisted of uniformly distributed series resistances and shunt capacitances. This was the beginning of transmission line theory. Later on, after the telephone was invented by Bell and Gray in 1876, a more detailed study of transmission lines was carried out by Oliver Heaviside, his analysis appears practically unaltered in today's text books.

A transmission line is often schematically represented as a two wire line, since transmission lines for TEM wave propagation always have at least two conductors. Figure 3-1 represents a short piece of transmission line, where Δ_z can always be chosen to be small compared to the operating wavelength, in the derivation $\Delta_z \to 0$, and hence the results are valid at all frequencies.

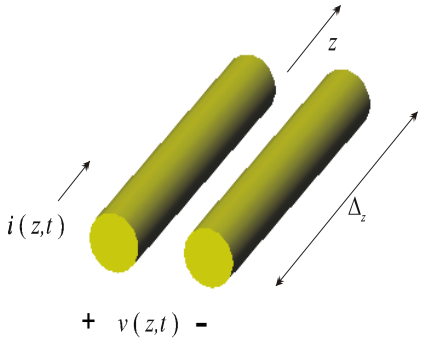

(a)

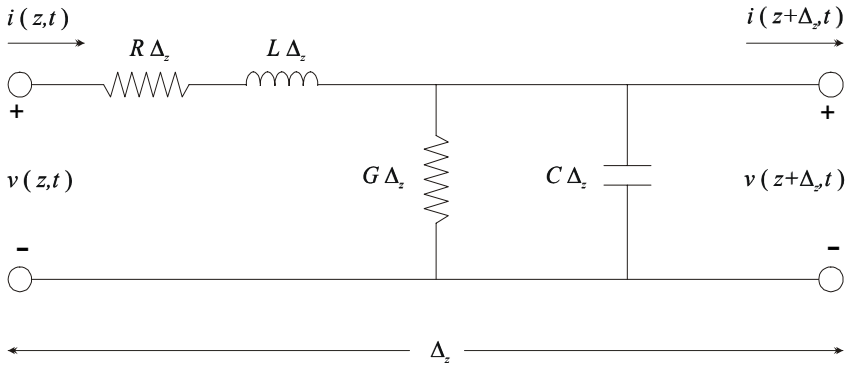

(b)

Figure 3-1 Short length of transmission line
(a) Voltage and current definitions (b) Lumped element equivalent circuit

Applying Kirchhoff's voltage and current law to the circuit in Figure 3-1b gives

$$v(z,t) - R\Delta_z i(z,t) - L\Delta_z \frac{\partial i(z,t)}{\partial t} - v(z+\Delta_z,t) = 0 \qquad \text{eq 3-1}$$

$$i(z,t) - G\Delta_z v(z+\Delta_z,t) - C\Delta_z \frac{\partial v(z+\Delta_z,t)}{\partial t} - i(z+\Delta_z,t) = 0 \qquad \text{eq 3-2}$$

Dividing eq 3-1 and eq 3-2 by Δ_z and taking the limit as $\Delta_z \to 0$, leads to the time domain form of the transmission line equation. This equation pair, shown below, is called the Telegrapher's equations

$$\frac{\partial v(z,t)}{\partial z} = -Ri(z,t) - L\frac{\partial i(z,t)}{\partial t} \quad \text{eq 3-3}$$

$$\frac{\partial i(z,t)}{\partial z} = -Gv(z,t) - C\frac{\partial v(z,t)}{\partial t} \quad \text{eq 3-4}$$

The Telegrapher's equations are general, relating voltages and currents on the transmission line to any point in time and space, via the line parameters *R, L, G* and *C*. The negative signs indicate that the voltage and current will decrease with an increasing distance *z*.

Frequently we are concerned with a single frequency steady state sinusoidal voltage or current that can be represented by the phasors

$$v(t) = v_o e^{j\omega t} \quad \text{eq 3-5}$$

$$i(t) = i_o e^{j\omega t} \quad \text{eq 3-6}$$

Differentiating these equations results in

$$\frac{\partial v}{\partial t} = j\omega v_o e^{j\omega t} = j\omega v(t) \quad \text{eq 3-7}$$

$$\frac{\partial i}{\partial t} = j\omega i_o e^{j\omega t} = j\omega i(t) \quad \text{eq 3-8}$$

In this case eq 3-3 and eq 3-4 simplify to

$$\frac{\partial v(z)}{\partial z} = -(R + j\omega L)i(z) \quad \text{eq 3-9}$$

$$\frac{\partial i(z)}{\partial z} = -(G + j\omega C)v(z) \quad \text{eq 3-10}$$

Eliminating $i(z)$ and $v(z)$ from eq 3-9 and eq 3-10 respectively by cross substitution yields

$$\frac{\partial^2 v(z)}{\partial z^2} = (R + j\omega L)(G + j\omega C)v(z) = \gamma^2 v(z) \qquad \text{eq 3-11}$$

$$\frac{\partial^2 i(z)}{\partial z^2} = (R + j\omega L)(G + j\omega C)i(z) = \gamma^2 i(z) \qquad \text{eq 3-12}$$

Where

$$\gamma = \alpha + j\beta = \sqrt{(R + j\omega L)(G + j\omega C)} \qquad \text{eq 3-13}$$

In eq 3-13, γ is called the Propagation constant, the real part of γ is called the attenuation constant represented by α, the units of α are in Np per unit length. The imaginary part of γ is called the phase constant represented by β, which describes the variation in phase of the travelling waves; its units are in radians per unit length. From the illustration in Figure 3-2, two points a wavelength distant are separated by 2π radians, hence

$$\lambda\beta = 2\pi \quad \text{or} \quad \beta = \frac{2\pi}{\lambda} \qquad \text{eq 3-14}$$

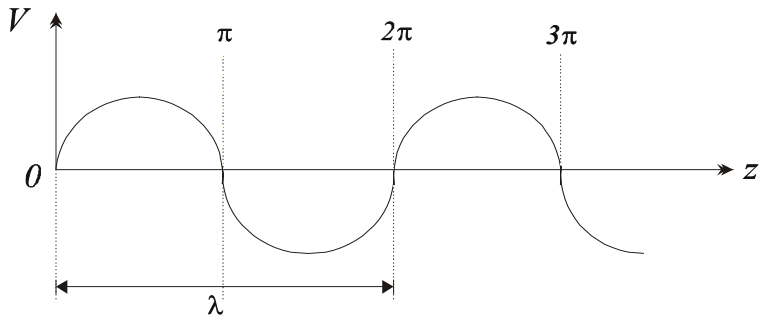

Figure 3-2 Variation in phase of a travelling wave

The second order differential equations, eq 3-11 and eq 3-12, are of standard form and by differentiation and back substitution, the solutions are readily shown to be

$$v(z) = V_1^+ e^{-\gamma z} + V_2^- e^{\gamma z} \qquad \text{eq 3-15}$$

$$i(z) = I_1^+ e^{-\gamma z} + I_2^- e^{\gamma z} \qquad \text{eq 3-16}$$

Where V_1^+, V_2^-, I_1^+, I_2^- are arbitrary amplitude constants, and the terms with $e^{-\gamma z}$ represent wave propagation in the $+z$ direction, and the terms with $e^{\gamma z}$ represent wave propagation in the $-z$ direction. By substitution of eq 3-9 in the voltage of eq 3-15 gives the current of the line

$$i(z) = \frac{\gamma}{R + j\omega L}(V_1^+ e^{-\gamma z} - V_2^- e^{\gamma z}) \qquad \text{eq 3-17}$$

Knowing that the characteristic impedance of the line is equal to the ratio of the voltage to current of the line, when the line is matched, and comparing eq 3-17 with eq 3-16, show that the characteristic impedance of the transmission line is

$$Zo = \frac{R + j\omega L}{\gamma} = \sqrt{\frac{R + j\omega L}{G + j\omega C}} \qquad \text{eq 3-18}$$

The current on the line is related to the voltage and the characteristic impedance of the transmission line in the following ways

$$I_1^+ = \frac{V_1^+}{Z_O} \qquad \text{eq 3-19}$$

$$I_2^- = \frac{-V_2^-}{Z_O} \qquad \text{eq 3-20}$$

The negative sign in eq 3-20 derives from the fact that the current I_2^- is travelling in the negative z direction.

3.3 STANDING WAVES

Two travelling waves of the same amplitude and with the same frequency travelling in the opposite direction will interfere and produce an interference pattern. Because the observed wave pattern is characterized by points which appear to be standing still, the pattern is called a standing wave pattern.

In this section, a reflection coefficient will be defined for a voltage travelling down the transmission line as shown in Figure 3-3, followed by the definition of the standing wave ratio. This is a measure of mismatch of a transmission line to the load. Finally an expression for calculating the input impedance seen at a distance l from the load will be defined. The objective of this section will be to illustrate the standing waves on a transmission line, and therefore a lossless transmission line will be assumed.

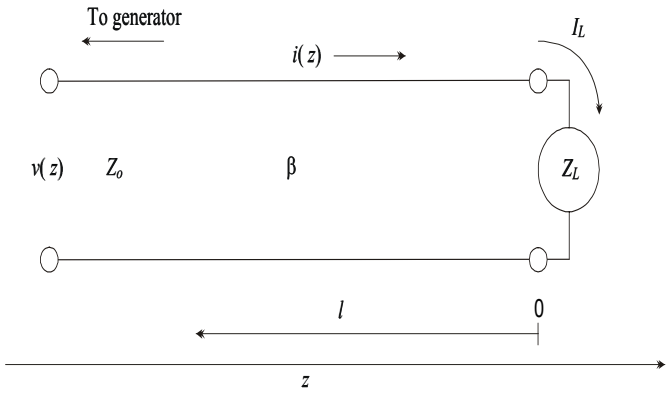

Figure 3-3 Lossless transmission line terminated in a load impedance Z_L

A travelling wave is generated from a source at $z<0$, as shown on Figure 3-3. The wave has the following form

$$v(z) = V_1^+ e^{-j\beta z} \qquad \text{eq 3-21}$$

As seen previously, the ratio of the voltage to current for the travelling wave is the characteristic impedance Z_O. If the transmission line is terminated in an arbitrary load $Z_L \neq Z_O$ the ratio of voltage to current at the load must be equal to Z_L. Therefore a reflected wave must be generated at the load with the appropriate amplitude to satisfy this condition.

The load impedance is related to the total voltage and current in the following way, using eq 3-19 and eq 3-20, at the load, we find

$$Z_L = \frac{v(l=0)}{i(l=0)} = \frac{V_1^+ + V_2^-}{V_1^+ - V_2^-} Z_O \qquad \text{eq 3-22}$$

Solving for the ratio V_2^-/V_1^+, that is the amplitude of the reflected wave normalized to the amplitude of the incident wave, defined as the voltage reflection coefficient Γ

$$\Gamma = \frac{V_2^-}{V_1^+} = \frac{Z_L - Z_O}{Z_L + Z_O} \qquad \text{eq 3-23}$$

A current reflection coefficient can also be defined as the ratio of the reflected current to the incident current. From eq 3-19 and eq 3-20 we can observe that it will be equal to the negative of the voltage reflection coefficient. The rest of the section will deal only with the voltage reflection coefficient.

When a load is mismatched, not all the available power from the generator is delivered to the load. This loss is referred as the return loss *RL* in dB, and is defined as

$$RL = -20\log|\Gamma| \qquad \text{eq 3-24}$$

If Γ=0 then we have $Z_L=Z_O$, in this case there is no reflected wave, and the transmission line is said to be matched to the load. If Γ≠0 then the voltage at any point of the line will be the phasor sum of the forward and reflected voltages.

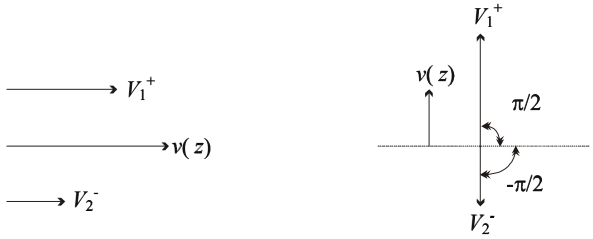

(a) (b)

Figure 3-4 Phasor diagram for the incident and reflected voltages when Γ≠0
(a) In phase (b) Out of phase

Figure 3-4 shows the phasor diagram of the incident voltage and the reflected voltage. The case when they add up is illustrated in Figure 3-4a, and the case when they cancel each other is shown in Figure 3-4b. Now we can conclude that the voltage will oscillate with position down the transmission line, due to the fact that the incident and reflected voltages will create a standing wave, where the voltage maximum will occur when

$$v_{\max} = V_1^+ + |\Gamma|V_1^+ = (1+\Gamma)V_1^+ \qquad \text{eq 3-25}$$

And a voltage minimum will occur when

$$v_{\min} = V_1^+ - |\Gamma|V_1^+ = (1-\Gamma)V_1^+ \qquad \text{eq 3-26}$$

A measure of the mismatch of the line is the standing wave ratio, and it is defined as the ratio of the voltage maximum to the voltage minimum of the standing wave

$$SWR = \frac{v_{\max}}{v_{\min}} = \frac{1+|\Gamma|}{1-|\Gamma|} \qquad \text{eq 3-27}$$

SWR can take values from 1 to ∞, a *SWR*=1 implies that the line is matched to the load.

Taking eq 3-23, that is the refection coefficient at the load, and solving for the load impedance results in

$$Z_L = \frac{(1+\Gamma)}{(1-\Gamma)} Z_O \qquad \text{eq 3-28}$$

The reflection coefficient can be generalized to any point on the line, with $z=-l$, the ratio of the reflected voltage to the incident voltage is

$$\Gamma(l) = \frac{V_2^- e^{-j\beta l}}{V_1^+ e^{j\beta l}} = \Gamma(0) e^{-2j\beta l} \qquad \text{eq 3-29}$$

Where Γ(0) is the reflection coefficient at $l=0$, now from eq 3-28 and eq 3-29, the input impedance seen looking toward the load at a distance $l=-z$ from the load is

$$Z_{in} = Z_O \frac{1+\Gamma e^{-2j\beta l}}{1-\Gamma e^{-2j\beta l}} \qquad \text{eq 3-30}$$

By using eq 3-23 in eq 3-30 gives

$$Z_{in} = Z_O \frac{(Z_L+Z_O)e^{j\beta l} + (Z_L-Z_O)e^{-j\beta l}}{(Z_L+Z_O)e^{j\beta l} - (Z_L-Z_O)e^{-j\beta l}} \qquad \text{eq 3-31}$$

Using the following Euler's identities relating trigonometric and exponential functions

$$e^{j\theta} = \cos(\theta) + j\sin(\theta) \qquad \text{eq 3-32}$$

$$e^{-j\theta} = \cos(\theta) - j\sin(\theta) \qquad \text{eq 3-33}$$

eq 3-31 becomes

$$Z_{in} = Z_O \frac{Z_L \cos(\beta l) + jZ_O \sin(\beta l)}{Z_O \cos(\beta l) + jZ_L \sin(\beta l)} = Z_O \frac{Z_L + jZ_O \tan(\beta l)}{Z_O + jZ_L \tan(\beta l)} \qquad \text{eq 3-34}$$

The input impedance of a length of transmission line terminated in an arbitrary load can be calculated with eq 3-34.

3.3.1 THE QUARTER WAVE TRANSFORMER

The quarter wavelength section of transmission line in Figure 3-5, can be used to match the load resistance R_L and the feed line characteristic impedance Z_O. Both are real and assumed to be given.

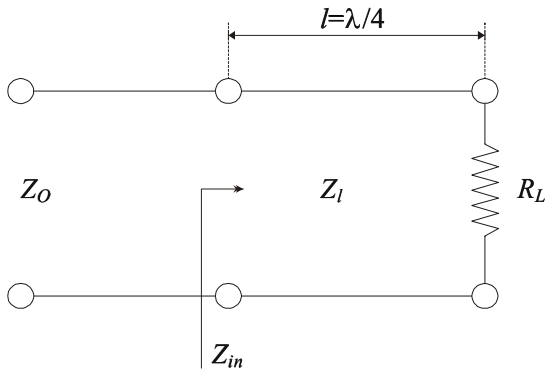

Figure 3-5 The quarter wave transformer

Using eq 3-34 for the quarter wave transformer in Figure 3-5, results in

$$Z_{in} = Z_l \frac{R_L + jZ_l \tan(\beta l)}{Z_l + jR_L \tan(\beta l)} \qquad \text{eq 3-35}$$

Now by using eq 3-14, we can see that for a quarter wavelength section of transmission line

$$\beta l = \frac{\pi}{2} \qquad \text{eq 3-36}$$

By dividing the numerator and denominator in eq 3-35 by tan(βl), and taking the limit as $\beta l \rightarrow \pi/2$, results in

$$Z_{in} = \frac{Z_l^{\,2}}{R_L} \qquad \text{eq 3-37}$$

From eq 3-37 we can see that a quarter wavelength section of a transmission line has the effect of transforming the load impedance in an inverse manner. In order to have no reflections, we must have $Z_{in}=Z_O$, so the characteristic impedance of the quarter wavelength section of transmission line is given by

$$Z_l = \sqrt{Z_O R_L} \qquad \text{eq 3-38}$$

This condition applies only when the length of the matching line is λ/4 long, or an odd multiple (2n+1) of λ/4. Note that this condition can be reached at one frequency, and a mismatch will occur at other frequencies.

3.3.2 A HALFWAVELENGTH TRANSMISSION LINE TERMINATED IN AN OPEN CIRCUIT

For a transmission line, the voltage and current on the transmission line, can be written as

$$v(z) = V_o^+ \left[e^{-\gamma z} + \Gamma e^{\gamma z} \right] \quad \text{eq 3-39}$$

$$i(z) = \frac{V_o^+}{Z_O} \left[e^{-\gamma z} - \Gamma e^{\gamma z} \right] \quad \text{eq 3-40}$$

Where V_o^+ is the amplitude of the voltage of an incident wave generated from a source, similar to eq 3-21. If the transmission line is terminated in an open circuit, such that $Z_L=\infty$, from eq 3-23, we find that the reflection coefficient for this case is $\Gamma=1$, and from eq 3-27 we find that the standing wave ratio is $SWR=\infty$, and the input impedance of the line is given by

$$Z_{in} = \frac{v(-l)}{i(-l)} \quad \text{eq 3-41}$$

Now by substituting eq 3-39 and eq 3-40 into eq 3-41, results in

$$Z_{in} = \frac{Z_O \left[e^{\gamma l} + \Gamma e^{-\gamma l} \right]}{e^{\gamma l} - \Gamma e^{-\gamma l}} \quad \text{eq 3-42}$$

Using the following identity

$$\coth(\theta) = \frac{e^{\theta} + e^{-\theta}}{e^{\theta} - e^{-\theta}} \quad \text{eq 3-43}$$

The input impedance in eq 3-42, for $\Gamma=1$, reduces to

$$Z_{in} = Z_O \coth \gamma l \quad \text{eq 3-44}$$

Note that eq 3-44 includes losses in the transmission line, since it contains the propagation constant γ, while eq 3-34 is valid for a lossless case.

3.4 WAVE PROPAGATION

This section deals with important characteristics of plane wave propagation; the result will be used later in Chapter 4, section 4.4.1, where conductor loss is discussed. The first section deals with the wave equations; in the second section the transverse electromagnetic wave propagation will be discussed, followed by a description of dispersion. Related to this are the phase and group velocities of the signals that travel through a transmission line, which concludes the section.

3.4.1 THE WAVE EQUATION

In this section the wave equation that governs the propagation of electromagnetic waves will be derived, the objective will be to derive the propagation constant and the general formulation for a wave from an electromagnetic point of view. This contrasts with the propagation constant in eq 3-13, which was derived from a lumped element model. For this purpose we will consider a linear, isotropic and homogeneous medium, where we will assume that the net free charge in the region is zero, so ρ=0. Any currents in the region are conduction currents σE, in the medium

$$\overline{D} = \varepsilon \overline{E} \qquad \text{eq 3-45}$$

$$\overline{B} = \mu \overline{H} \qquad \text{eq 3-46}$$

$$\overline{J} = \sigma \overline{E} \qquad \text{eq 3-47}$$

Where $\overline{D}$ is the electric flux density, $\overline{E}$ is the electric field intensity, $\overline{B}$ is the magnetic flux density, $\overline{H}$ is the magnetic field intensity, ε is the permittivity and μ is the permeability. Maxwell's equations in point form for this region become

$$\nabla \times \overline{E} = -\mu \frac{\partial \overline{H}}{\partial t} \qquad \text{eq 3-48}$$

$$\nabla \times \overline{H} = \sigma \overline{E} + \varepsilon \frac{\partial \overline{E}}{\partial t} \qquad \text{eq 3-49}$$

$$\nabla \cdot \overline{E} = 0 \qquad \text{eq 3-50}$$

$$\nabla \cdot \overline{H} = 0 \qquad \text{eq 3-51}$$

Taking the curl of eq 3-48 and substituting into eq 3-49, results in

$$\nabla \times \nabla \times \overline{E} = -\mu\sigma \frac{\partial \overline{E}}{\partial t} - \mu\varepsilon \frac{\partial^2 \overline{E}}{\partial t^2} \qquad \text{eq 3-52}$$

Similarly, by taking the curl of eq 3-49 and substituting into eq 3-48, results in

$$\nabla \times \nabla \times \overline{H} = -\mu\sigma \frac{\partial \overline{H}}{\partial t} - \mu\varepsilon \frac{\partial^2 \overline{H}}{\partial t^2} \qquad \text{eq 3-53}$$

In order to interpret these results the following vector identity will be used

$$\nabla \times \nabla \times A = \nabla\left(\nabla \cdot A\right) - \nabla^2 A \qquad \text{eq 3-54}$$

Now, substituting eq 3-54 into eq 3-52 and eq 3-53 gives the wave equations, namely

$$\nabla^2 \overline{E} = \mu\sigma \frac{\partial \overline{E}}{\partial t} + \mu\varepsilon \frac{\partial^2 \overline{E}}{\partial t^2} \qquad \text{eq 3-55}$$

$$\nabla^2 \overline{H} = \mu\sigma \frac{\partial \overline{H}}{\partial t} + \mu\varepsilon \frac{\partial^2 \overline{H}}{\partial t^2} \qquad \text{eq 3-56}$$

Now considering a sinusoidal steady state variation of the field vectors, the wave equations become

$$\nabla^2 \hat{E} = \mu\sigma\left(j\omega\hat{E}\right) + \mu\varepsilon\left(j\omega\right)^2 \hat{E} \qquad \text{eq 3-57}$$

$$\nabla^2 \hat{H} = \mu\sigma\left(j\omega\hat{H}\right) + \mu\varepsilon(j\omega)^2 \hat{H} \qquad \text{eq 3-58}$$

Rearranging terms

$$\nabla^2 \hat{E} = j\omega\mu(\sigma + j\omega\varepsilon)\hat{E} \qquad \text{eq 3-59}$$

$$\nabla^2 \hat{H} = j\omega\mu(\sigma + j\omega\varepsilon)\hat{H} \qquad \text{eq 3-60}$$

Where

$$\gamma^2 = j\omega\mu(\sigma + j\omega\varepsilon) \qquad \text{eq 3-61}$$

The positive square root of γ^2 is referred as the propagation constant of the medium given by

$$\gamma = \alpha + j\beta \qquad \text{eq 3-62}$$

$$\gamma = \sqrt{j\omega\mu(\sigma + j\omega\varepsilon)} \qquad \text{eq 3-63}$$

The propagation constant in eq 3-63 describes the propagation characteristics of an electromagnetic field, in contrast to the propagation constant in eq 3-13, which describes the propagation characteristics of a voltage or a current.

The general equations of a wave in terms of the phasor field vectors eq 3-59 and eq 3-60, can be expanded in terms of components. These will be useful for the derivation of the surface resistance in chapter 4 section 4.4.1, since

$$\nabla^2 \hat{E}_x = \frac{\partial^2 \hat{E}_x}{\partial x^2} + \frac{\partial^2 \hat{E}_x}{\partial y^2} + \frac{\partial^2 \hat{E}_x}{\partial z^2} \qquad \text{eq 3-64}$$

Resulting in

$$\frac{\partial^2 \hat{E}_x}{\partial x^2} + \frac{\partial^2 \hat{E}_x}{\partial y^2} + \frac{\partial^2 \hat{E}_x}{\partial z^2} = \gamma^2 \hat{E}_x \quad \text{eq 3-65}$$

$$\frac{\partial^2 \hat{E}_y}{\partial x^2} + \frac{\partial^2 \hat{E}_y}{\partial y^2} + \frac{\partial^2 \hat{E}_y}{\partial z^2} = \gamma^2 \hat{E}_y \quad \text{eq 3-66}$$

$$\frac{\partial^2 \hat{E}_z}{\partial x^2} + \frac{\partial^2 \hat{E}_z}{\partial y^2} + \frac{\partial^2 \hat{E}_z}{\partial z^2} = \gamma^2 \hat{E}_z \quad \text{eq 3-67}$$

$$\frac{\partial^2 \hat{H}_x}{\partial x^2} + \frac{\partial^2 \hat{H}_x}{\partial y^2} + \frac{\partial^2 \hat{H}_x}{\partial z^2} = \gamma^2 \hat{H}_x \quad \text{eq 3-68}$$

$$\frac{\partial^2 \hat{H}_y}{\partial x^2} + \frac{\partial^2 \hat{H}_y}{\partial y^2} + \frac{\partial^2 \hat{H}_y}{\partial z^2} = \gamma^2 \hat{H}_y \quad \text{eq 3-69}$$

$$\frac{\partial^2 \hat{H}_z}{\partial x^2} + \frac{\partial^2 \hat{H}_z}{\partial y^2} + \frac{\partial^2 \hat{H}_z}{\partial z^2} = \gamma^2 \hat{H}_z \quad \text{eq 3-70}$$

3.4.2 TEM AND QUASI TEM MODES

As a consequence of Maxwell's equations, we know that electromagnetic waves are 'self-propagating'. This propagation results from the fact that a time varying magnetic field produces a time varying electric field from Faraday's law, which in turn, produces a time varying magnetic field from Ampere's law and so forth. One type of field produces the other at a point in a plane normal to it; the electric and magnetic field are always perpendicular to each other and travel at the same speed.

In this thesis, the transmission line structures used to design the microwave filters in Chapter 7 propagate a TEM (transverse electromagnetic wave) or a "quasi" TEM wave, as will be defined in the following paragraphs.

Figure 3-6 illustrates the propagation of an electromagnetic wave for an instant of time t=0; we can observe that the power flow determined by the poynting vector is along the z axis. A TEM wave propagation is one in which the electric and magnetic field vectors at each point in space have no components in the direction of propagation,

so the electric and magnetic field vectors in space lie in a plane which is transverse to the direction of propagation.

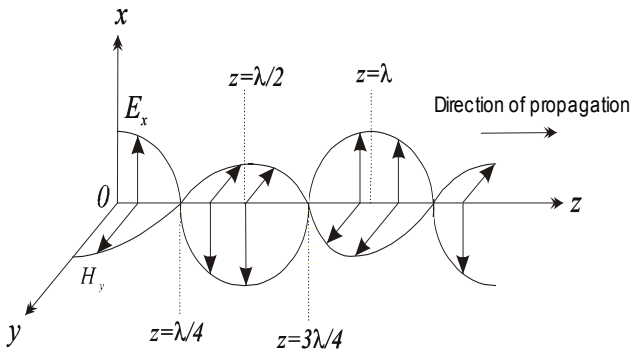

Figure 3-6 Electromagnetic wave travelling in the positive *z* direction at a time *t*=0

There are other possible field structures for which the electric and magnetic field vectors are not transverse to the direction of propagation. However, these modes have cutoff frequencies associated with them. Above these cutoff frequencies modes will propagate through the transmission line, and below the cutoff frequency they will be deeply attenuated in relatively short distances along the transmission line. The cutoff frequencies of the higher modes depend on the cross section of the transmission line, specifically on the separation between conductors, if these dimensions are electrically small, meaning that if the conductors are separated by a distance much less than a wavelength, then the higher modes are cutoff. The waveguide, which consists of a single conductor, can propagate TM and TE modes, which have cutoff frequencies associated with them.

If the conductors used in a transmission line are not perfect conductors, then a pure TEM mode cannot propagate through the line, even at dc, since there will be a component of the electric field in the direction of propagation due to the currents passing through the imperfect conductors. In practice, good conductors behave sufficiently well to assume a TEM approximation that is commonly referred to as Quasi TEM propagation.

The phase velocity V_p, that is the velocity at which a fixed phase point on the wave in Figure 3-6 travels, is related to the propagation constant by

$$V_p = \frac{\omega}{\beta} \qquad \text{eq 3-71}$$

3.4.3 DISPERSION

Phase velocity is defined as the velocity of a point of constant phase down the transmission line, while group velocity is defined as the velocity at which a group of frequencies travels down the transmission line. Group velocity can be defined as

$$V_g = \frac{d\omega}{d\beta} \qquad \text{eq 3-72}$$

Since most communication systems carry information in groups of frequencies, in base band or radio frequency, it will be of extreme importance that all the frequencies arrive at the receiving point as a delayed version of the input signal. This implies that all components of the signal spectrum must be transmitted with the same phase velocity. This is not always the case; when the phase and group velocities are a function of frequency, the transmission line is said to be dispersive, as it will disperse or spread a signal in time. How severe this effect is will depend on the range of velocities, and the length of the transmission line.

An example of a dispersive transmission line is the rectangular waveguide. The square coaxial transmission lines used in Chapter 7 are designed to operate in the pure TEM mode, so they are dispersionless, which is one advantage over the waveguide.

3.5 BASIC MICROWAVE TRANSMISSION LINES

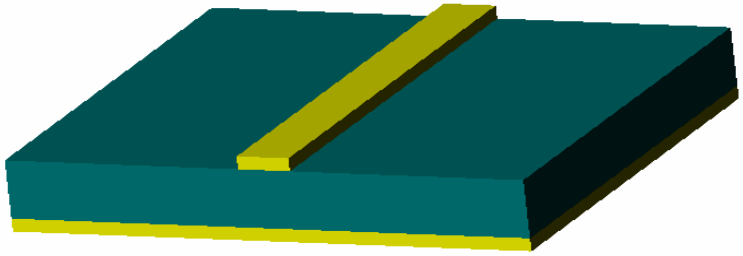

Figure 3-7 Microstrip

The Microstrip in Figure 3-7 is a very common transmission line in microwave engineering. It consists of a thin conductor and a ground plane separated by a low loss dielectric. The microstrip is simple to manufacture, and has a good range of characteristic impedance, and it is relatively low loss (it is often completely shielded to avoid radiation losses).

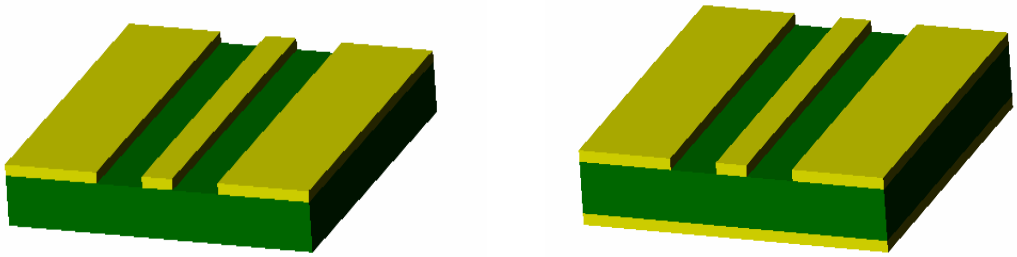

(a) (b)

Figure 3-8 The coplanar line

(a) Without ground plane, (b) With ground plane

The Coplanar line in Figure 3-8 has a ground plane on each side of the signal strip on top of the dielectric, and may have a ground plane at the bottom (Figure 3-8b).

The coplanar structure is good for mounting active devices due to the proximity of the ground and signal line. A deep air filled coplanar transmission line will be demonstrated and discussed later in Chapter 6.

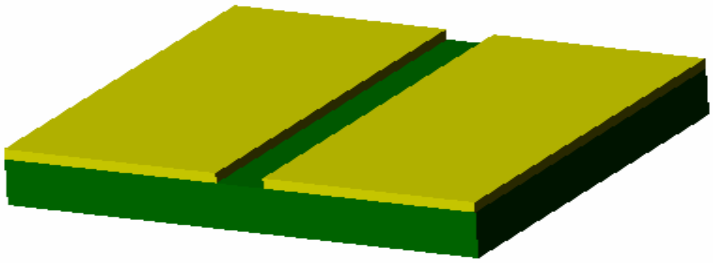

Figure 3-9 Slotline

The slotline in Figure 3-9 also has the advantage of mounting active devices due to the proximity of the signal and ground strips, however, the main disadvantage is that it is relatively lossy.

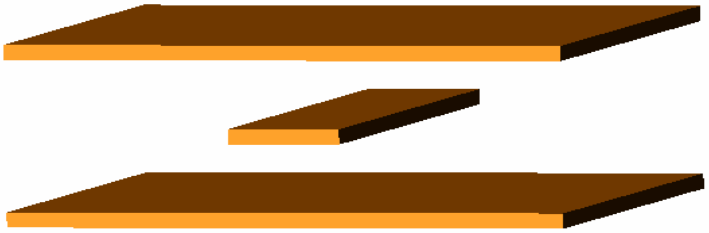

Figure 3-10 Stripline

The stripline in Figure 3-10 has two parallel ground planes with a strip in the middle. Propagation is pure TEM, and it is similar to a coaxial cable. The centre strip can be supported by a thin dielectric and the two ground planes can be confined in a box, making it a low loss structure.

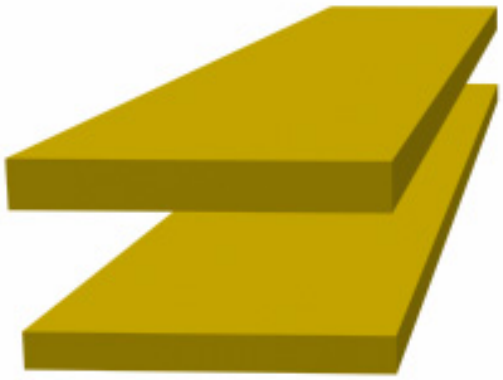

Figure 3-11 Parallel plate waveguide

The parallel plate waveguide in Figure 3-11 consists of two parallel conducting plates. The strip width is assumed to be much greater than the separation between the plates, and it is generally too large to use in typical circuits. In Chapter 6 a parallel plate waveguide made out of aluminium will be discussed.

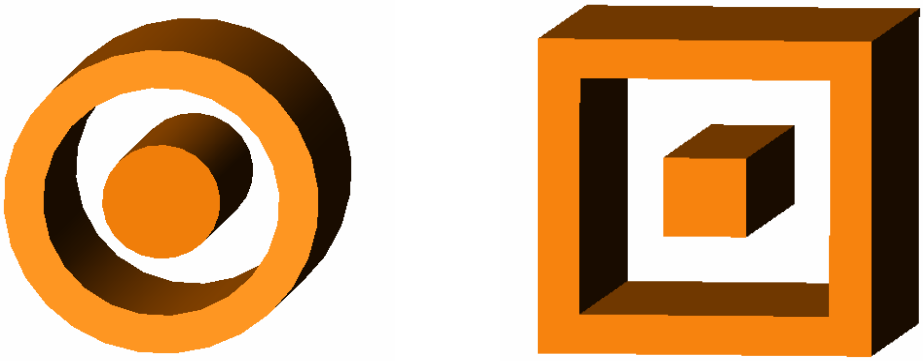

(a) (b)

Figure 3-12 Coaxial line
(a) Round coaxial (b) Square coaxial

The coaxial line in Figure 3-12a is widely used in microwave engineering; it is a low loss transmission line. It consists of a central conductor with an outer shielding. The square coaxial transmission line in Figure 3-12b is the main structure of this thesis, and will be discussed in detail in Chapters 6 and 7, where the square coaxial transmission

line shows an outstanding performance and provides a good way of making low loss microwave filters and resonators.

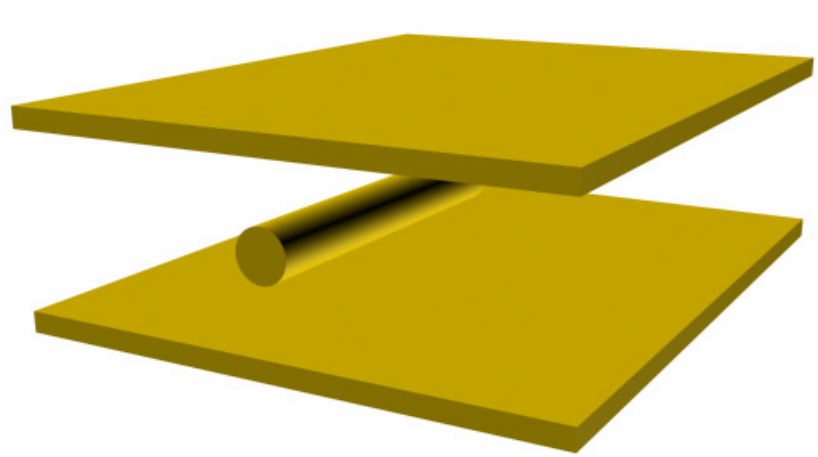

Figure 3-13 Slabline

The slabline in Figure 3-13 has a similar structure to the stripline in Figure 3-10. It consists of three conductors; the round centre conductor will give a better current distribution than the stripline.

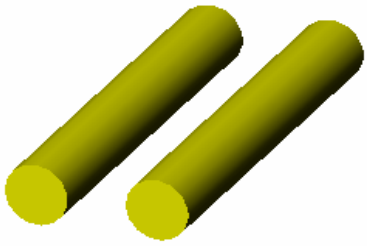

Figure 3-14 Two wires

The two wire transmission line in Figure 3-14 is used mainly at the lower frequencies over short distances. Its main disadvantage is that it tends to radiate energy; enclosing the conductors with a shield could solve this problem.

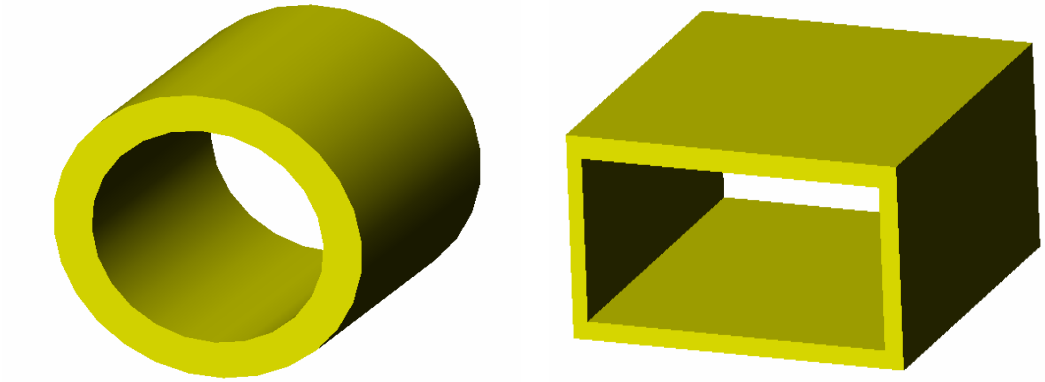

(a) (b)

Figure 3-15 Waveguide
(a) Circular waveguide (b) Rectangular waveguide

The waveguide in Figure 3-15 is a hollow metal tube that has high power capability. It was extensively used in the early days of microwave engineering, and it has some clear disadvantages like weight, cost, and size. It also has a limited bandwidth.

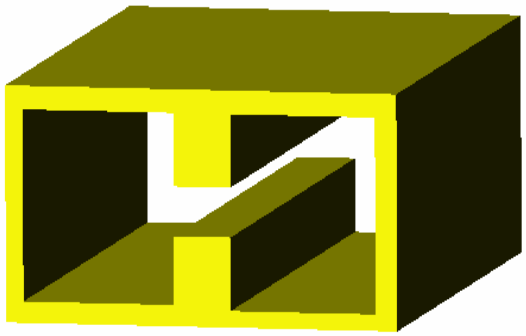

Figure 3-16 Ridge waveguide

The ridge waveguide in Figure 3-16 is a rectangular waveguide with two ridges on the top and bottom conductor. It can also have just one ridge in just one of the conductors. These ridges broaden the bandwidth, over the rectangular waveguide, and give better characteristic impedances. This makes it suitable for impedance matching purposes, the introduction of the ridges reduces the power handling of the waveguide.

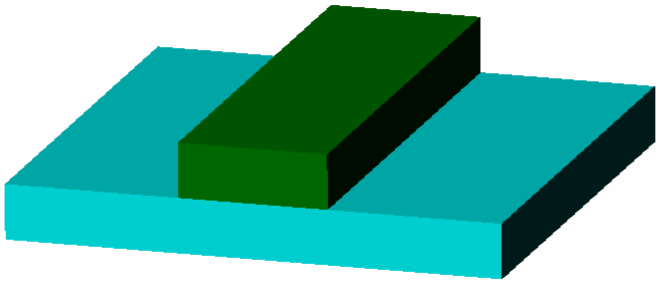

Figure 3-17 Dielectric waveguide

The dielectric waveguide in Figure 3-17 has no metal conductors. It consists of two dielectrics bounded together. The dielectric constant of the strip is greater than the substrate beneath it. It is small in size, which makes it useful at millimetre waves and optical frequencies. It can be very lossy at bends or junctions.

3.6 CONCLUSIONS

In this chapter a review of the lumped element model of a transmission line was carried out, which will be useful, and is directly related to other lumped models used in Chapters 4 and 5. Out of this model the propagation constant was derived. The propagation constant was also derived from the electromagnetic propagation point of view; this result will be useful for the derivation of the skin depth and the surface resistance in Chapter 4.

Standing waves were discussed, and the result for the input impedance of a low loss transmission line terminated in an open circuit was derived. This will be used to extract the unloaded quality factor of a half wavelength resonator in Chapter 4.

The final part of this chapter has the objective of illustrating different microwave transmission lines.

3.7 REFERENCES

[3-1] C.W. Davidson, "Transmission lines for communications", *MacMillan Education Ltd*, 1992

[3-2] D.M. Pozar, "Microwave engineering", *John Wiley and Sons Inc.*, 1998

[3-3] D.M.Pozar, "Microwave and RF design of wireless systems", *John Wiley and Sons Inc*., 2001

[3-4] C.R. Paul *et al.* "Introduction to electromagnetic fields", *McGraw Hill Co.*1998

[3-5] P.A. Rizzi, "Microwave engineering passive circuits", *Prentice Hall Inc.* 1988

[3-6] K.F. Sander & G.A.L. Reed, "Transmission and propagation of electromagnetic waves", *Cambridge University Press*, 1986

[3-7] J.C. Slater, "Microwave transmission", *McGraw Hill Co*., 1942

[3-8] S.R. Pennock & P.R. Shepherd, "Microwave engineering with wireless applications", *MacMillan Press Ltd*, 1998

[3-9] F.R. Connor, "Waves", *Edward Arnold*, 1992

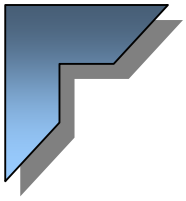

CHAPTER FOUR
MICROWAVE RESONATORS

4.1. INTRODUCTION

In this chapter, resonator theory is reviewed; the theory used in this chapter can be found in references [3-2] to [3-5], [3-8] and from [4-1] to [4-9]. In section 4.2 lumped element resonant circuits are analysed, since the operation of microwave distributed element resonators can be explained with the help of these circuits. In section 4.3 the unloaded quality factor for a half wavelength distributed element resonator will be derived. In section 4.4 material losses will be considered, especially the conductor loss, since the main structures of this thesis are conductor loss limited transmission lines. In section 4.5 a practical way of extracting the unloaded quality factor directly from experimental measurements is presented. Finally, in section 4.6 the unloaded quality factor for different square coaxial cross sections will be presented, as

well as a conclusion on the higher modes propagating throughout the square coaxial line.

4.2. THE UNLOADED QUALITY FACTOR

In this section, the unloaded quality factor Q_O will be derived for a series and parallel resonant circuit. The unloaded quality factor is a very important parameter when designing microwave filters. A higher Q_O means a lower insertion loss and better out of passband rejection characteristics in the filter response. The resistance R in the circuits represents the loss of the resonators.

4.2.1. SERIES RESONANCE

A lumped element series resonant circuit is shown in Figure 4-1

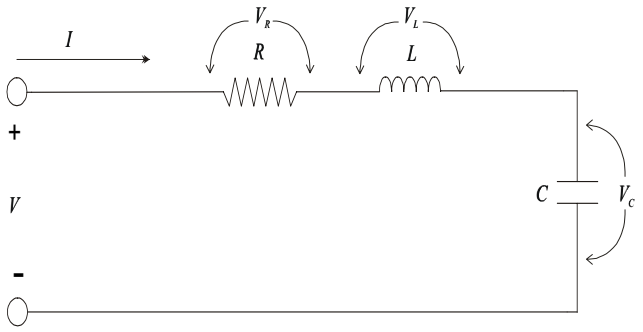

Figure 4-1 Series resonant circuit

The input impedance is

$$Z_{in} = R + j\omega L - j\frac{1}{\omega C} \qquad \text{eq 4-1}$$

The resonant condition in the circuit is when the inductive reactance cancels the capacitive reactance, so the resonant frequency ω_o is

$$\omega_o L = \frac{1}{\omega_o C} \quad \text{or} \quad \omega_o = \frac{1}{\sqrt{LC}} \qquad \text{eq 4-2}$$

At resonance the input impedance from eq 4-1 is purely resistive. If the current and voltage are known at the input of the resonant circuit, then the complex power delivered to the resonator P_{in} is one half of the product of the voltage and the conjugate of the current, so

$$P_{in} = \frac{1}{2} V I^* = \frac{1}{2} |I|^2 Z_{in} \qquad \text{eq 4-3}$$

$$P_{in} = \frac{1}{2} |I|^2 \left(R + j\omega L - j\frac{1}{\omega C} \right) \qquad \text{eq 4-4}$$

So the power dissipated by the resistor is

$$P_R = \frac{1}{2} R |I|^2 \qquad \text{eq 4-5}$$

The energy stored in the capacitor is

$$W_C = \frac{1}{2} C V_C^{\,2} \qquad \text{eq 4-6}$$

And the average electric energy stored in the capacitor under a sinusoidal voltage is

$$W_{C_{av}} = \frac{1}{4} C |V_C|^2 = \frac{1}{4} |I|^2 \frac{1}{\omega^2 C} \qquad \text{eq 4-7}$$

The energy stored in the inductor is

$$W_L = \frac{1}{2} L I^2 \qquad \text{eq 4-8}$$

And the average magnetic energy stored in the inductor under a sinusoidal current is

$$W_{L_{av}} = \frac{1}{4} L |I|^2 \qquad \text{eq 4-9}$$

The unloaded quality factor for the resonant circuit, is defined as the ratio of the energy stored in the resonant circuit to the power loss in the resonant circuit at the resonant frequency, such that

$$Q_O = \omega_o \frac{W_{c_{av}} + W_{L_{av}}}{P_R} \qquad \text{eq 4-10}$$

We can obtain the unloaded quality factor for the series resonant circuit, and as $W_C = W_L$ at resonance eq 4-10 becomes

$$Q_O = \frac{\omega_o L}{R} = \frac{1}{\omega_o RC} \qquad \text{eq 4-11}$$

4.2.2 PARALLEL RESONANCE

A lumped element parallel resonant circuit is shown in Figure 4-2

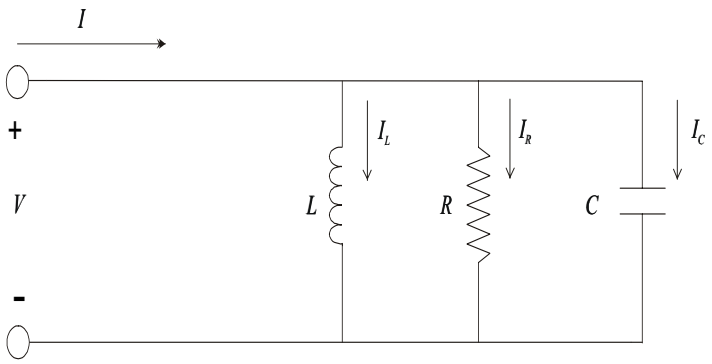

Figure 4-2 Parallel resonant circuit

The input impedance is

$$Z_{in} = \left(\frac{1}{R} + \frac{1}{j\omega L} + j\omega C \right)^{-1} \qquad \text{eq 4-12}$$

As in the series resonant circuit, the resonant condition in the circuit is when the inductive reactance cancels the capacitive reactance, so the resonant frequency ω_o is

$$\omega_o = \frac{1}{\sqrt{LC}} \qquad \text{eq 4-13}$$

So at resonance the input impedance from eq 4-12 is purely resistive. Now the complex power delivered to the resonator is

$$P_{in} = \frac{1}{2} V I^* = \frac{1}{2} V \left(\frac{V}{Z_{in}} \right)^* = \frac{1}{2} |V|^2 \left(\frac{1}{Z_{in}^*} \right) \qquad \text{eq 4-14}$$

$$P_{in} = \frac{1}{2} |V|^2 \left(\frac{1}{R} + \frac{j}{\omega L} - j\omega C \right) \qquad \text{eq 4-15}$$

So the power dissipated by the resistor is

$$P_R = \frac{1}{2}\frac{|V|^2}{R} \qquad \text{eq 4-16}$$

The average electric energy stored in the capacitor is

$$W_{C_{av}} = \frac{1}{4}|V|^2 C \qquad \text{eq 4-17}$$

And the average magnetic energy stored in the inductor is

$$W_{L_{av}} = \frac{1}{4}|I_L|^2 L = \frac{1}{4}|V|^2 \frac{1}{\omega^2 L} \qquad \text{eq 4-18}$$

From eq 4-10 we can find the unloaded quality factor for the parallel resonant circuit, remembering that $W_C = W_L$ at resonance yields

$$Q_O = \frac{R}{\omega_o L} = \omega_o RC \qquad \text{eq 4-19}$$

4.3. UNLOADED QUALITY FACTOR OF A HALF WAVELENGTH TRANSMSISSION LINE RESONATOR

By using the input impedance for an open circuited line eq 3-44, and the following identity

$$\tanh(\theta + j\phi) = \frac{\tanh\theta + j\tan\phi}{1 + j\tan\phi\tanh\theta} \qquad \text{eq 4-20}$$

The input impedance for an open circuited line of length l can be written as

$$Z_{in} = Z_O \frac{1 + j \tan \beta l \tanh \alpha l}{\tanh \alpha l + j \tan \beta l} \qquad \text{eq 4-21}$$

Considering ω near resonance

$$\omega = \omega_o + \Delta\omega \qquad \text{eq 4-22}$$

Where $\Delta\omega$ is small. Using eq 3-70 and eq 4-22, results in

$$\beta l = \frac{\omega_o l}{V_p} + \frac{\Delta\omega l}{V_p} \qquad \text{eq 4-23}$$

The length of a half wavelength transmission line resonator for $\omega=\omega_o$ can be written as

$$l = \frac{\lambda}{2} = \frac{\pi V_p}{\omega_o} \qquad \text{eq 4-24}$$

This result can be verified by substituting eq 3-14 and eq 3-70 into eq 4-24. Substituting eq 4-24 into eq 4-23, results in

$$\beta l = \pi + \frac{\Delta\omega\pi}{\omega_o} \qquad \text{eq 4-25}$$

Now

$$\tan \beta l = \tan\left(\pi + \frac{\Delta\omega\pi}{\omega_o}\right) = \tan \frac{\Delta\omega\pi}{\omega_o} \approx \frac{\Delta\omega\pi}{\omega_o} \qquad \text{eq 4-26}$$

The transmission line is assumed to have a small loss such that $\alpha l << 1$, so

$$\tanh \alpha l \approx \alpha l \qquad \text{eq 4-27}$$

By substituting eq 4-26 and eq 4-27 into eq 4-21 results in

$$Z_{in} = Z_O \frac{1 + j\frac{\Delta\omega\pi}{\omega_o}\alpha l}{\alpha l + j\frac{\Delta\omega\pi}{\omega_o}} \qquad \text{eq 4-28}$$

The second term in the numerator is small, namely

$$\frac{\Delta\omega\pi}{\omega_o}\alpha l << 1 \qquad \text{eq 4-29}$$

So the input impedance can be found by

$$Z_{in} \approx \frac{Z_O}{\alpha l + j\frac{\Delta\omega\pi}{\omega_o}} \qquad \text{eq 4-30}$$

Now the input impedance for a parallel resonant circuit eq 4-12 will be compared to the input impedance of a half wavelength transmission line resonator eq 4-30, for this, near resonance eq 4-12 can be rewritten using the result that [3-2]

$$\frac{1}{1+x} \approx 1 - x + \ldots \qquad \text{eq 4-31}$$

Now using eq 4-22 and eq 4-13, the input impedance for the parallel resonant circuit eq 4-12 results in [4-5]

$$Z_{in} \approx \left(\frac{1}{R} + \frac{1 - \frac{\Delta\omega}{\omega_o}}{j\omega_o L} + j\omega_o C + j\Delta\omega C \right)^{-1} \quad \text{eq 4-32}$$

$$Z_{in} \approx \left(\frac{1}{R} + j\frac{\Delta\omega}{\omega_o^{\,2} L} + j\Delta\omega C \right)^{-1} \quad \text{eq 4-33}$$

$$Z_{in} \approx \left(\frac{1}{R} + 2j\Delta\omega C \right)^{-1} \quad \text{eq 4-34}$$

$$Z_{in} \approx \frac{R}{1 + 2j\Delta\omega RC} \quad \text{eq 4-35}$$

By comparing eq 4-30 and eq 4-35, the resistance of the equivalent *RLC* circuit for the half wavelength resonator is given by

$$R = \frac{Z_O}{\alpha l} \quad \text{eq 4-36}$$

Similarly the capacitance of the equivalent *RLC* circuit for the half wavelength resonator is

$$C = \frac{\pi}{2\omega_o Z_O} \quad \text{eq 4-37}$$

And the inductance of the equivalent *RLC* circuit for the half wavelength resonator is

$$L = \frac{1}{\omega_o^{\,2} C} \quad \text{eq 4-38}$$

Finally the unloaded quality factor for the half wavelength transmission line resonator can be calculated by using eq 4-19 and eq 4-37

$$Q_O = \omega_o RC = \frac{\pi}{2\alpha l} = \frac{\beta}{2\alpha} \qquad \text{eq 4-39}$$

4.4. MATERIAL LOSSES

In this section, the losses due to the materials used to form transmission line resonators will be presented.

Ampere's law for sinusoidal signals in the lossless dielectric case (σ=0), can be written as

$$\nabla \times \hat{H} = j\omega\varepsilon\hat{E} \qquad \text{eq 4-40}$$

If we include losses, $\sigma \neq 0$, the expression can be written as

$$\nabla \times \hat{H} = (\sigma + j\omega\varepsilon)\hat{E} \qquad \text{eq 4-41}$$

$$\nabla \times \hat{H} = j\omega\varepsilon\left(1 - j\frac{\sigma}{\omega\varepsilon}\right)\hat{E} \qquad \text{eq 4-42}$$

Comparing Ampere's law for both cases, we can see that the losses can be included into the lossless case by replacing ε with a complex permittivity given by

$$\hat{\varepsilon} = \varepsilon\left(1 - j\frac{\sigma}{\omega\varepsilon}\right) \qquad \text{eq 4-43}$$

Where the term in the right hand side of the parenthesis is referred as the loss tangent of the material, namely

$$\tan\delta = \frac{\sigma}{\omega\varepsilon} \qquad \text{eq 4-44}$$

The loss tangent arises from the two components of current involved in Ampere's law, a conduction current density

$$\hat{J}_c = \sigma\hat{E} \qquad \text{eq 4-45}$$

And a displacement current density

$$\hat{J}_d = j\omega\varepsilon\hat{E} \qquad \text{eq 4-46}$$

The ratio of these two currents is the measure of the lossy nature of the material, so Ampere's law can written as

$$\nabla \times \hat{H} = \hat{J}_c + \hat{J}_d \qquad \text{eq 4-47}$$

$$\hat{J}_{total} = \hat{J}_c + \hat{J}_d \qquad \text{eq 4-48}$$

The conduction and displacement current are 90° out of time phase. In Figure 4-3, a plot of the conduction and displacement current is shown in the complex plane.

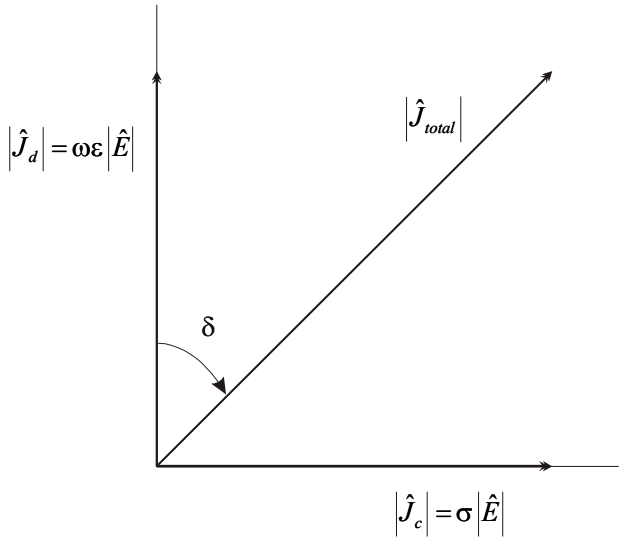

Figure 4-3 Loss tangent

The loss tangent is related to the conduction current density and the displacement current density from Figure 4-3 as

$$\tan\delta = \frac{\left|\hat{J}_c\right|}{\left|\hat{J}_d\right|} = \frac{\sigma}{\omega\varepsilon} \qquad \text{eq 4-49}$$

Materials can be classified according to whether the conduction current is much larger than the displacement current, which corresponds to a good conductor eq 4-50, or whether the displacement current is much larger than the conduction current, which corresponds to a good dielectric eq 4-51.

$$\frac{\sigma}{\omega\varepsilon} >> 1 \quad \text{good conductor} \qquad \text{eq 4-50}$$

$$\frac{\sigma}{\omega\varepsilon} << 1 \quad \text{good dielectric} \qquad \text{eq 4-51}$$

The expressions of the attenuation constant due to dielectrics are a function of the loss tangent of the material.

4.4.1 CONDUCTOR LOSS

Rearranging terms from the propagation constant eq 3-62, we obtain

$$\gamma = \sqrt{j\omega\mu\sigma\left(1 + j\frac{\omega\varepsilon}{\sigma}\right)} \qquad \text{eq 4-52}$$

Since for a good conductor we have the condition stated in eq 4-50, the propagation constant for a good conductor becomes

$$\gamma \approx \sqrt{j\omega\mu\sigma} = \sqrt{\omega\mu\sigma}\angle 45^\circ \qquad \text{eq 4-53}$$

So that

$$\alpha = \beta \approx \sqrt{\frac{\omega\mu\sigma}{2}} \qquad \text{eq 4-54}$$

The electric field for a forward travelling wave can be written as

$$\overline{E} = E_m e^{-\alpha z}\cos(\omega t - \beta z)a_x \qquad \text{eq 4-55}$$

Where E_m is the magnitude of the field, and a_x. is the unit vector in the x direction in Figure 4-4. As the wave travels through the material, its amplitude will be attenuated by the factor $e^{-\alpha z}$, now the skin depth δ is the distance over which the current density falls to 1/e or 37% of its initial value, so

$$\delta_s = \frac{1}{\alpha} \qquad \text{eq 4-56}$$

Substituting the relation for the attenuation constant α for a good conductor given in eq 4-54, the skin depth becomes

$$\delta_s = \sqrt{\frac{2}{\omega\mu\sigma}} = \frac{1}{\sqrt{\pi f \mu\sigma}} \qquad \text{eq 4-57}$$

As seen from the formula, as frequency increases, the skin depth becomes smaller; the units of the skin depth are meters. In practice, metals of several skin depths are used to form microwave circuits.

Now the skin effect resistance will be derived, which will be used extensively in Chapter 6. First consider the section of the conductor in Figure 4-4, where the current density decreases in the *x* direction

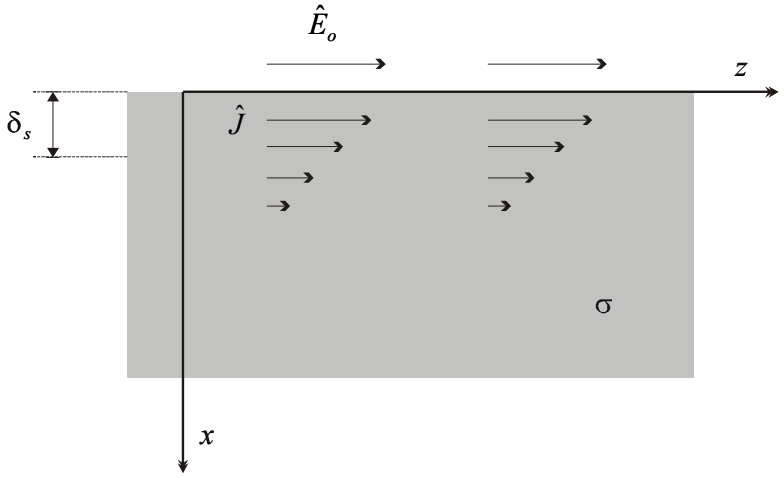

Figure 4-4 Section of a conductor illustrating the decay of current

By using the propagation constant in eq 4-52, for a good conductor eq 4-50 results in

$$\gamma = \sqrt{j\omega\mu\sigma} \qquad \text{eq 4-58}$$

And the wave equation for the electric field, from eq 3-66, becomes

$$\frac{d^2\hat{E}_z}{dx^2} = \gamma^2 \hat{E}_z \qquad \text{eq 4-59}$$

Since the current density and the electric field are related by the conductivity of the conductor, eq 4-59 also relates the current density, so

$$\frac{d^2\hat{J}_z}{dx^2} = \gamma^2 \hat{J}_z \qquad \text{eq 4-60}$$

The solution to differential equation eq 4-60, is of the form

$$\hat{J}_z = C_1 e^{-\gamma x} + C_2 e^{\gamma x} \qquad \text{eq 4-61}$$

The second term of eq 4-61 is discarded (otherwise, the current density would be increasing in the *x* direction) the current density in Figure 4-4 decreases exponentially into the conductor as

$$\hat{J}_z = \hat{J}_o e^{-\frac{x}{\delta_s}} e^{-j\frac{x}{\delta_s}} \qquad \text{eq 4-62}$$

The total current per unit width in the *y* direction, which is pointing into the page in Figure 4-4, is

$$\hat{I}_z = \int_0^\infty \hat{J}_z dx = \frac{J_o \delta_s}{1+j} \qquad \text{eq 4-63}$$

At x=0 we find that

$$\hat{J}_o = \sigma \hat{E}_o \qquad \text{eq 4-64}$$

The impedance per unit length and per unit width is

$$\hat{Z}_s = \frac{\hat{E}_o}{\hat{I}_z} \qquad \text{eq 4-65}$$

By substituting eq 4-63 and eq 4-64 into eq 4-65, we obtain

$$\hat{Z}_s = \frac{1+j}{\sigma\delta_s} \qquad \text{eq 4-66}$$

Where the units of Z_s are in Ohms, now we define the impedance as

$$\hat{Z}_s = R_s + j\omega L_i \qquad \text{eq 4-67}$$

From eq 4-66 and eq 4-67, it is possible to identify the slab's resistance and its internal inductance per unit width and length as

$$R_s = \frac{1}{\sigma\delta_s} \qquad \text{eq 4-68}$$

$$\omega L_i = \frac{1}{\sigma\delta_s} \qquad \text{eq 4-69}$$

So the block of conducting material in Figure 4-4, that has infinite depth in the *x* direction and a surface area of 1m^2, will have the impedance of eq 4-68 and eq 4-69, with units of Ohms per square.

4.5. EXTRACTING Q FROM MEASUREMENTS

The quality factor is defined in terms of the energy stored and the energy lost at the resonant frequency. Considering the resonant cavity in Figure 4-5

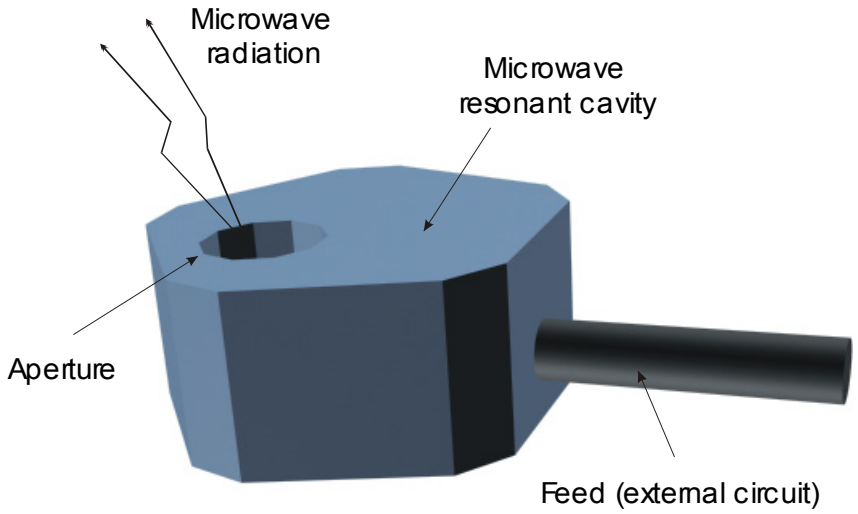

Figure 4-5 Microwave resonant cavity

It is possible to define three different quality factors for a loaded resonator, depending on which loss is being considered, namely,

$$Q_l = \omega_o \frac{\text{energy stored in the resonant circuit}}{\text{total power loss}} \qquad \text{eq 4-70}$$

$$Q_O = \omega_o \frac{\text{energy stored in the resonant circuit}}{\text{power loss in the resonant circuit}} \qquad \text{eq 4-71}$$

$$Q_e = \omega_o \frac{\text{energy stored in the resonant circuit}}{\text{power loss in the external circuit}} \qquad \text{eq 4-72}$$

The three expressions in eq 4-70, eq 4-71 and eq 4-72 are evaluated at the resonant frequency. The loaded quality factor Q_l, depends on the degree of coupling between the resonant circuit and the external circuit. The unloaded quality factor Q_O is a measure of the losses of the resonant circuit; a lower loss implies a higher Q_O. The

external quality factor Q_e is related to the degree to which the resonant circuit is coupled to the external circuits. The three quality factors are related in the following way

$$\frac{1}{Q_l} = \frac{1}{Q_e} + \frac{1}{Q_O} \qquad \text{eq 4-73}$$

When designing a transmission line resonator, some power may not be available in the load, which was not caused by material losses, or an impedance mismatch at the ports of the device. This power may be lost as a result of radiation losses. These losses mainly depend on the physical structure of the transmission line. When the transmission line uses semiconductors, leakage losses must be taken into account. Leakage losses are normally present in dielectrics having finite resistivity, such as the case of semiconductors.

The losses present in the resonant circuit can be conductor losses Q_c, dielectric losses Q_d, radiation losses Q_r, or leakage losses Q_k. The unloaded quality factor for a resonant circuit can be calculated by adding these losses, resulting in

$$\frac{1}{Q_O} = \frac{1}{Q_c} + \frac{1}{Q_d} + \frac{1}{Q_r} + \frac{1}{Q_k} \qquad \text{eq 4-74}$$

Next, a practical method to extract the unloaded quality factor from the measurements of a loaded resonator will be described [4-6] [4-7]. First, consider a symmetrically loaded resonator. The resonator's typical transmission response is shown in Figure 4-6

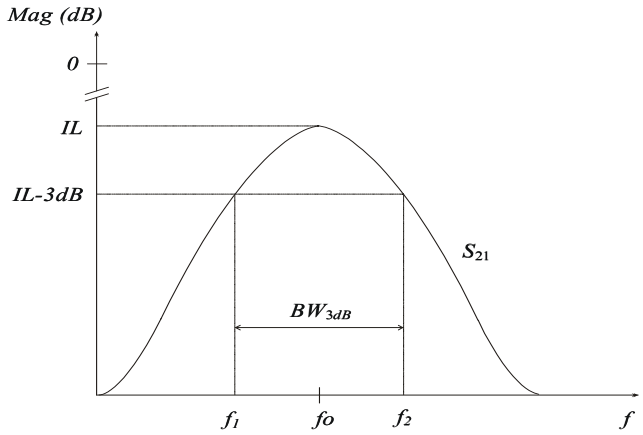

Figure 4-6 Frequency response of a single resonator

Directly from the measurement the loaded quality factor is given by

$$Q_l = \frac{fo}{BW_{3dB}} = \frac{fo}{f_2 - f_1} \qquad \text{eq 4-75}$$

Where BW_{3dB} is the bandwidth taken at $3dB$ as illustrated in Figure 4-6. Now the unloaded quality factor can be extracted by

$$Q_o = \frac{Q_l}{1 - |S_{21}|} \qquad \text{eq 4-76}$$

Where $|S_{21}|$ is the absolute magnitude of S_{21} at the resonant frequency fo, namely

$$|S_{21}| = 10^{\frac{IL}{20}} \qquad \text{eq 4-77}$$

It is desired to weakly couple the resonator to the external circuit in order to obtain an $IL > -20\ dB$, so that $Q_l \approx Q_o$.

4.6. FINDING Q_O USING CAD

This section describes a way of finding the Q_O of a transmission line resonator, and to do this, the example of a square coaxial transmission line resonator will be used. The calculations performed in this section were done with the aid of a 3D CAD simulator [4-10], in which different square coaxial transmission line resonators were simulated. All of them have the same resonant frequency and the differences between them is the cross section of the square coaxial line used to form a half wavelength resonator.

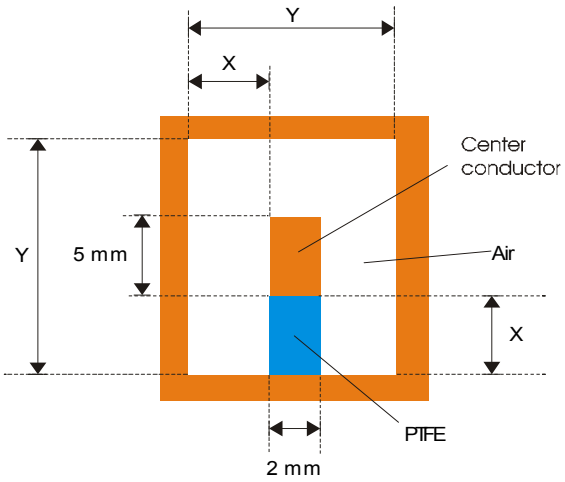

Figure 4-7 Cross section of a square coaxial resonator

The square coaxial transmission line in Figure 4-7 is used to compute the Q_O for the different cross sections by varying the distance Y, and the resonators are adjusted to resonate at 9 GHz. The properties of the materials used in the simulations are as follows, the loss tangent of the PTFE is 0.001 with a dielectric constant of 2.1, and the conductivity used for the copper is 5.8×10^7 S/m.

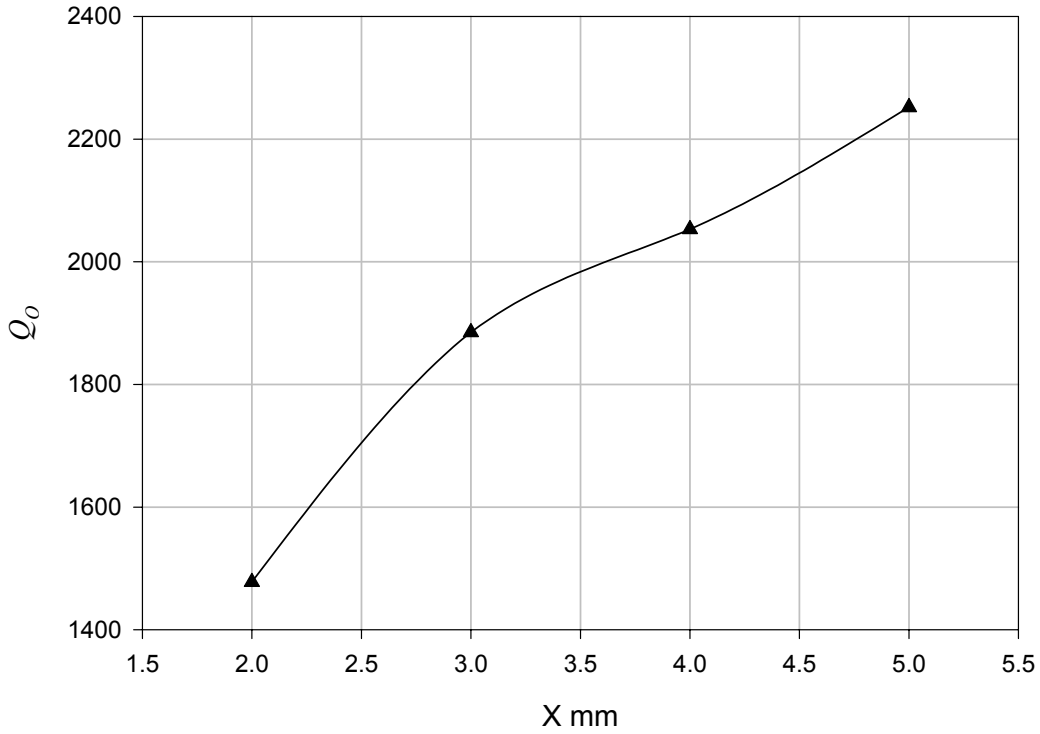

Figure 4-8 Square coaxial resonator Q_O

The simulated results for Q_O are shown on Figure 4-8. The graph clearly indicates that a higher Q_O is obtained by making the cross section bigger, but there is a very important issue to consider here. By changing the cross section's dimensions, higher order modes will begin to propagate beyond a certain frequency. In Figure 4-9 we can observe on the y axis, the frequency at which the higher modes begin to propagate for the different cross section dimensions.

It is desired to propagate a TEM mode through the coaxial transmission line, which is the lowest order mode in a coaxial line; higher order (TE and TM) modes can also exist [4-11]. Normally, the line is designed in such a way that the cutoff frequencies of the higher order modes are well above the operating frequency.

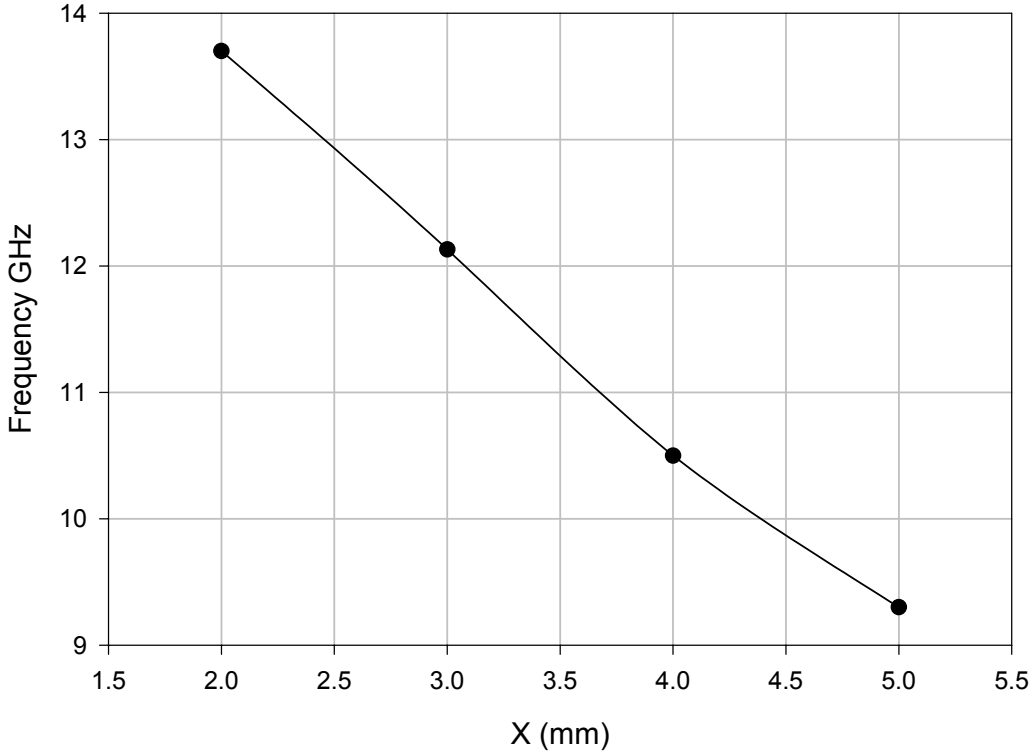

Figure 4-9 Presence of higher modes in a square coaxial transmission line

The consequence of deciding at which frequency the higher order modes should propagate is crucial for the filter design. They should and will be placed out of the desired passband in all the filter designs of Chapter 7. The higher modes will not be studied further in this thesis, since the main interest is to propagate a TEM mode only through the structure.

4.7. CONCLUSIONS

In this chapter, the unloaded quality factor for a half wavelength transmission line resonator was introduced. This result will be used as a measure of the losses involved in the resonators that will be compared in Chapter 6, and the resonators that compose the filters of Chapter 7.

The lumped element resonant circuits presented in this chapter will be extensively used in the filter theory of Chapter 5, as well as to make calculations of the losses directly from the measured responses of the filters of Chapter 7, although this procedure will be further explained in Chapter 5.

Material losses were also introduced in this chapter. The surface resistance will be used to make the analytical calculations of the attenuation constant due to conductor loss, and the unloaded quality factor for different half wavelength resonators will be described and compared in Chapter 6.

The way of extracting the unloaded quality factor from measurements, will be the method used to make calculations of the different fabricated resonators presented in Chapter 6.

Finally the unloaded quality factor for a square coaxial transmission line was presented, including a discussion on higher modes in coaxial lines.

4.8. REFERENCES

[4-1] M.J. Lancaster, "Passive microwave device applications of high temperature superconductors", *Cambridge University press,* 1996

[4-2] S. Ramo, J.R. Whinnery and T.Van Duzer, "Fields and waves in communication electronics", *John Wiley and Sons Inc,* 1984

[4-3] J.W. Nilsson, "Electric circuits", *Addison-Wesley publishing company,* 1990

[4-4] J. Carr and J. Davies "Radio and RF engineer's pocket handbook", *Newnes an imprint of Butterworth-Heinemann,* 2000

[4-5] R.E. Collin, "Foundations for microwave engineering", *Mc Graw Hill,* 1992

[4-6] G. Matthaei, L. Young and E.M.T. Jones, "Microwave filters, impedance matching networks and coupling structures", *Artech house Inc,* 1964

[4-7] Jia-Sheng Hong and M.J. Lancaster, "Microstrip filters for RF/Microwave applications", *John Wiley and Sons Inc,* 2001

[4-8] M. Makimoto and S. Yamashita, "Microwave resonators and filters for wireless communication", *Springer-Verlag Berlin Heidelberg,* 2001

[4-9] H.A. Wheeler, "Formulas for the skin effect", *Proc. IRE*., Vol. 30, pp. 412-424, September 1942

[4-10] *Agilent HFSS V 5.5*

[4-11] L. Gruner, "Higher order modes in square coaxial lines", *IEEE transactions on microwave theory and techniques,* Vol. 31, No 9, September 1983.

CHAPTER FIVE
GENERAL FILTER DESIGN

5.1. INTRODUCTION

This chapter contains the theory used to design the filters presented in Chapter 7. These filters have a Chebyshev response. The design procedure for each filter will be shown individually in Chapter 7. The theory used in this Chapter can be found in [4-6] to [4-8].

Section 5.2 contains a discussion of the low pass filter prototype, which will be converted to give a bandpass response in section 5.3; where narrowband coupled resonator filters will be addressed. The rest of section 5.3 contains the theory on how to develop a Chebyschev bandpass filter, touching important issues like the use of impedance and admittance inverters, and a general procedure of calculating the design parameters with the aid of a CAD simulator.

In section 5.4, the design formulae for a wideband bandpass filter using quarter wavelength stubs as resonators, with quarter wavelength transmission lines connecting the resonators, will be presented. This will be used in the design of the filter in Chapter 7, section 7.3. Finally in section 5.5, a method of extracting the unloaded quality factor from experimental filter measurements will be presented; this method uses the lumped element models discussed throughout this chapter in a CAD circuit simulator. This section also contains an important formula that can be used to calculate the insertion loss of a bandpass filter, knowing the unloaded quality factors of the resonant elements composing the filter.

5.2. THE LOW PASS PROTOTYPE

This section describes the lowpass prototype that will be used in the design of the bandpass filters in this thesis; the lowpass prototype can be converted to give highpass, bandpass, or bandstop characteristics. The lowpass filter prototype discussed in this section has the Chebyshev response shown in Figure 5-1

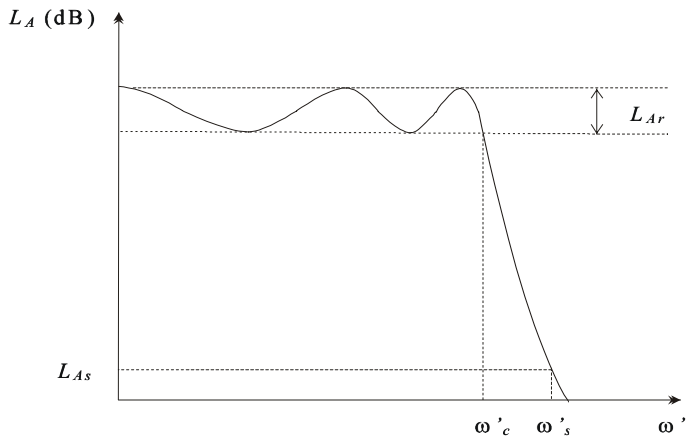

Figure 5-1 Chebyshev low pass prototype response

The Chebyschev response has a ripple L_{Ar} in the passband. And a roll off at the transition to the stopband, which can be specified as a given attenueation L_{As} at a wanted frequency ω'_s. The attenuation characteristics of the Chebyshev low pass prototype may be mathematically specified as [4-6]

$$L_A(\omega) = 10\log_{10}\left[1+\varepsilon\cos^2\left[n\cos^{-1}\left(\frac{\omega'}{\omega'_c}\right)\right]\right] \quad if\ \omega<\omega_c \qquad \text{eq 5-1}$$

$$L_A(\omega) = 10\log_{10}\left[1+\varepsilon\cosh^2\left[n\cosh^{-1}\left(\frac{\omega'}{\omega'_c}\right)\right]\right] \quad if\ \omega\geq\omega_c \qquad \text{eq 5-2}$$

Where n is the number of reactive elements in the low pass prototype filter, and ε is the ripple constant defined by

$$\varepsilon = 10^{\frac{L_{Ar}}{10}} - 1 \qquad \text{eq 5-3}$$

The response in Figure 5-1 can be achieved by the low pass prototype filters shown on Figure 5-2

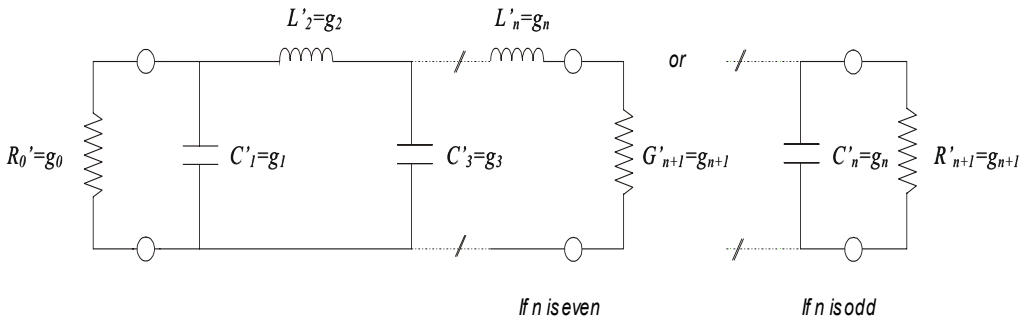

(a)

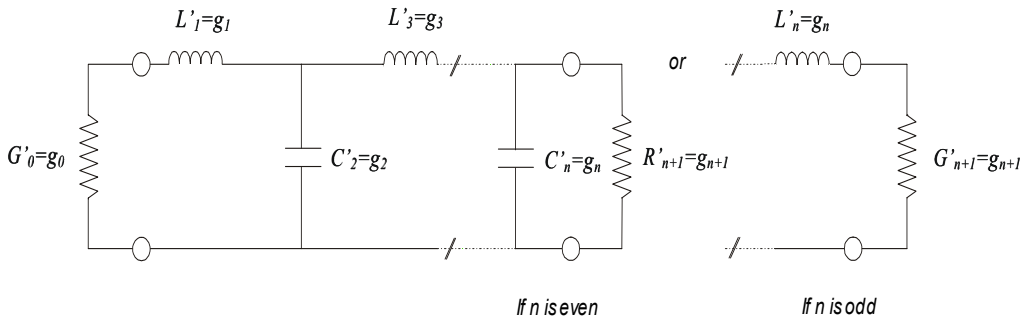

(b)

Figure 5-2 Low pass prototype filer
(a) ladder network structure (b) its dual

Either form in Figure 5-2 will give identical responses. The elements of the low pass filter prototypes are normalized to make g_o=1 and ω'_c=1. The prototypes are changed to other cut off frequencies and impedance levels by the following transformations, for resistances or conductances

$$R = R_0 R' \quad \text{or} \quad G = G_0 G' \qquad \text{eq 5-4}$$

For the capacitances

$$C = \frac{C'}{Ro\omega_c} \quad \text{or} \quad C = \frac{GoC'}{\omega_c} \qquad \text{eq 5-5}$$

And for inductances

$$L = \frac{RoL'}{\omega_c} \quad \text{or} \quad L = \frac{L'}{Go\omega_c} \qquad \text{eq 5-6}$$

In eq 5-4, eq 5-5 and eq 5-6, the elements with the prime are the values of the normalized low pass filter prototype, ω_c is the new cutoff frequency of the filter, and *Ro* or *Go* is the new impedance or conductance for the scaled filter.

The element values for the low pass prototype filters in Figure 5-2 can be computed by using the following formulas [4-7]

$$g_1 = \frac{2}{\gamma}\sin\left(\frac{\pi}{2n}\right) \qquad \text{eq 5-7}$$

$$g_k = \frac{1}{g_{k-1}} \frac{4\sin\left[\frac{(2k-1)\pi}{2n}\right]\sin\left[\frac{(2k-3)\pi}{2n}\right]}{\gamma^2 + \sin^2\left[\frac{(k-1)\pi}{n}\right]} \quad \text{for } k=2,3,\ldots n \qquad \text{eq 5-8}$$

$$g_{n+1} = 1 \qquad \text{if } n \text{ is odd} \qquad \text{eq 5-9}$$

$$g_{n+1} = \coth^2\left(\frac{\beta}{4}\right) \qquad \text{if } n \text{ is even} \qquad \text{eq 5-10}$$

Where

$$\beta = \ln\left[\coth\left(\frac{L_{Ar}}{17.37}\right)\right] \qquad \text{eq 5-11}$$

$$\gamma = \sinh\left(\frac{\beta}{2n}\right) \qquad \text{eq 5-12}$$

The degree of the Chebyschev low pass prototype, or the number of reactive elements in the prototype to meet the minimum stopband attenuation L_{As} at ω'_s as shown on Figure 5-1, for a required bandpass ripple L_{Ar} can be calculated from [4-7]

$$n \geq \frac{\cosh^{-1}\sqrt{\frac{10^{0.1L_{As}}-1}{10^{0.1L_{Ar}}-1}}}{\cosh^{-1}(\omega'_s)} \qquad \text{eq 5-13}$$

5.3. NARROW BAND COUPLED RESONATOR BANDPASS FILTERS

In this section, the low pass prototype in section 5.2 will be transformed to bandpass circuits in section 5.3.1. After this, impedance and admittance inverters will be used to achieve a bandpass circuit having only one kind of resonant element, as discussed in section 5.3.2, which is a useful result to implement a practical distributed element filter. In section 5.3.3, the calculations used to obtain the design parameters and their relation to a practical design are discussed. Finally in section 5.3.4, a general procedure of how to calculate the design parameters for a practical transmission line filter, with the aid of a CAD will be discussed.

5.3.1 BANDPASS TRANSFORMATION

In this section the lowpass prototype presented in section 5.2 will be transformed to give the bandpass response in Figure 5-3

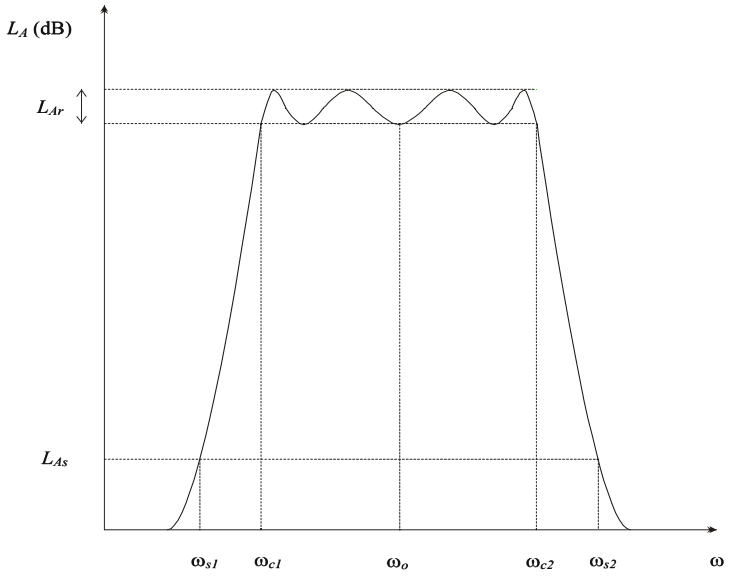

Figure 5-3 Bandpass response

The lowpass prototype filters in Figure 5-2, can related to the bandpass response in Figure 5-3 by a well known lowpass to bandpass mapping as follows [4-6]

$$\frac{\omega'}{\omega'_C} = \frac{1}{\Delta}\left(\frac{\omega}{\omega_o} - \frac{\omega_o}{\omega}\right) \qquad \text{eq 5-14}$$

$$\Delta = \frac{\omega_{c2} - \omega_{c1}}{\omega_o} \qquad \text{eq 5-15}$$

$$\omega_o = \sqrt{\omega_{c2}\omega_{c1}} \qquad \text{eq 5-16}$$

Now the lowpass prototype can be transformed to give the bandpass response in Figure 5-3, as the low pass filter elements are transformed to series and parallel resonant circuits as shown in Figure 5-4, [4-7]

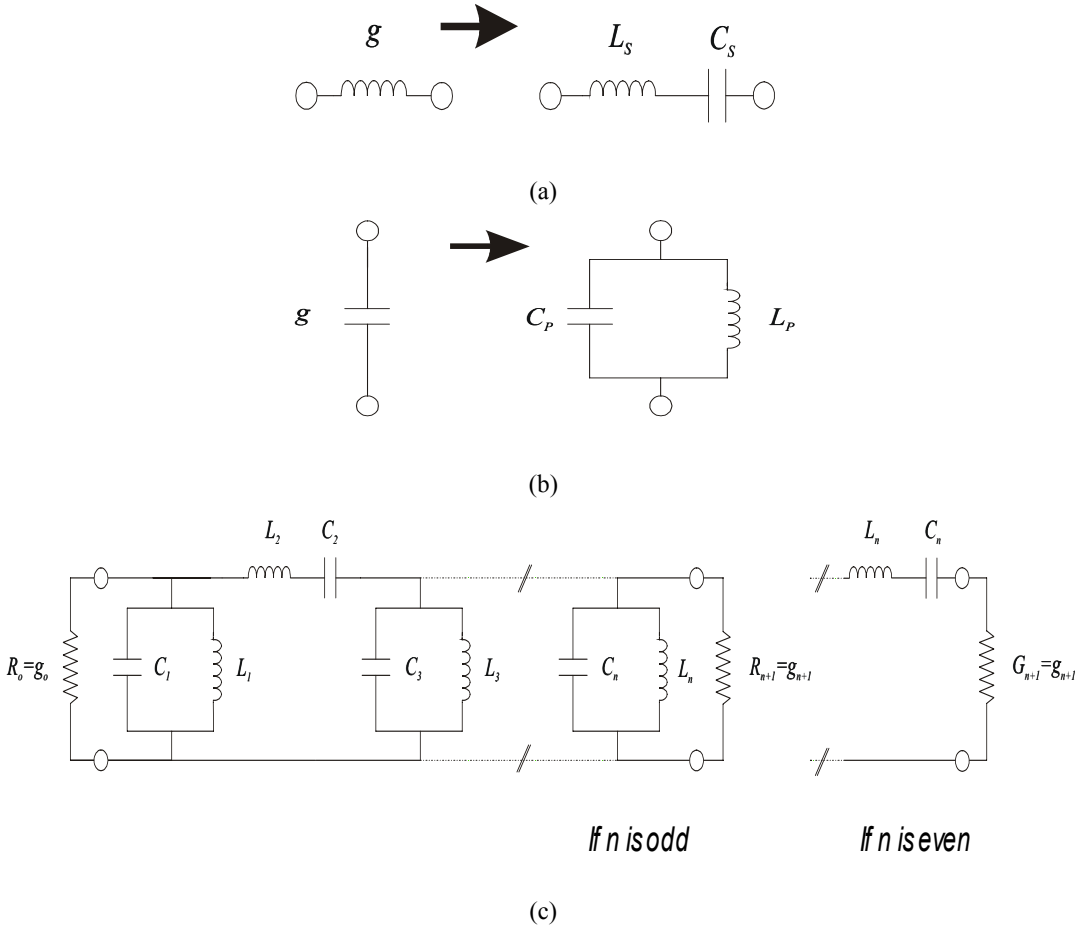

Figure 5-4 Bandpass filter transformation

(a) for a series inductance (b) for a shunt capacitance (c) bandpass filter ladder network

The impedance scaling is independent of the frequency transformation, and can be obtained by multiplying the impedances of the low pass prototype by the new characteristic impedance *Zo*.

A series inductor in the low pass prototype is transformed to a series LC circuit as in Figure 5-4a, with element values given by

$$L_S = \frac{gZo}{\Delta\omega o} \qquad \text{eq 5-17}$$

$$C_S = \frac{\Delta}{g\omega o Zo} \qquad \text{eq 5-18}$$

A shunt capacitor in the low pass prototype is transformed to a parallel LC circuit as in Figure 5-4b with element values given by

$$L_P = \frac{\Delta Zo}{g\omega o} \qquad \text{eq 5-19}$$

$$C_P = \frac{g}{\Delta\omega o Zo} \qquad \text{eq 5-20}$$

5.3.2 FILTERS USING IMPEDANCE OR ADMITTANCE INVERTERS

When designing bandpass filters, it is desirable to convert the low pass prototype that uses both series inductances and shunt capacitances, to an equivalent circuit that will only use series inductances or shunt capacitances. This will make the filter easier to implement. This can be done with an impedance or admittance inverter.

An idealized impedance inverter operates like the quarter wavelength section of transmission line discussed in Chapter 3, section 3.3.1, having an impedance *K* at all frequencies. If such a transmission line is terminated in an impedance *Zb* at one end, the impedance Za seen looking at the other end, from eq 3-37 is

$$Za = \frac{K^2}{Zb} \qquad \text{eq 5-21}$$

Similarly an idealized admittance inverter operates like a quarter wavelength section of a transmission line, with a characteristic admittance *J* at all frequencies. Thus if the transmission line is terminated in an admittance *Yb* on one end, the admittance *Ya* seen looking at the other end is

$$Ya = \frac{J^2}{Yb} \qquad \text{eq 5-22}$$

An impedance or admittance inverter has a phase shift of ±90 degrees or an odd multiple thereof. Because of the inverting action of the impedance and admittance inverters, the circuit conversions shown on Figure 5-5 can be made

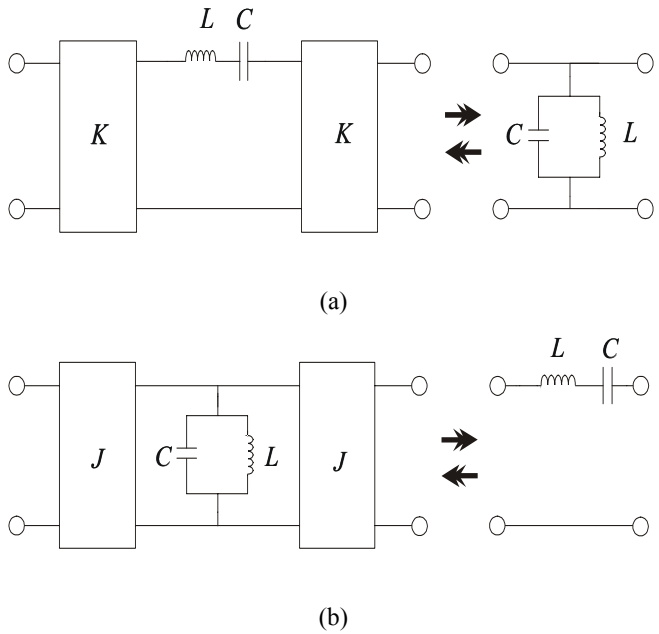

Figure 5-5 Conversions using impedance or admittance inverters
(a) Impedance inverter used to convert a shunt resonator into an equivalent circuit with a series resonance (b) admittance inverter used to convert a series resonator into an equivalent circuit with a shunt resonance

The impedance and admittance inverters used in practical cases are sensitive to frequency, meaning that practical realizations of *J* or *K* inverters are relatively narrowband in nature, so the following equations represent approximations which are best for narrow bandwidths. Good results can be obtained for bandwidths as great as 20% when half wavelength resonators are used, and bandwidths approaching 40% can be obtained when using quarter wavelength resonators [4-6].

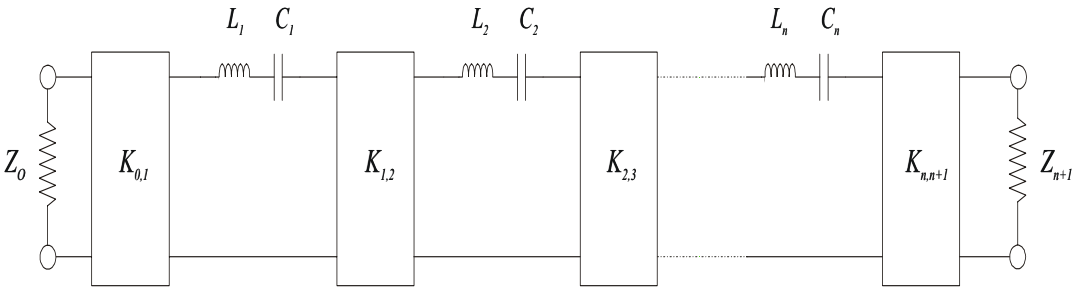

Figure 5-6 Band pass filter using impedance inverters and only series resonators

The *K* inverter values in Figure 5-6 are computed using the following formulas [4-7] [4-6]

$$K_{0,1} = \sqrt{\frac{\chi_1 Z_O \Delta}{g_1}} \qquad \text{eq 5-23}$$

$$K_{j,j+1} = \Delta\sqrt{\frac{\chi_j \chi_{j+1}}{g_j g_{j+1}}} \quad \text{where } j=1 \text{ to } n\text{-}1 \qquad \text{eq 5-24}$$

$$K_{n,n+1} = \sqrt{\frac{\chi_n Z_{n+1} \Delta}{g_n g_{n+1}}} \qquad \text{eq 5-25}$$

Where χ_n is the reactance slope parameter of a series resonator having zero reactance at ω_O, and is given by

$$\chi_n = \omega_O L_n = \frac{1}{\omega_O C_n}$$

Where L_n and C_n are the scaled L and C values from the lowpass prototype g values.

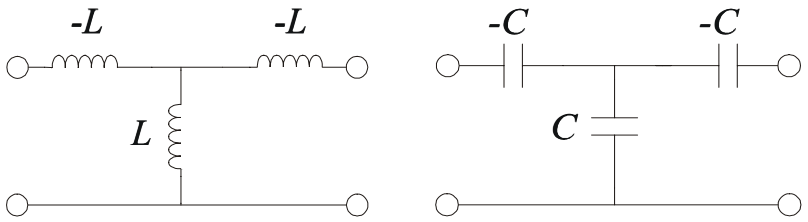

(a) (b)

Figure 5-7 Lumped element impedance inverters

The lumped element impedance inverter K in Figure 5-7 (a) is given by

$$K = \omega L \qquad \text{eq 5-26}$$

And the lumped element impedance inverter K in Figure 5-7 (b) is given by

$$K = \frac{1}{\omega C} \qquad \text{eq 5-27}$$

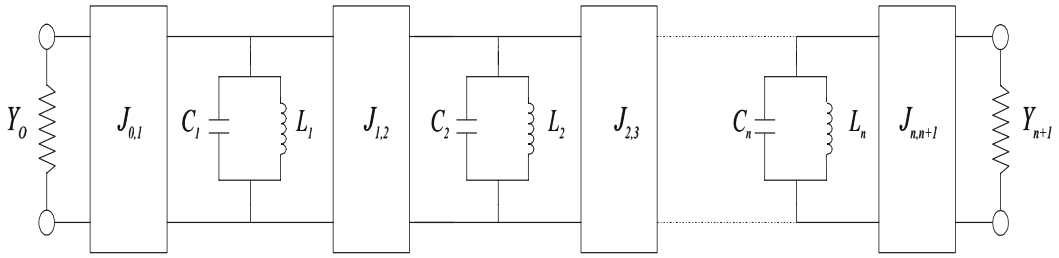

Figure 5-8 Band pass filter using admittance inverters and only shunt resonators

The J inverter values in Figure 5-8 are computed using the following formulas[4-7] [4-6]

$$J_{0,1} = \sqrt{\frac{\vartheta_1 Y_O \Delta}{g_1}} \qquad \text{eq 5-28}$$

$$J_{j,j+1} = \Delta\sqrt{\frac{\vartheta_j \vartheta_{j+1}}{g_j g_{j+1}}} \quad \text{where } j=1 \text{ to } n\text{-}1 \qquad \text{eq 5-29}$$

$$J_{n,n+1} = \sqrt{\frac{\vartheta_n Y_{n+1} \Delta}{g_n g_{n+1}}} \qquad \text{eq 5-30}$$

Where ϑ_n is the susceptance slope parameter of a shunt resonator having zero susceptance at ω_O, and is given by

$$\vartheta_n = \omega_O C_n = \frac{1}{\omega_O L_n} \qquad \text{eq 5-31}$$

Where L_n and C_n are the scaled L and C values from the lowpass prototype g values.

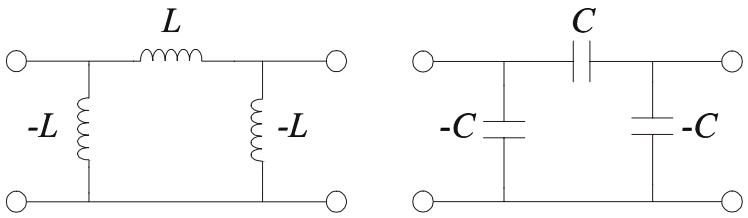

(a) (b)

Figure 5-9 Lumped element admittance inverters

The lumped element admittance inverter J in Figure 5-9 (a) is given by

$$J = \frac{1}{\omega L} \qquad \text{eq 5-32}$$

And the lumped element admittance inverter J in Figure 5-9 (b) is given by

$$J = \omega C \qquad \text{eq 5-33}$$

5.3.3 OBTAINING THE DESIGN PARAMETERS FOR A BANDPASS DISTRIBUTED ELEMENT FILTER FROM THE LOW PASS PROTOTYPE

In this section, important formulation used to obtain the design parameters for a bandpass filter directly from the lowpass prototype in sections 5.2 and 5.3.1 will be presented. Once the number of resonators is defined, the design parameters to be found are the couplings between resonators and the external quality factors as shown in Figure 5-10.

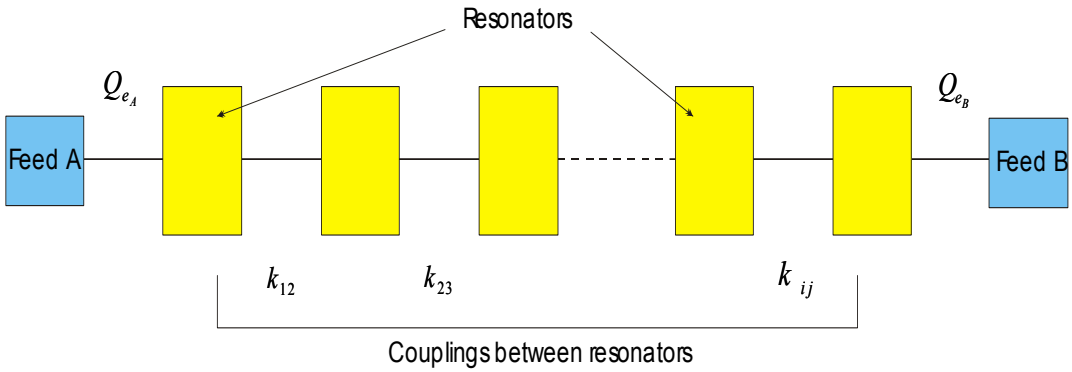

Figure 5-10 Design parameters of a bandpass filter

The design parameters can be directly obtained from the lowpass prototype g values, the low pass prototype derived Q_e for the bandpass filter in Figure 5-10, is given by [4-7]

$$Q_{e_A} = \frac{g_1 f_o}{\Delta BW} \qquad \text{eq 5-34}$$

$$Q_{e_B} = \frac{g_n g_{n+1} f_o}{\Delta BW} \qquad \text{eq 5-35}$$

Where f_o in eq 5-34 and eq 5-35 is the desired centre frequency for the bandpass filter response, the *g's* are the low pass element values, and ΔBW is the desired bandpass bandwidth for the filter as in Figure 5-3 given by

$$\Delta BW = \omega_{C2} - \omega_{C1} \qquad \text{eq 5-36}$$

Next, the coupling coefficients derived from the low pass prototype are given by [4-7]

$$k_{ij} = \frac{\Delta BW}{f_o \sqrt{g_i g_j}} \qquad \text{eq 5-37}$$

Where f_o in eq 5-37 is the desired centre frequency for the bandpass filter response, ΔBW is the desired bandpass bandwidth for the filter as in Figure 5-3, given by eq 5-36, and the *g's* are the low pass element values.

5.3.4 DETERMINATION OF COUPLINGS WITH THE AID OF A CAD SIMULATOR

In this section, important formulation will be presented to calculate the couplings within a practical filter. The couplings will be computed with the aid of an electromagnetic CAD simulator, to match the ones obtained directly from the low pass element *g* values, described in section 5.3.3. The details of how the parameters were calculated for each filter of this thesis will be discussed in Chapter 7. Here only the main procedure will be addressed, with the example of coupled microstrip resonators.

The parameters involved in filter design are the couplings between the resonators, and the external quality factors. By determining these parameters, the

bandpass filter response is obtained. The rest of this section contains a subsection summarizing the general procedure used to calculate the filter's parameters.

5.3.4.1 CALCULATING Q_e

The external quality factor Q_e is related to the loading effect from coupling the first and last resonators to their respective feeds, as shown in Figure 5-10. The set up in Figure 5-11 can be used to extract Q_e with the aid of an electromagnetic CAD simulator, where a microstrip resonator is weakly coupled on one side.

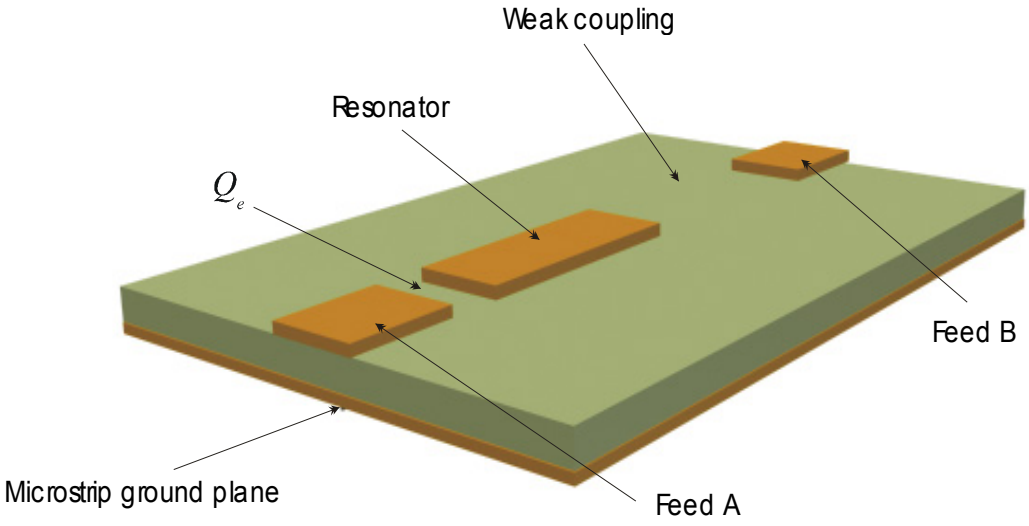

Figure 5-11 Extracting Q_e from simulations

By loading the microstrip resonator to its feed, the simulation response in Figure 5-12 is obtained for S_{21}

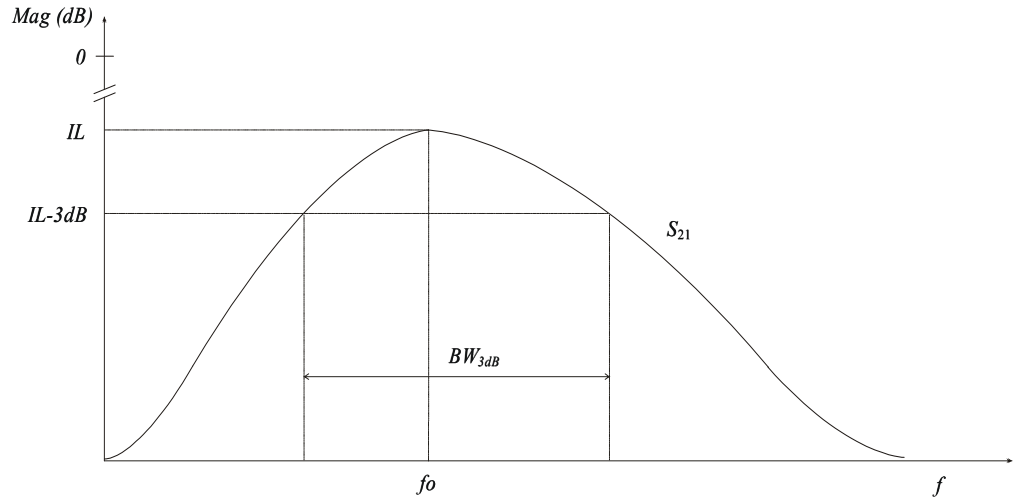

Figure 5-12 Typical S_{21} simulated response for Q_e

The asymmetry of the plot in Figure 5-12 is due to the asymmetric coupling used in Figure 5-11. The Q_e is now extracted from the simulated response in Figure 5-12 by computing

$$Qe = \frac{f_o}{BW_{3dB}} \qquad \text{eq 5-38}$$

Where f_o and BW_{3dB} in eq 5-38 are specified in Figure 5-12. Now by varying the coupling between the resonator and feed A in Figure 5-11, Q_e can be optimised for the filter specification. This is done by taking eq 5-38 to match the low pass prototype derived Q_e from eq 5-34 and eq 5-35, Such that the distance between the first and last resonator to its respective feed is the one that gives the appropriate Q_e for each case.

5.3.4.2 CALCULATING THE COUPLINGS BETWEEN RESONATORS

This section will focus on extracting the couplings between resonators. For this, the electric coupling between two resonators will be discussed by the use of the lumped

element model shown in Figure 5-13, which will lead to the derivation of a general formula that can be used to extract the couplings between resonators, regardless of whether the coupling is electric, magnetic or mixed [4-7]. The main objective of this section is to expose the method of extracting the coupling between resonators with the aid of a CAD.

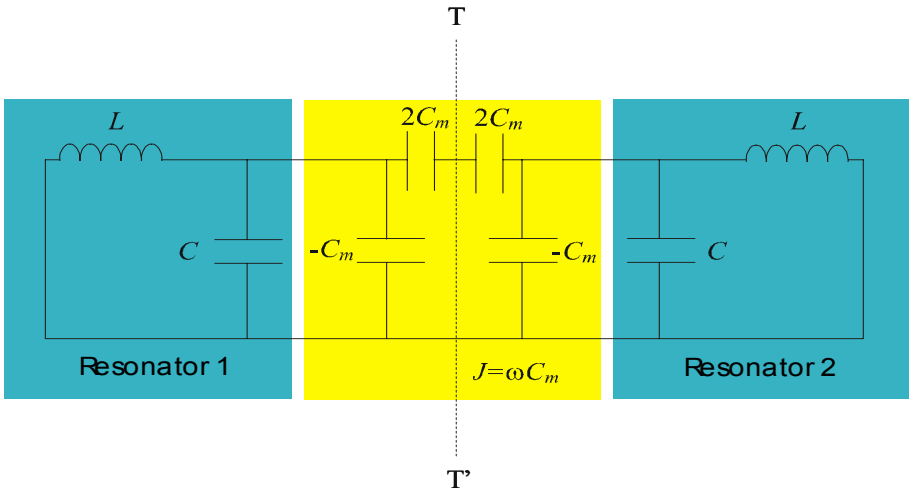

Figure 5-13 Theoretical lumped element model for the electric coupling between resonators

Figure 5-13 shows two resonators connected by a *J* inverter, which represents the electric coupling between the resonators. If the symmetry plane T-T' in Figure 5-13 is replaced by a short circuit or an electric wall, the resultant circuit has a resonant frequency given by

$$f_e = \frac{1}{2\pi\sqrt{L(C + C_m)}} \qquad \text{eq 5-39}$$

In this case, the coupling effect enhances the capability to store charge such that the resonant frequency is lower than that of an uncoupled single resonator. If the symmetry plane T-T' in Figure 5-13 is replaced by an open circuit or a magnetic wall, the resonant frequency of the resultant single resonant circuit is given by

$$f_m = \frac{1}{2\pi\sqrt{L(C - C_m)}} \qquad \text{eq 5-40}$$

In this case, the coupling effect reduces the capability to store charge, such that the resonant frequency with respect of an uncoupled single resonator is increased. Now by using eq 5-39 and eq 5-40, the electric coupling coefficient between the resonators of Figure 5-13 can be found by

$$k_E = \frac{f_m{}^2 - f_e^2}{f_m{}^2 + f_e^2} = \frac{C_m}{C} \qquad \text{eq 5-41}$$

As mentioned at the beginning of this section, a magnetic and a mixed coupling between resonators can also be defined; these models all converge in a general expression for the coupling between resonators eq 5-42, which will be treated in the rest of this section with the example of coupled microstrip resonators.

The set up in Figure 5-14 can be used to extract the couplings between the two microstrip resonators, with the aid of an electromagnetic CAD simulator. The resonators should be weakly coupled to their feeds in order to extract the coupling between the resonators.

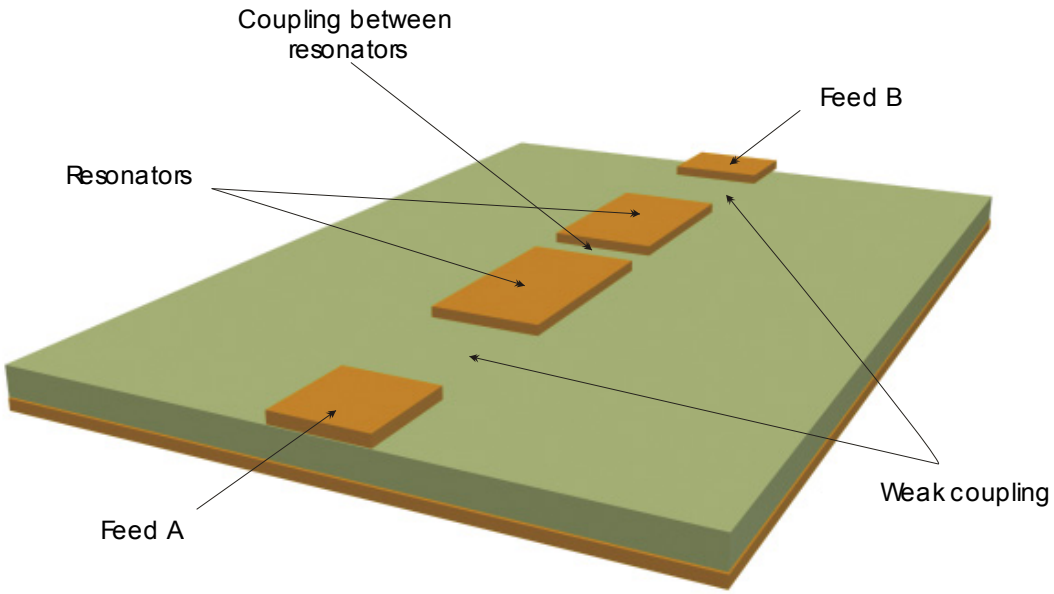

Figure 5-14 Extracting the coupling between resonators from simulations

A typical simulated S_{21} response produced by coupling two resonators is shown in Figure 5-15

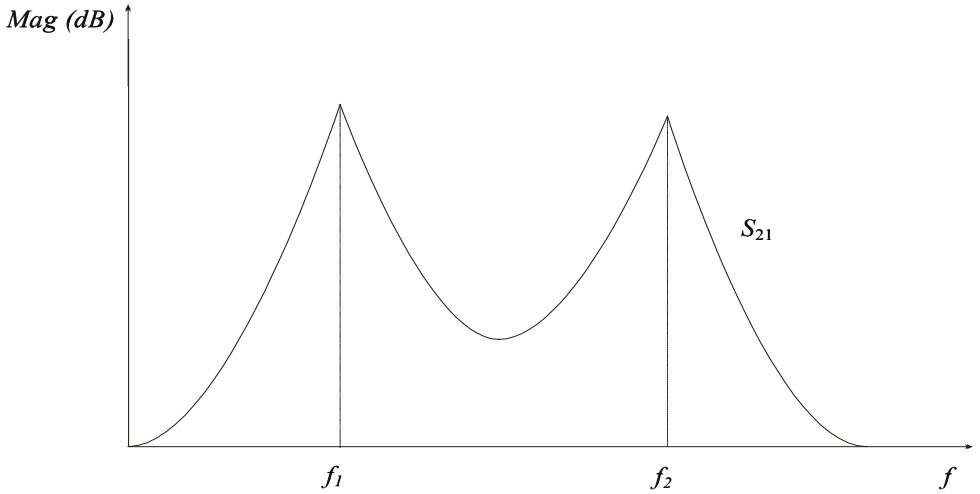

Figure 5-15 Typical S_{21} simulated response for two coupled resonators

The coupling coefficient between the *i*th and the *j*th resonator is now extracted from the simulated response in Figure 5-15 by using the general formulation for couplings given by

$$k_{ij} = \frac{f_2^{\,2} - f_1^{\,2}}{f_2^{\,2} + f_1^{\,2}} \qquad \text{eq 5-42}$$

Where f_1 and f_2 are the frequencies of the two coupled peaks generated by the electromagnetic interaction between the resonators as shown in Figure 5-15. Now by varying the coupling between resonators, the value of the couplings is optimised to the filter specification by making the coupling of eq 5-42 match the coupling coefficients derived from the low pass prototype, which are given by eq 5-37. With this data, the appropriate distances between resonators can be calculated.

5.4. WIDEBAND FILTER USING QUARTER WAVELENGTH STUBS

In this section, the design formulae for a wideband bandpass filter using quarter wavelength short circuited stubs as resonators, and quarter wavelength transmission lines connecting the resonators as admittance inverters will be introduced.

The filter in this section has an identical bandpass ladder network to the one shown on Figure 5-8. Here the shunt resonators are implemented by quarter wavelength long transmission lines. The resonators are connected by quarter wavelength long sections of transmission line, as admittance inverters.

This filter structure is not good for narrow band filters, as the stubs will have unreasonably low impedance levels, as the bandwidth becomes narrower. The filter structure defined in this section is shown on Figure 5-16.

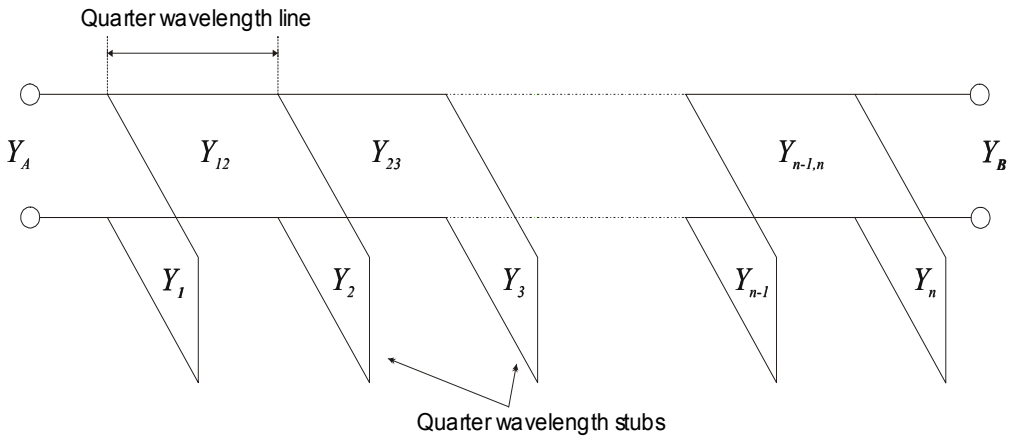

Figure 5-16 Wideband filter using quarter wavelength stubs and quarter wavelength connecting lines

The appropriate lowpass to bandpass mapping for this filter is given by [4-6]

$$\frac{\omega'}{\omega'_C} = \frac{-\cos\left(\frac{\pi}{2}\frac{\omega}{\omega_O}\right)\sqrt[n]{\left|\sin\left(\frac{\pi}{2}-\frac{\pi\Delta}{4}\right)\right|}}{\cos\left(\frac{\pi}{2}-\frac{\pi\Delta}{4}\right)\sqrt[n]{\left|\sin\left(\frac{\pi}{2}\frac{\omega}{\omega_O}\right)\right|}} \qquad \text{eq 5-43}$$

Where n is the number of reactive elements in the low pass prototype, Δ is defined in eq 5-15 and the rest of the elements refer to Figure 5-1 and Figure 5-3. After estimating the number of reactive elements to be used in the filter, the lowpass prototype element values are obtained using eq 5-7 to eq 5-12, the terminating admittances Y_A and Y_B for the filter in section 7.3 in Chapter 7 are set to be 0.02 Mhos, which corresponds to a characteristic impedance of 50 Ohm for the input and output ports. Now the admittances for the various sections of the filter are computed using the following formulas [4-6]

First compute

$$\theta_1 = \frac{\pi}{2}\left(1 - \frac{\Delta}{2}\right) \quad \text{eq 5-44}$$

$$\frac{J_{12}}{Y_A} = \sqrt{\frac{2g_1}{g_2}} \quad \text{eq 5-45}$$

$$\frac{J_{k,k+1}}{Y_A} = \frac{2g_1}{\sqrt{g_k g_{k+1}}} \quad \text{where } k\text{=2 to } n\text{-2} \quad \text{eq 5-46}$$

$$\frac{J_{n-1,n}}{Y_A} = \sqrt{\frac{2g_1 g_{n+1}}{g_{n-1}}} \quad \text{eq 5-47}$$

$$N_{k,k+1} = \sqrt{\left(\frac{J_{k,k+1}}{Y_A}\right)^2 + \left(\frac{2g_1 \tan(\theta_1)}{2}\right)^2} \quad \text{where } k\text{=1 to } n\text{-1} \quad \text{eq 5-48}$$

The characteristic admittances of the shunt subs are given by

$$Y_1 = Y_A\left(N_{12} - \frac{J_{12}}{Y_A}\right) \quad \text{eq 5-49}$$

$$Y_k = Y_A\left(N_{k-1,k} + N_{k,k+1} - \frac{J_{k-1,k}}{Y_A} - \frac{J_{k,k+1}}{Y_A}\right) \quad \text{where } k\text{=2 to } n\text{-1} \quad \text{eq 5-50}$$

$$Y_n = Y_A\left(g_n g_{n+1} - g_1\right)\tan(\theta_1) + Y_A\left(N_{n-1,n} - \frac{J_{n-1,n}}{Y_A}\right) \quad \text{eq 5-51}$$

Finally the characteristic admittances of the connecting lines are given by

$$Y_{k,k+1} = Y_A\left(\frac{J_{k,k+1}}{Y_A}\right) \quad \text{eq 5-52}$$

5.5. EXTRACTING *Qo* FROM AN EXPERIMENTAL FILTER

This section describes the procedure used to extract the resonator's unloaded quality factor, from a filter measurement using CAD. The theoretical model shown in

Figure 5-17 is used in the circuit simulator, where the values of the admittance inverters, or *J*'s in Figure 5-17 are calculated using eq 5-28 to eq 5-31, and the shunt lumped elements that form the resonators, are calculated using eq 5-19 and eq 5-20.

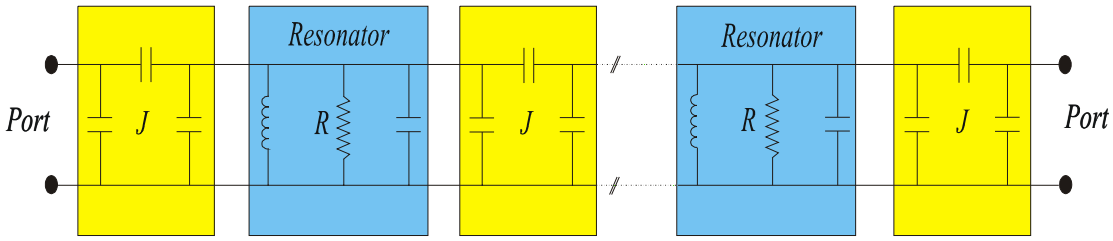

Figure 5-17 Theoretical model used to extract Q_O from filter measurements

Then the value of *R* is varied until the simulation's insertion loss matches the measured insertion loss. The unloaded quality factor of the resonators can now be calculated using eq 4-19.

The insertion loss for the bandpass filter in dB can be calculated directly from the low pass prototype *g* values by [4-7]

$$IL = 4.343 \sum_{i=1}^{n} \frac{g_i}{\Delta Q_{o_i}} \qquad \text{eq 5-53}$$

Where Δ is defined in eq 5-15, it can be assumed that all the resonators have the same Q_O, although in principle they may be unequal.

5.6. CONCLUSIONS

In this chapter, the low pass prototype filter, which is part of the procedure followed for many filter designs, was reviewed. This low pass prototype can be transformed to give the desired bandpass filter.

After this, the main focus was a discussion of the theory and the main procedure used to design the filters, which will be described individually in Chapter 7. For this, theoretical models were presented, as well as the general procedure to set the design parameters in a simulator.

CHAPTER SIX
MICROMACHINED TRANSMISSION LINES AND RESONATORS

6.1. INTRODUCTION

In section 6.2 experiments were carried out in order to define a good transmission line to make the filters described in Chapter 7 will be presented. This section starts with a shielded microstrip line, followed by a parallel plate waveguide, and a deep coplanar waveguide and finally the square coaxial transmission line.

In section 6.3 an analytical loss comparison of four transmission lines will be presented, in which the attenuation constant and the unloaded quality factor for a half wavelength resonator made out of its respective structure will be calculated and plotted versus the area of the cross section of the transmission line.

6.2. THE SEARCH FOR A HIGH *Q* TRANSMISSION LINE

In this section the steps that lead to the choice of the square coaxial transmission line structure from which the filters in Chapter 7 are made of, will be addressed. A number of transmission lines have been investigated experimentally. The objective was to look at different low loss transmission lines at low frequencies with test materials, with the aim to produce low loss transmission lines at higher frequencies later, made out of silicon or SU8 for example.

6.2.1 THE SHELDED MICROSTRIP RESONATOR

The first experiment that was carried out, was a foam suspended microstrip half wavelength transmission line resonator shown in Figure 6-1

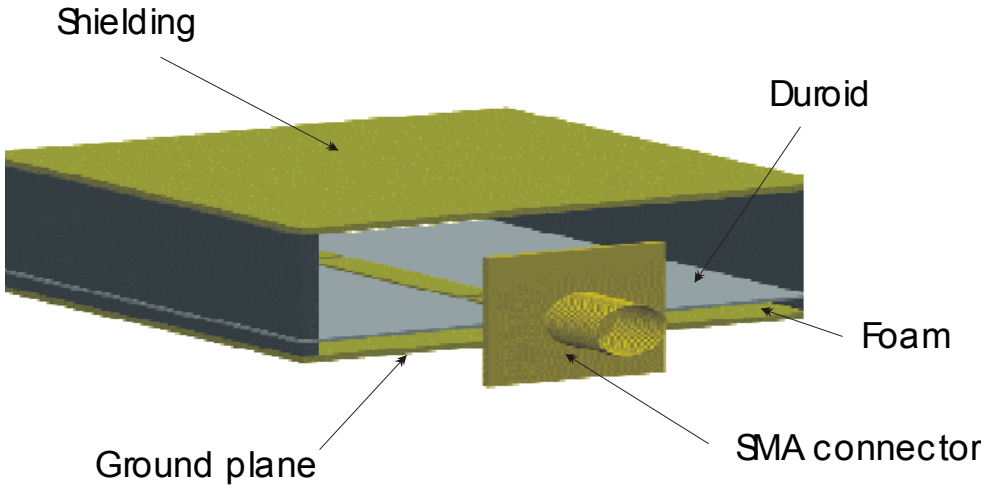

(a)

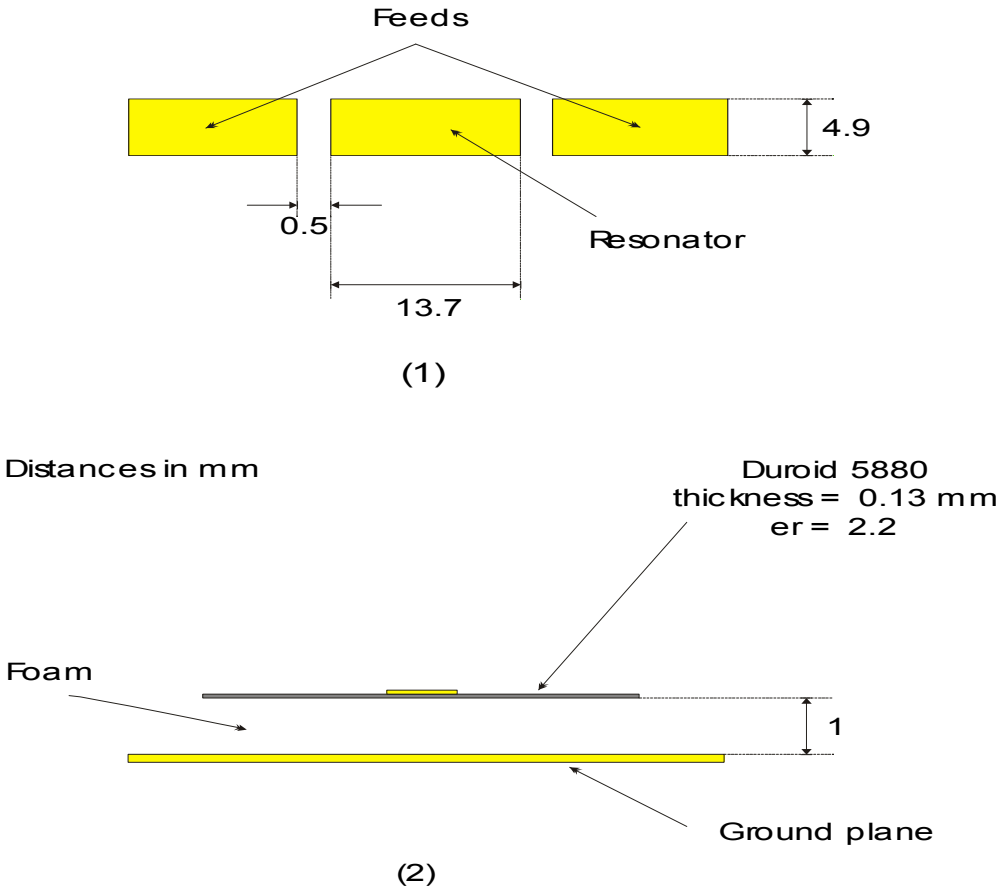

(b)

Figure 6-1 Half wavelength resonator on a foam-duroid substrate

(a) the shielded microstrip resonator (b) dimensions

(1) for the resonator (2) side view of the structure

The fabricated resonator has a low loss propagation media which consists of a 1mm foam layer and a 0.13 mm duroid substrate, and the height of the cavity is 8mm from the duroid substrate. The resonant frequency for the half wavelength resonator is 9.19 GHz and gave a measured *Qo* of 345. Some of the problems that occurred with this experiment were that the duroid is so thin that it started to bend very easily and the foam height was not strictly uniform. The characteristic impedance of a microstrip line can be calculated using the following formulae [3-2]

$$Zo = \frac{120\pi}{\sqrt{\frac{\varepsilon_r + 1}{2} + \frac{\varepsilon_r - 1}{2\sqrt{1 + \frac{12d}{W}}}\left[\frac{W}{d} + 1.393 + 0.667\ln\left(\frac{W}{d} + 1.444\right)\right]}} \quad \text{for } W/d \geq 1 \qquad \text{eq 6-1}$$

$$Zo = \frac{60}{\sqrt{\frac{\varepsilon_r + 1}{2} + \frac{\varepsilon_r - 1}{2\sqrt{1 + \frac{12d}{W}}}}}\ln\left(\frac{8d}{W} + \frac{W}{4d}\right) \quad \text{for } W/d \leq 1 \qquad \text{eq 6-2}$$

Where W, d and ε_r are as in Figure 6-2

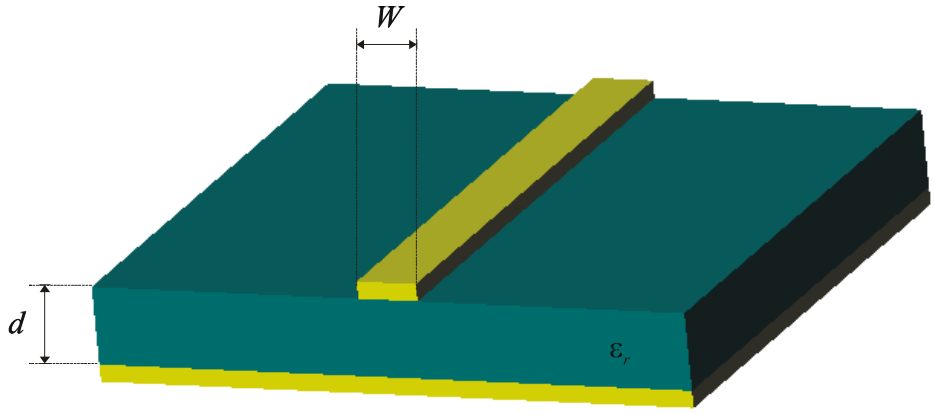

Figure 6-2 Microstrip transmission line

The dielectric constant was taken as 1, and the formula used to calculate the characteristic impedance of a 50 Ohm line was eq 6-1.

6.2.2 THE PARALLEL PLATE WAVEGUIDE

The structure in Figure 6-3 can be seen as a parallel plate transmission line. The main idea was to make the parallel plate waveguide out of aluminium, having an air propagation media, which had a measured attenuation constant of 0.4 dB/cm at 2 GHz.

This experiment can be considered for higher frequencies using micromachining techniques.

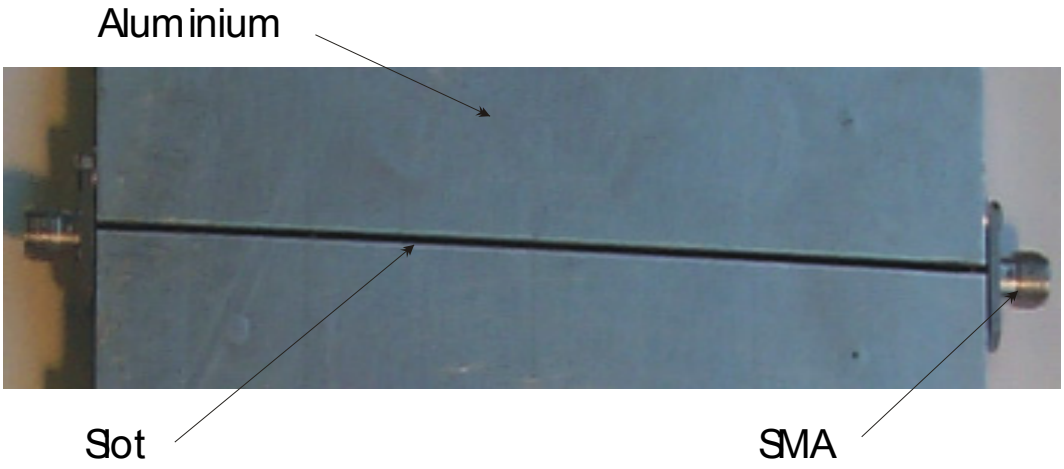

(a)

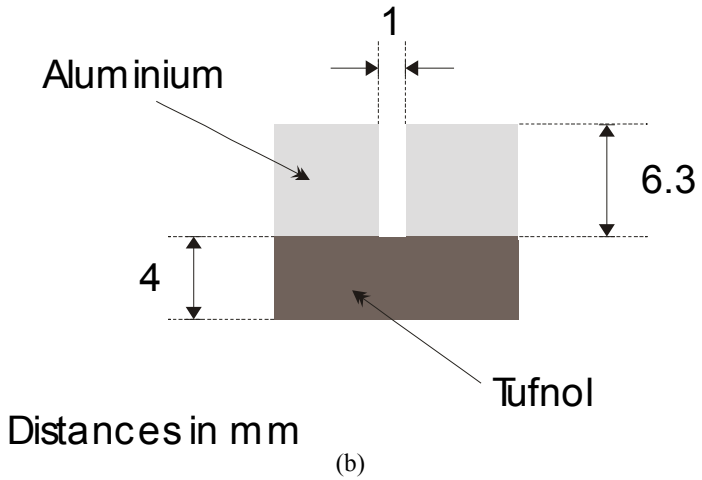

(b)

Figure 6-3 Aluminium parallel plate transmission line
(a) photo (b) cross section

The characteristic impedance for a parallel plate waveguide can be calculated using the following formulae [6-1]

$$Zo = \frac{\eta_o}{\sqrt{\varepsilon_r}}\left\{\frac{a}{b} + \frac{1}{\pi}\ln 4 + \frac{\varepsilon_r + 1}{2\pi\varepsilon_r}\ln\left[\frac{\pi\varepsilon_r\left(\frac{a}{b} + 0.94\right)}{2}\right] + \frac{\varepsilon_r - 1}{2\pi\varepsilon_r^{\,2}}\ln\frac{\varepsilon_r\pi^2}{16}\right\}^{-1} \qquad \text{eq 6-3}$$

for $a/b>1$

$$Zo = \frac{\eta_o}{\pi\sqrt{\varepsilon_r}}\left[\ln\frac{4b}{a} + \frac{1}{8}\left(\frac{a}{b}\right)^2 - \frac{\varepsilon_r - 1}{2(\varepsilon_r + 1)}\left(\ln\frac{\pi}{2} + \frac{\ln\frac{4}{\pi}}{\varepsilon_r}\right)\right] \qquad \text{for } a/b<1 \qquad \text{eq 6-4}$$

Where

$$a = \frac{w}{2} \qquad \text{eq 6-5}$$

$$b = \frac{h}{2} \qquad \text{eq 6-6}$$

And ε_r is the dielectric constant of the material between the conducting plates, η_o is the impedance of free space and w and h are as in Figure 6-4.

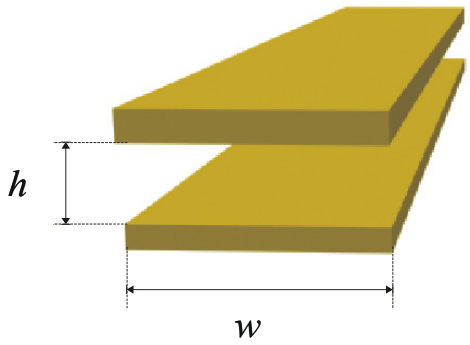

Figure 6-4 Parallel plate transmission line

The characteristic impedance for the parallel plate waveguide was calculated using eq 6-3 to give a characteristic impedance of 50 Ohms. The structure was mounted on a block of tufnol that has a dielectric constant of 5.1 and a loss tangent of 0.037.

6.2.3 THE DEEP COPLANAR WAVEGUIDE

The structure in Figure 6-5, shows the deep coplanar waveguide, which is made of aluminium and tufnol. No precise formulas to calculate the characteristic impedance for this structure were found in the literature. The measured *Qo* of the structure was found to be 25.15 with a resonant frequency of 1.45 GHz. The same structure with a partial shielding to reduce radiation losses, and covering just one side of the structure, gave a *Qo* of 37.5 with a resonant frequency of 1.49 GHz.

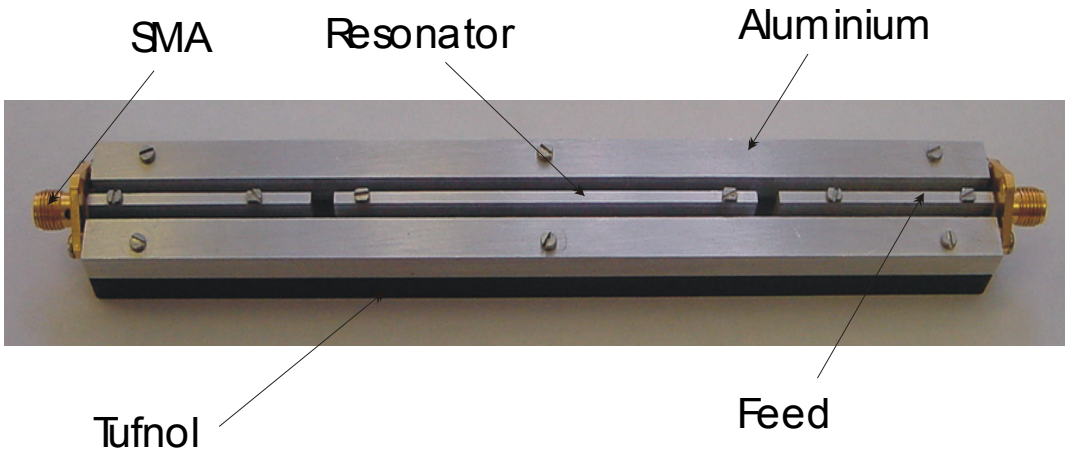

(a)

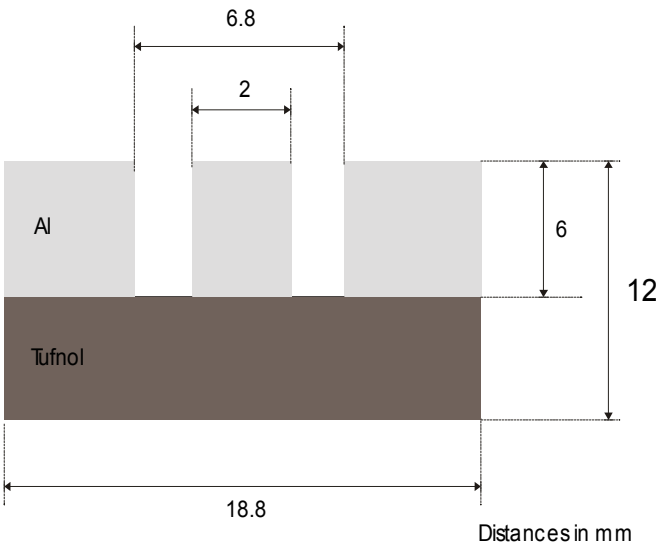

(b)

Figure 6-5 Deep coplanar waveguide
(a) photo (b) cross section

6.2.4 A SQUARE COAXIAL RESONATOR

The main structure in this thesis is the square coaxial transmission line. Here a half wavelength resonator at 1.6 GHz was designed having a measured *Qo* of 960, compared to the simulated result that gave a *Qo* of 1047 using a 3D CAD simulator [4-10]. The structure is shown on Figure 6-6.

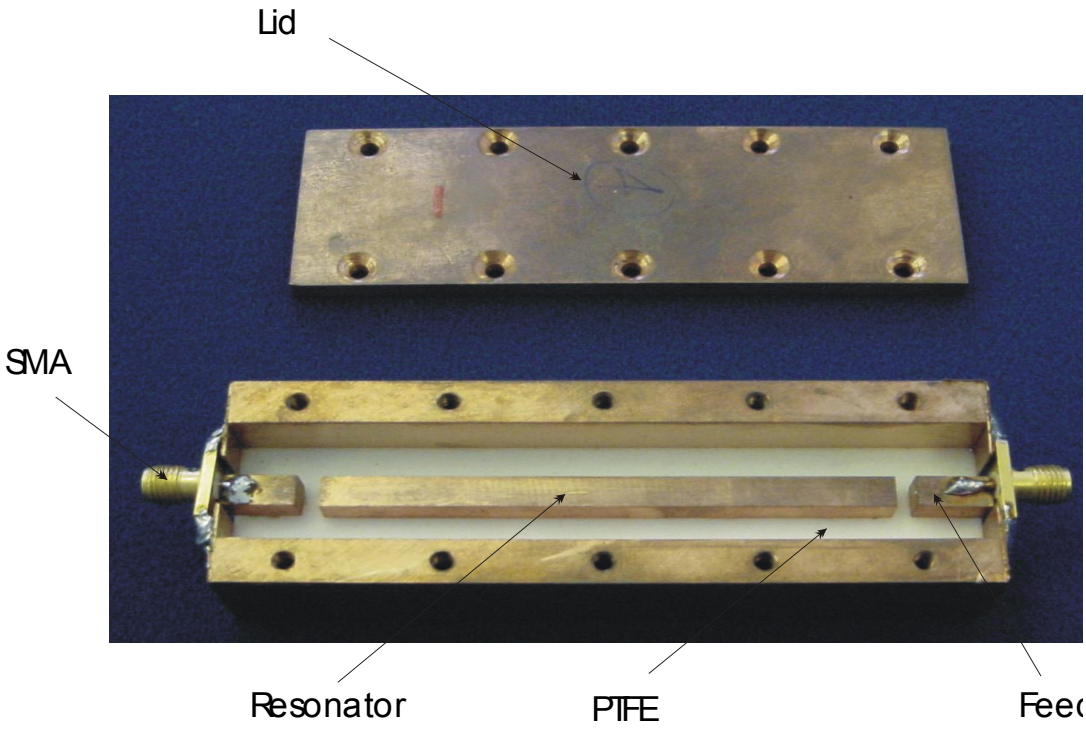

(a)

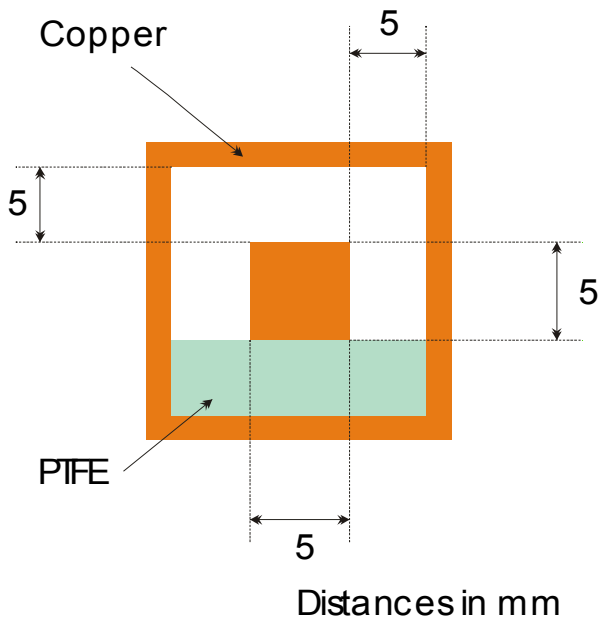

(b)

Figure 6-6 Square coaxial resonator
(a) photo (b) cross section

The design equations for a square coaxial transmission line are given in section 6.4. The dielectric used to support the centre conductor is PTFE with a dielectric constant of 2.1 and a loss tangent of 0.001.

6.3. ANALYTICAL LOSS COMPARISON OF LOW LOSS TRANSMISSION LINES

In this section, a loss comparison between a round coaxial, square coaxial, microstrip and stripline transmission line resonators will be discussed. This section will be divided into three sub-subsections. The first one contains the formulae that will be used to calculate the attenuation constant for the different transmission line structures to be compared. The second section contains the area of the transmission line's cross section that will be considered for comparison between structures in the calculations; and the third subsection contains the results of the loss comparison between the exposed structures.

6.3.1 LOW LOSS TRANSMISSION LINES

In this section the focus will be on comparing the conductor loss from the four structures shown in Figure 6-7. The structures have been compared as if they were suspended, having no dielectric or radiation loss.

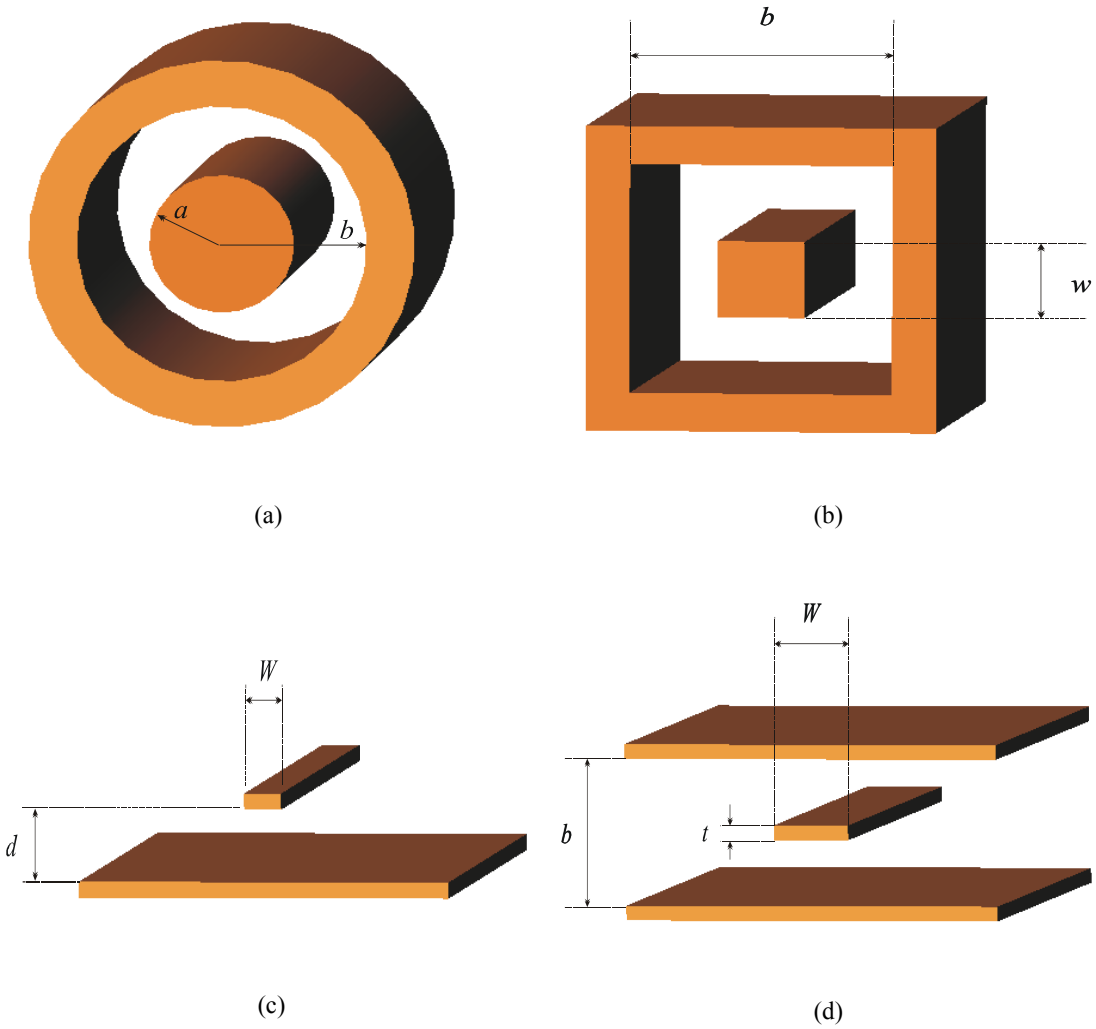

(a) (b) (c) (d)

Figure 6-7 Low loss transmission lines

(a) coaxial (b) square coaxial (c) microstrip (d) stripline

In the next paragraphs of this section the calculation of the skin depth and surface resistivity for the copper plates will be given. The frequency at which these structures will be compared is f_o=50 GHz. The conductivity of the ideal copper used for the calculations is σ=5.8 x 10^7 S/m at 20°C, and a relative permeability μ_r equal to one is assumed. Since the structure is made only of a high conductivity metal, and the rest of the space surrounding the conductors is air, the relative permittivity, ε_r is equal to one.

The skin depth is calculated by using eq 4-57, which gives a value of 2.955 x 10^{-7}m, using the values discussed in last paragraph, the surface resistance calculated using eq 4-68 is equal to 0.58 Ω/square.

6.3.2 LOSS CALCULATION

In this section, the loss calculation for the four different structures will be presented individually, following the order of Figure 6-7. The formulae given are used in the calculation of the characteristic impedance Z_O, the attenuation constant due to conductor losses, α_c, and the unloaded quality factor Q_O of a half wavelength resonator. As the structures to be compared are air filled, only the conductor loss will be considered; and in the microstrip case, it will be assumed that no radiation losses are present, since it is common practice to enclose the microstrip transmission line to avoid radiation losses, obtaining a better performance of the circuit.

6.3.2.1 COAXIAL

The first structure to be analysed is the coaxial transmission line shown on Figure 6-7a, the impedance of this coaxial line, can be calculated by

$$Z_O = 60\sqrt{\frac{\mu_r}{\varepsilon_r}}\ln\frac{b}{a} \qquad \text{eq 6-7}$$

Where b and a are the radius of the coaxial line's conductors shown on Figure 6-7a. Now the attenuation due to conductor for this structure can be obtained by [3-5]

$$\alpha_c = 1.5657\frac{\delta_s\sqrt{\varepsilon_r}\left(1+\frac{b}{a}\right)}{\lambda_o b\ln\frac{b}{a}} \qquad \text{eq 6-8}$$

Where δ_s is the skin depth and λ_o is the wavelength at the operating frequency, α_c in eq 6-8 has units of Np/m.

6.3.2.2 SQUARE COAXIAL

The impedance for the square coaxial structure shown on Figure 6-7b can be calculated using [6-2]

$$Z_O = \frac{47.09}{\sqrt{\varepsilon_r}} \frac{(b-w)}{(0.2794b + 0.7206w)} \qquad \text{for} \quad b/w < 2.5 \qquad \text{eq 6-9}$$

$$Z_O = \frac{136.7}{\sqrt{\varepsilon_r}} \log_{10}\left(0.9259\frac{b}{w}\right) \qquad \text{for} \quad 2.5 \le b/w \le 4 \qquad \text{eq 6-10}$$

$$Z_O = \frac{138.06}{\sqrt{\varepsilon_r}} \log_{10}\left(0.914\frac{b}{w}\right) \qquad \text{for} \quad b/w > 4 \qquad \text{eq 6-11}$$

And the attenuation due to conductor for this structure can be obtained by [6-2]

$$\alpha_c = \frac{47.09R_s}{\eta_o Z_O}\left(1+\frac{b}{w}\right)\frac{w}{(0.2794b + 0.7206w)^2} \qquad \text{for} \quad b/w < 2.5 \qquad \text{eq 6-12}$$

$$\alpha_c = \frac{59.37R_s}{\eta_o Z_O}\left(1+\frac{b}{w}\right)\frac{1}{b} \qquad \text{for} \quad 2.5 \le b/w \le 4 \qquad \text{eq 6-13}$$

$$\alpha_c = \frac{59.96R_s}{\eta_o Z_O}\left(1+\frac{b}{w}\right)\frac{1}{b} \qquad \text{for} \quad b/w > 4 \qquad \text{eq 6-14}$$

Where R_s is the surface resistance calculated by using eq 4-68, η_o in the impedance of free space and b and w are as in Figure 6-7b, the units of α_c are Np/m.

6.3.2.3 MICROSTRIP

The impedance of the microstrip structure, which was discussed earlier in section 6.3.1, is presented again, but now the effective dielectric constant is shown separately. The impedance of the microstrip can be calculated by [3-2]

$$Z_O = \frac{60}{\sqrt{\varepsilon_e}} \ln\left(\frac{8d}{W} + \frac{W}{4d}\right) \qquad \text{for} \quad w/d \le 1 \qquad \text{eq 6-15}$$

$$Z_O = \frac{120\pi}{\sqrt{\varepsilon_e}\left[\frac{W}{d} + 1.393 + 0.667 \ln\left(\frac{W}{d} + 1.444\right)\right]} \qquad \text{for} \quad w/d \ge 1 \qquad \text{eq 6-16}$$

Where ε_e is the effective dielectric constant of the air and dielectric regions of the microstrip shown on Figure 6-2. For the microstrip shown on Figure 6-7c, the effective dielectric constant is equal to one, since it is an air filled transmission line. The effective dielectric constant for a microstrip line is given approximately by [3-2]

$$\varepsilon_e = \frac{\varepsilon_r + 1}{2} + \frac{\varepsilon_r - 1}{2}\left(\frac{1}{\sqrt{1 + 12\frac{d}{W}}}\right) \qquad \text{eq 6-17}$$

The attenuation due to conductor loss for the microstrip can be obtained by [3-2]

$$\alpha_c = \frac{R_s}{W Z_O} \qquad \text{eq 6-18}$$

The units of α_c are in Np/m and R_s is the surface resistance that can be calculated by using eq 4-68.

6.3.2.4 STRIPLINE

The impedance for the stripline structure shown in Figure 6-7d, can be calculated by[3-2]

$$Z_O = \frac{30\pi}{\sqrt{\varepsilon_r}}\left(\frac{b}{W_e + 0.441b}\right) \qquad \text{eq 6-19}$$

Where W_e is the effective width of the centre conductor given by

$$W_e = W \qquad \text{for } W/b > 0.35 \qquad \text{eq 6-20}$$

$$W_e = W - b\left(0.35 - \frac{W}{b}\right)^2 \qquad \text{for } W/b < 0.35 \qquad \text{eq 6-21}$$

And the attenuation due to conductor in Nepers/m for this structure can be obtained by [3-2]

$$\alpha_c = \frac{2.7\text{x}10^{-3} R_s \varepsilon_r Z_O}{30\pi(b-t)} A \qquad \text{for } Zo\sqrt{\varepsilon_r} < 120 \qquad \text{eq 6-22}$$

$$\alpha_c = \frac{0.16 R_s}{b Z_O} B \qquad \text{for } Zo\sqrt{\varepsilon_r} > 120 \qquad \text{eq 6-23}$$

With

$$A = 1 + \frac{2W}{b-t} + \frac{1}{\pi}\left(\frac{b+t}{b-t}\right)\ln\left(\frac{2b-t}{t}\right) \qquad \text{eq 6-24}$$

$$B = 1 + \left(\frac{b}{0.5W + 0.7t}\right)\left(0.5 + \frac{0.414t}{W} + \frac{1}{2\pi}\ln\left(\frac{4\pi W}{t}\right)\right) \qquad \text{eq 6-25}$$

Where t is the thickness of the strip, in the calculations t is taken to be 10 microns, which satisfies the skin depth penetration for the operating frequency.

6.3.3 LOSS COMPARISON

In this section, a way of comparing the losses of a half wavelength transmission line resonator made out of the structures of Figure 6-7 will be presented. For this we have considered the unloaded quality factor and the conductor attenuation constant versus the area of the cross section of the transmission line. The area taken for each transmission line is represented by the area enclosed by the black line in Figure 6-8. The areas considered for the microstrip and the stripline were taken approximately to confine most of the electromagnetic field, as well as considering typical dimensions used in practical circuits.

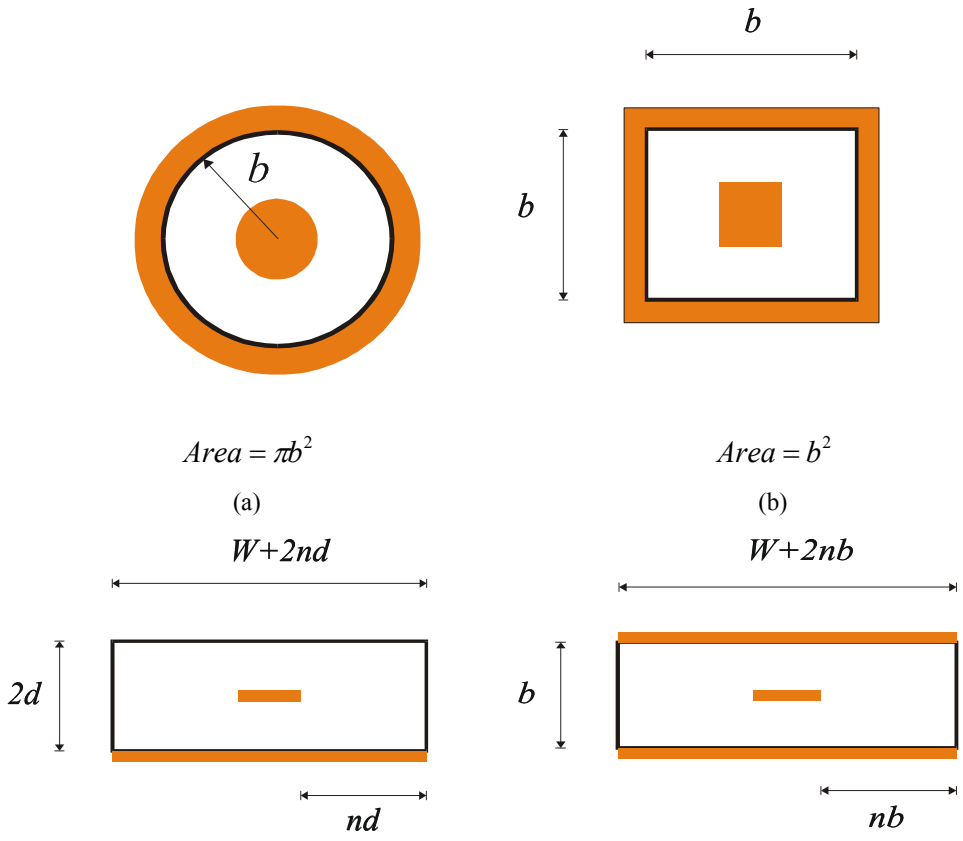

Figure 6-8 Transmission line cross section areas
(a) round coaxial (b) square coaxial (c) microstrip (d) stripline

The attenuation constant in nepers per meter for the low loss structures is plotted versus the area defined in Figure 6-8 for each transmission line in Figure 6-9. For the calculation, the formulae of section 6.4.2 were used in a CAD software [6-3] to compute the values obtained. The structures are considered to be air filled transmission lines, with ideal copper metalizations, and they all have a 50 Ohm characteristic impedance.

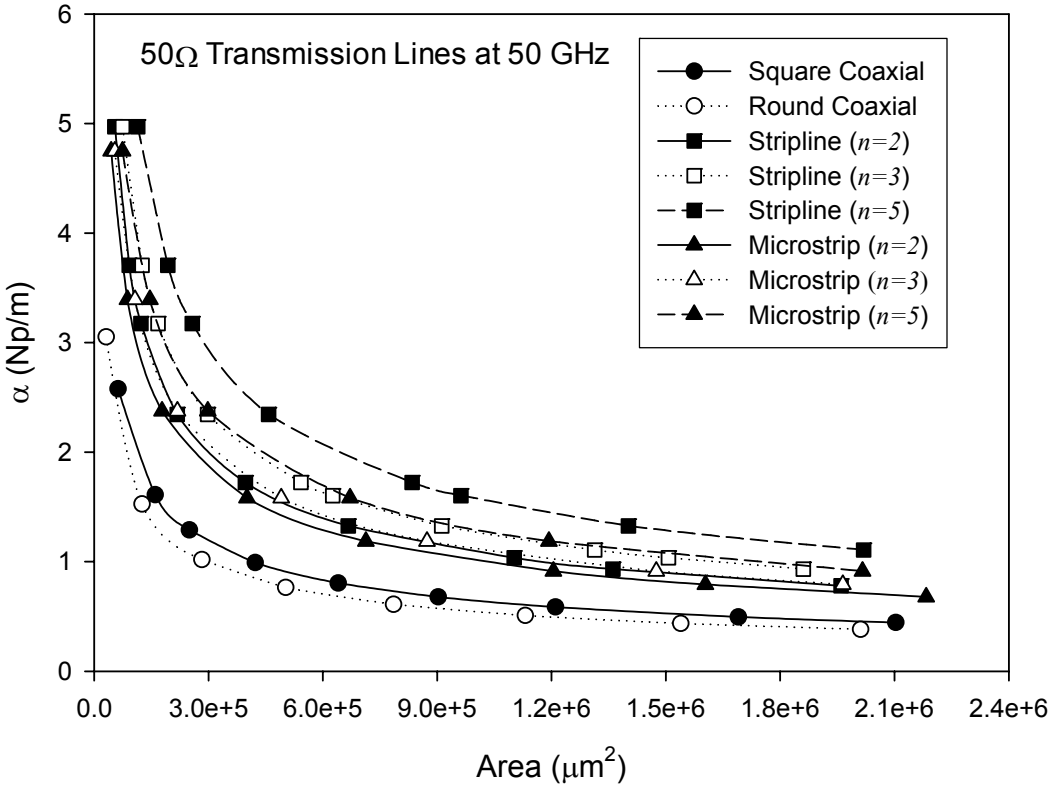

Figure 6-9 Attenuation constant versus area

The unloaded quality factor for a half wavelength resonator made out of these transmission lines, can be extracted by using eq 4-39 and the value of alpha obtained above, giving as a result the graph in Figure 6-10.

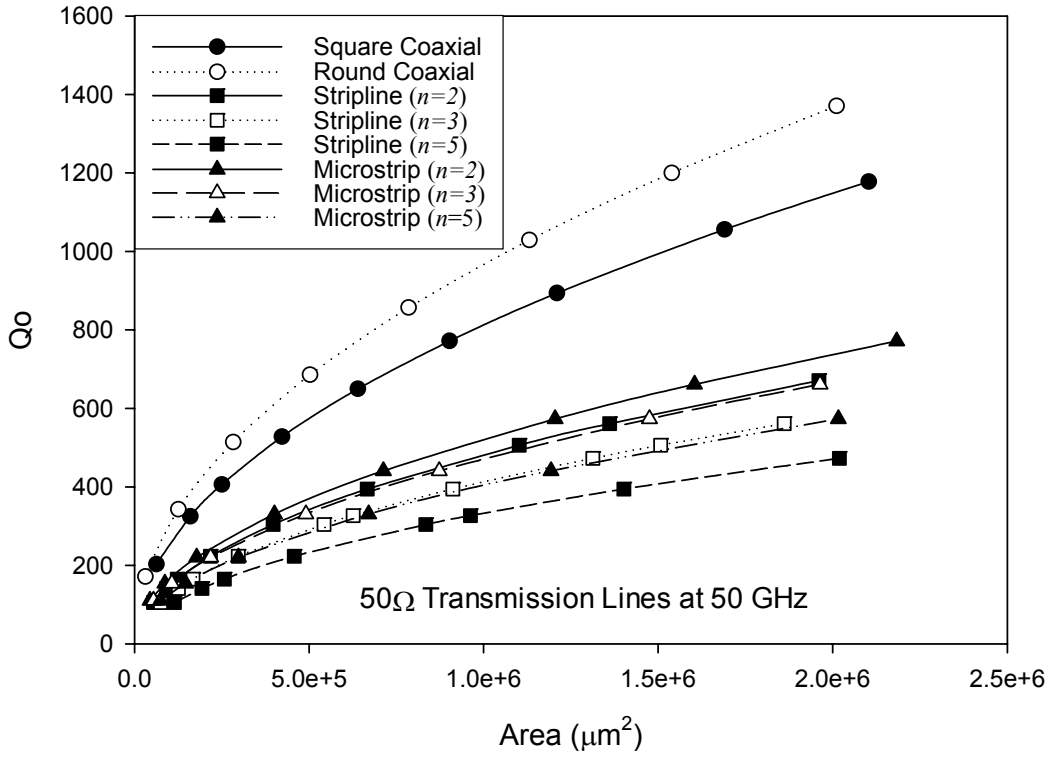

Figure 6-10 *Qo* versus area

The calculations indicate that the coaxial structures have higher *Qo*'s than the microstrip and stripline transmission lines. The round coaxial has higher *Qo* values because it has a smoother current distribution compared with the square coaxial.

6.4. CONCLUSIONS

In this chapter, the initial experiments in the search for a low loss transmission line were presented, these led to the decision to adopt the square coaxial transmission line structure, used in the filters described in Chapter 7. The square coaxial line was

chosen over the round coaxial line, because stacking thick planar layers of material allow an easier manufacturing process compared to the round coaxial.

Finally a conductor loss comparison of different low loss transmission lines was done analytically, with the objective of showing the advantages of using a square coaxial transmission line.

6.5. REFERENCES

[6-1] Brian C. Wadell, "Transmission line design handbook" *Artech House, Inc.*, 1991

[6-2] K.H.Lau, "Loss calculations for rectangular coaxial lines" *IEE proceedings,* Vol. 135, pt. H, No. 3, pp. 207-209, June 1988

[6-3] *Mathcad 8 professional by Mathsoft Inc.*

CHAPTER SEVEN
SQUARE COAXIAL MICROWAVE BANDPASS FILTERS

7.1. INTRODUCTION

This chapter will be divided into two parts. Part I contains a description of filters, which were designed using a coaxial structure, which has its centre conductor supported with a bar of dielectric. Part II describes filters, which were designed out of all-metal structures that have an air propagation media, enhancing filter performance by avoiding substrate losses.

Each section details how the design parameters were calculated, and also includes the technical drawings of the pieces that compose the filter. All the filters presented in this chapter have a Chebycheff response, and all simulated results presented are assumed to have perfect conductors.

PART I. DIELECTRIC SUPPORTED FILTERS

7.2. X BAND NARROW BAND FILTER

The filter discussed in this section is a three pole, 1% fractional bandwidth band pass filter with a centre frequency of 9 GHz, with a pass band ripple of 0.01 dB. The filter is formed by using a square coaxial transmission line with its centre conductor supported on a bar of dielectric. The dielectric used is PTFE with the same properties as the one used in the square coaxial resonator discussed in Chapter 6, section 6.2.4. The filter uses half wavelength resonators, and the filter design parameters are shown in Table 7-1.

g_1= 0.6291	g_2= 0.9702
Q_e= 62.91	k_c= 0.013

Table 7-1 Design parameters for the narrow band X band filter

7.2.1. DESIGN PARAMETERS

In this section, the method of finding the external quality factor and the coupling coefficients will be addressed; this section uses the techniques discussed in Chapter 5, section 5.3.3 to extract the values of the external quality factor, and the coupling coefficients involved with this particular design. To find the external quality factor, the set up illustrated in Figure 7-1 is used in a 3D electromagnetic CAD simulator [4-10].

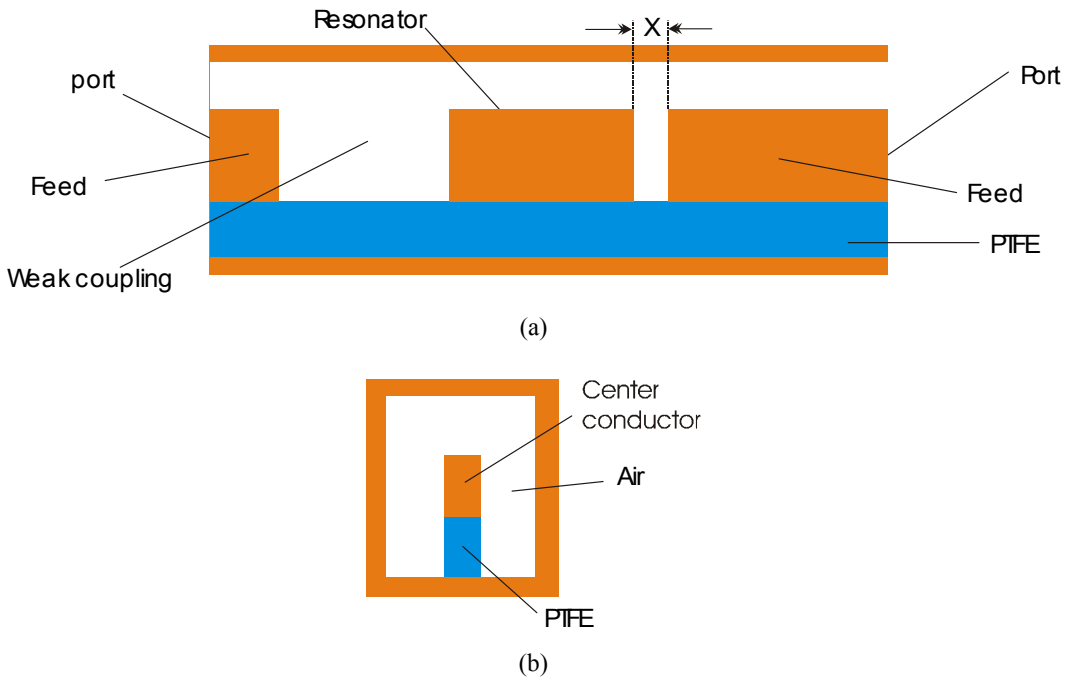

Figure 7-1 Extracting Q_e for the narrowband X-band filter
(a) side view, (b) end view

The distance X in Figure 7-1a is varied, and the external quality factor is calculated for each distance. The external quality factor for various values of X is plotted in Figure 7-2.

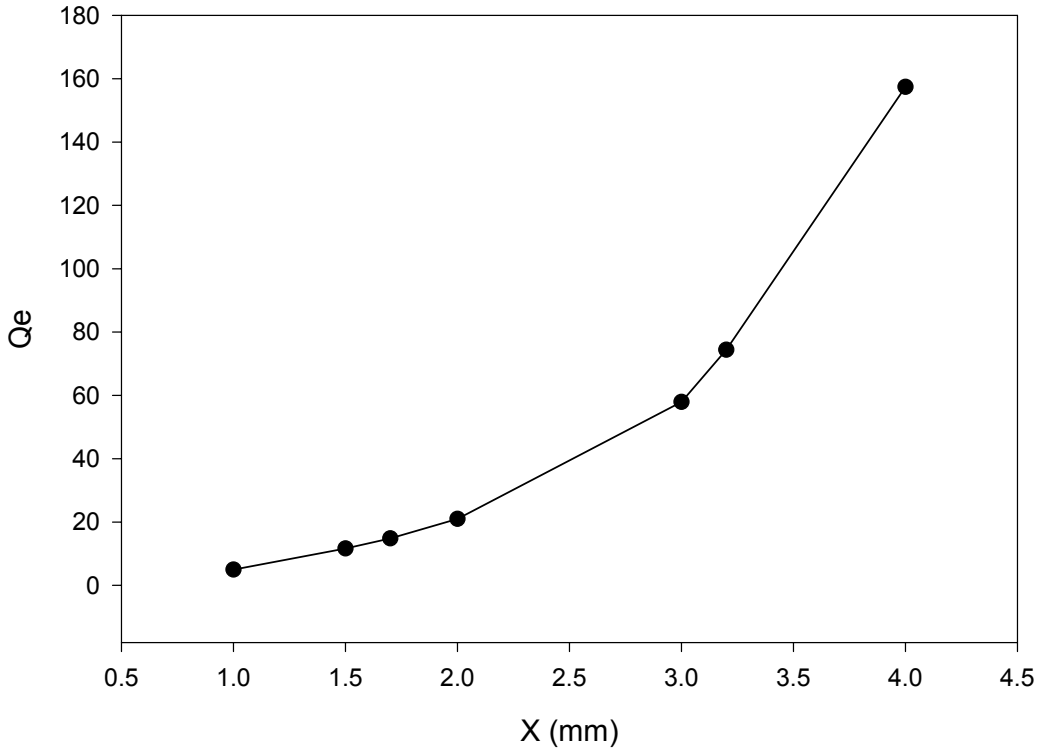

Figure 7-2 Q_e for the narrowband X-band filter

To calculate the couplings between resonators, the set up in Figure 7-3 is used in a 3D electromagnetic CAD simulator [4-10]

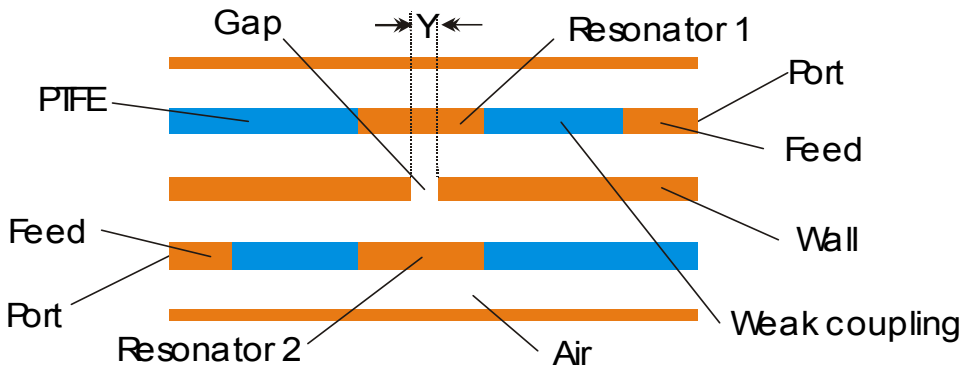

Figure 7-3 Extracting k_c for the narrowband X-band filter (top view)

The distance Y in Figure 7-3 is varied and the coupling coefficient for different values is plotted in Figure 7-4.

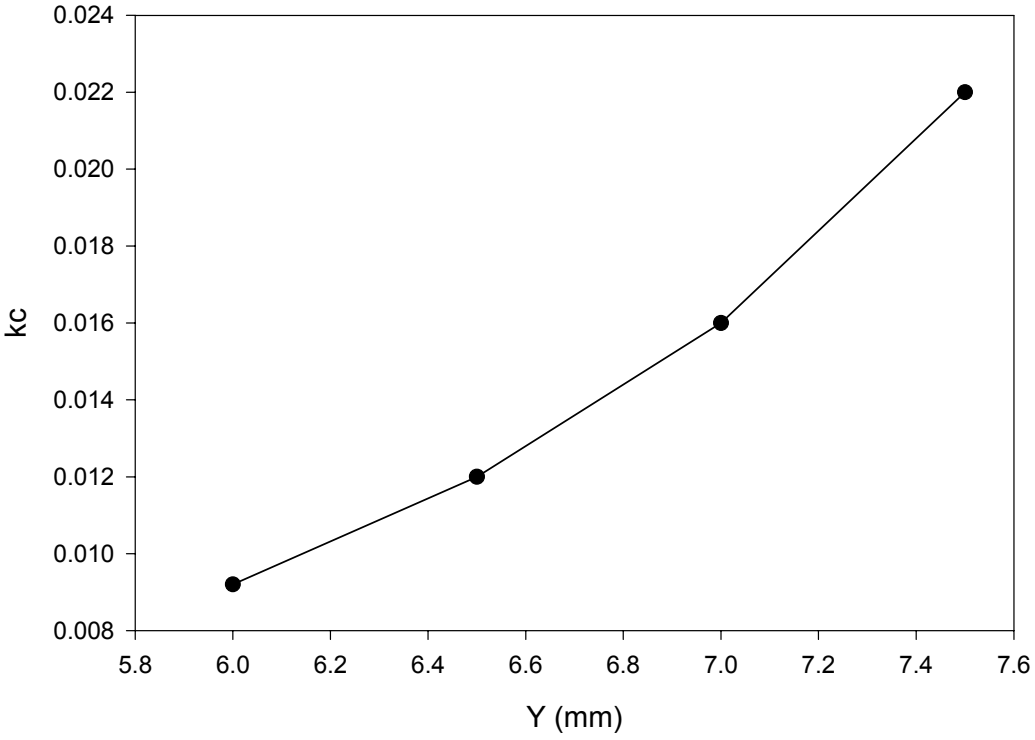

Figure 7-4 k_c for the narrowband X-band filter

From the calculations made in this section, the correct value of the external quality factor, together with the correct coupling coefficients are taken to form the final filter dimensions shown in the next section.

7.2.2. FILTER ASSEMBLY AND TECHNICAL DRAWINGS

The filter assembly is shown in Figure 7-5. The filter was fabricated with conventional machining techniques, and it was made in two parts, the lid, and the main filter structure.

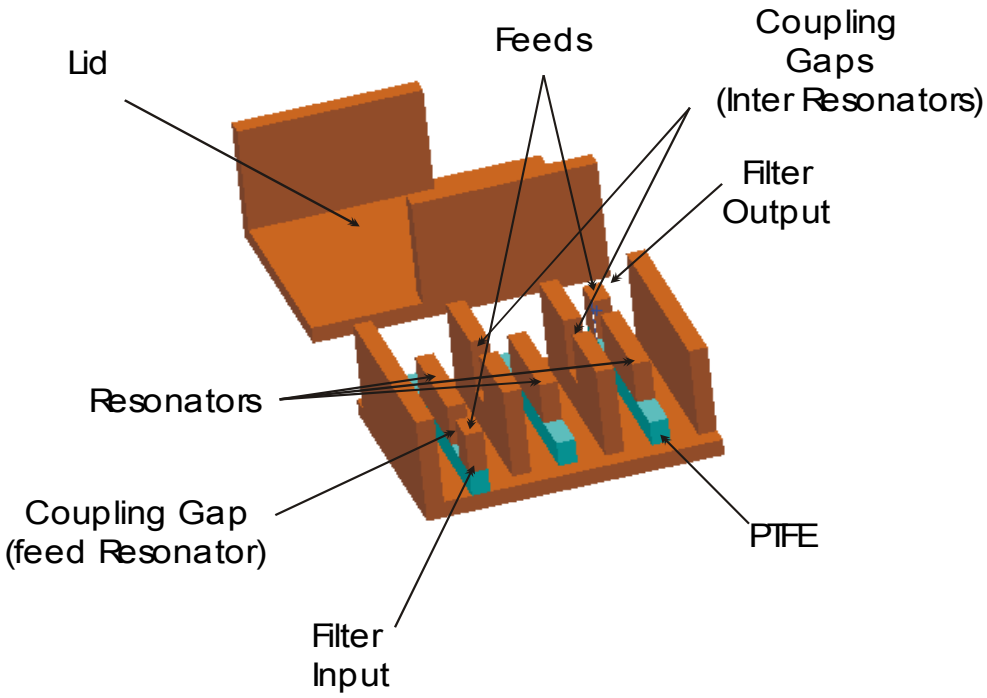

Figure 7-5 Assembly for the narrowband X-band filter

The technical drawings of the filter are shown in Figure 7-6. The gap in the walls of the square coaxial cable used to set the coupling coefficients between resonators has a depth of 6.5mm.

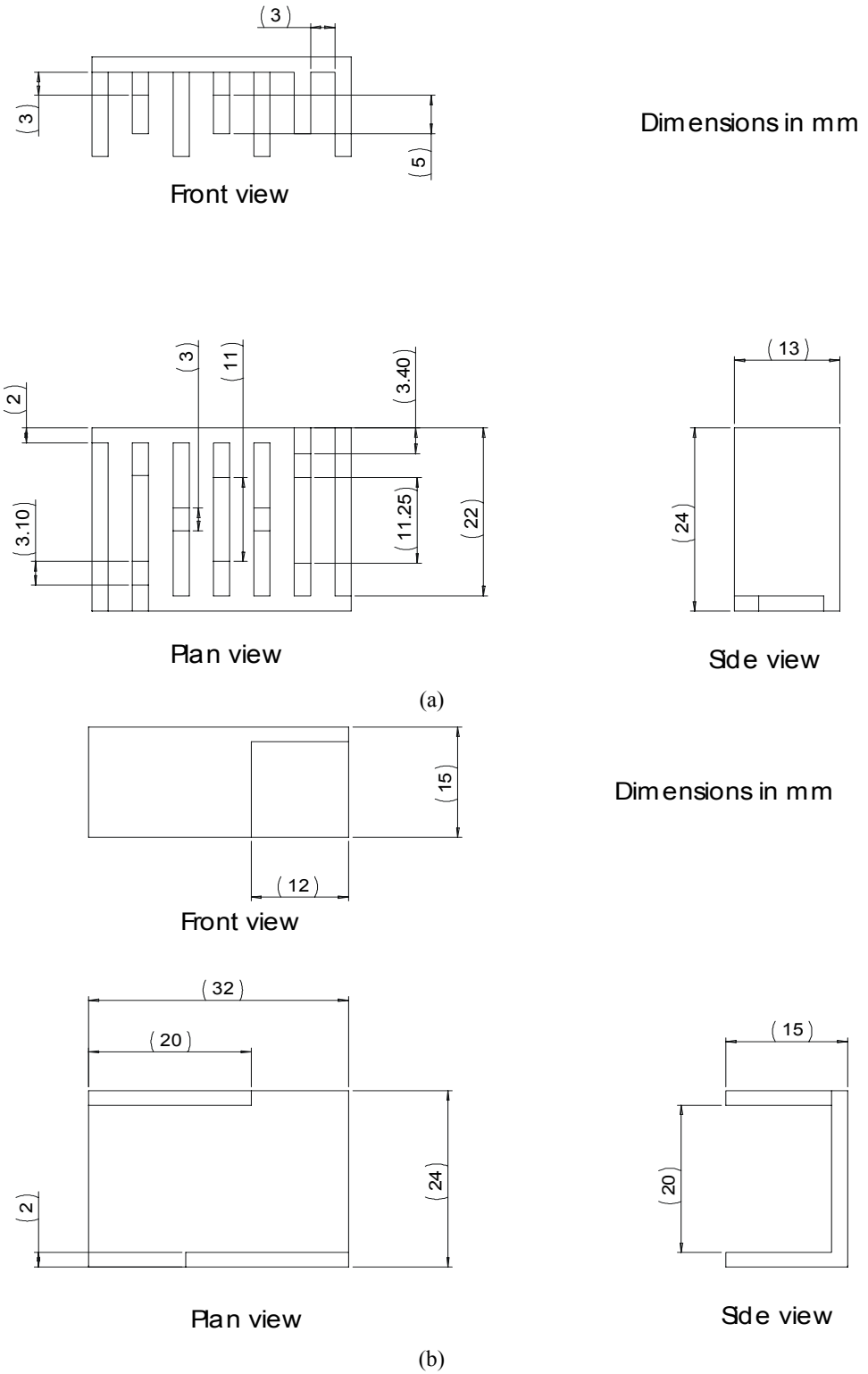

Figure 7-6 Technical drawings of the narrowband X-band filter
(a) main filter structure (b) lid

7.2.3. TUNING

During the development of this filter, fabrication tolerances became critical, especially when the resonators were mounted on the bar of PTFE. To compensate these tolerances, sapphire tuning screws with a dielectric constant of 9.6 were inserted in the lid, and the screws were placed at the end of each resonator, as shown in Figure 7-7, since the electric field presents a maximum at this point.

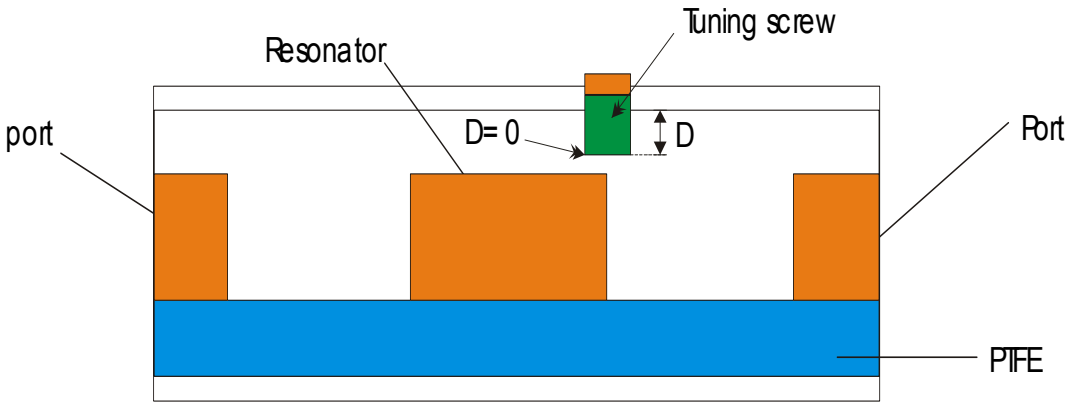

Figure 7-7 Tuning the narrowband X band filter (side view)

The simulated [4-10] frequency shift produced by moving the tuning screw up from the distance D=0 in Figure 7-7, is shown in Figure 7-8. Here the objective was to ensure that the three resonators would resonate at the same frequency. Additional tuning screws were set between the feed and the first resonator to adjust the $Q_{e,}$ giving a total of 5 tuning screws to obtain the response shown in section 7.2.4.

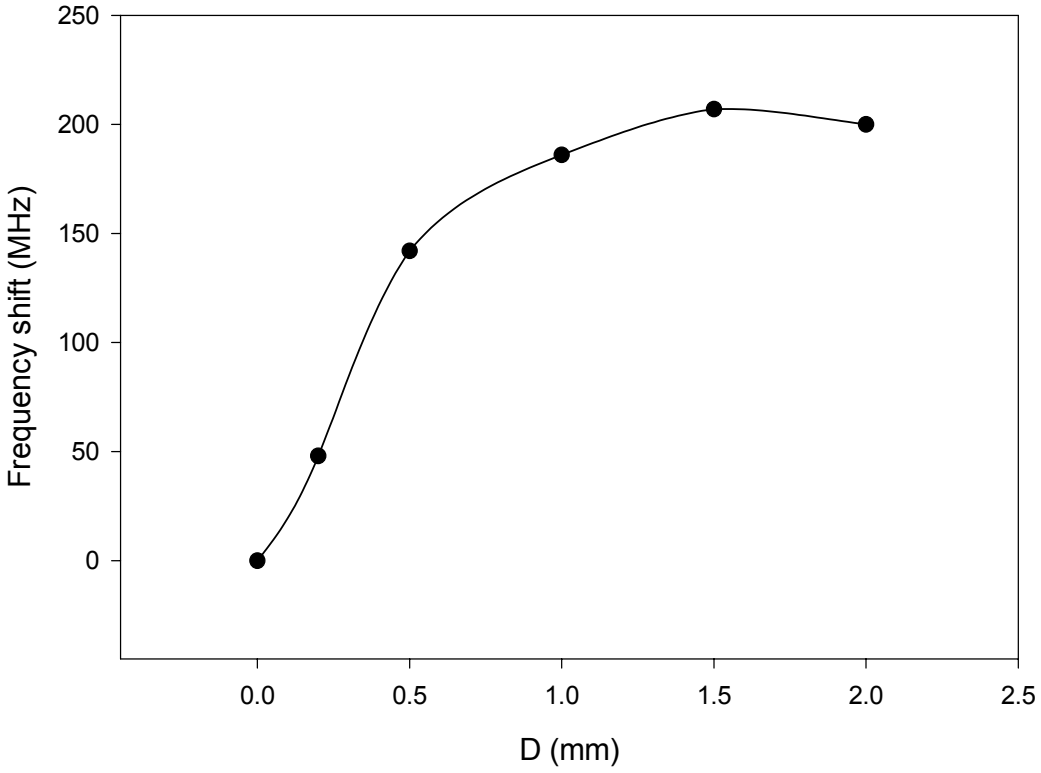

Figure 7-8 Frequency shift produced while tuning a single resonator for the narrowband X band filter

7.2.4. RESPONSE

In this section, the measured and simulated response of the X band narrowband filter will be presented.

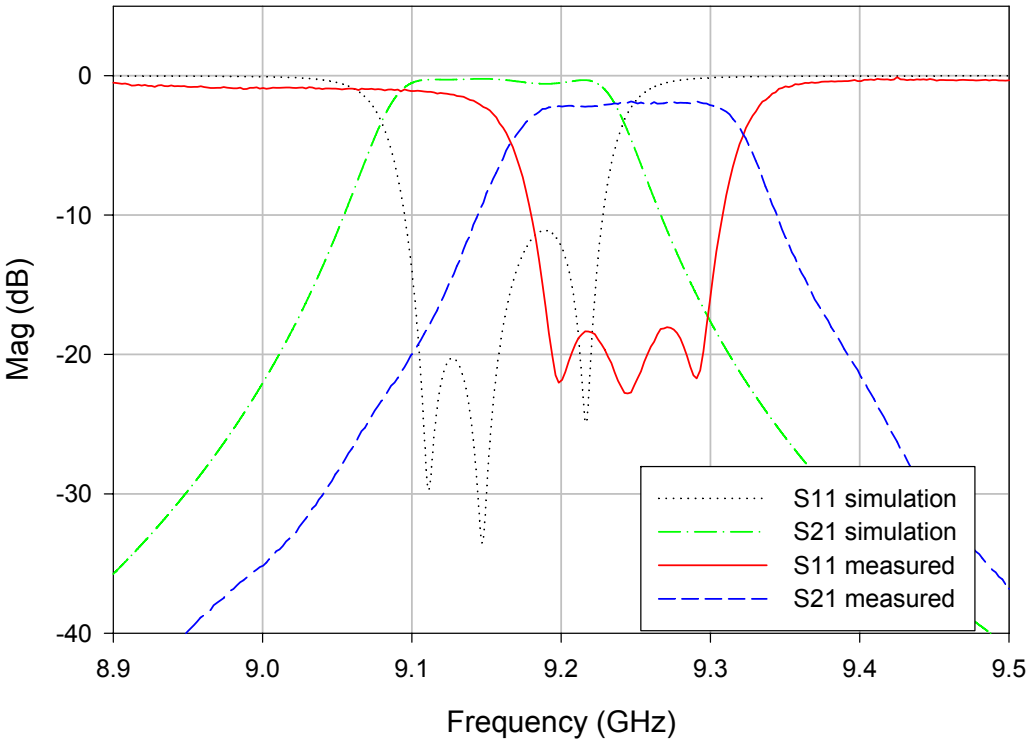

Figure 7-9 Bandpass response of the narrowband X band filter

The bandpass response is shown in Figure 7-9, where a good agreement between theory and experiment was obtained. There is a frequency shift in the response of approximately 0.8 GHz between the simulated and the measured response. This was mainly caused by the effects of the tuning screws on the final response, the fabrication tolerances involved in the realization of this filter, the tolerance in the dielectric constant of the PTFE, and the CAD inaccuracy in the final prediction of the response.

The measured insertion loss for the filter was found to be 2dB. From this measurement, the unloaded quality factor for the half wavelength resonators was extracted using the method presented in Chapter 5, section 5.5, with the aid of a CAD circuit simulator [7-1], which gave an unloaded quality factor of approximately 460, which is in agreement with the value of 480 using 5-53.

Figure 7-10 is a photograph of the X-band narrowband bandpass filter showing its two parts, note the tuning screws on the lid. SMA connectors were used to connect the device. The gaps between the connector and the feed were sealed with copper tape to avoid radiation losses at the transition.

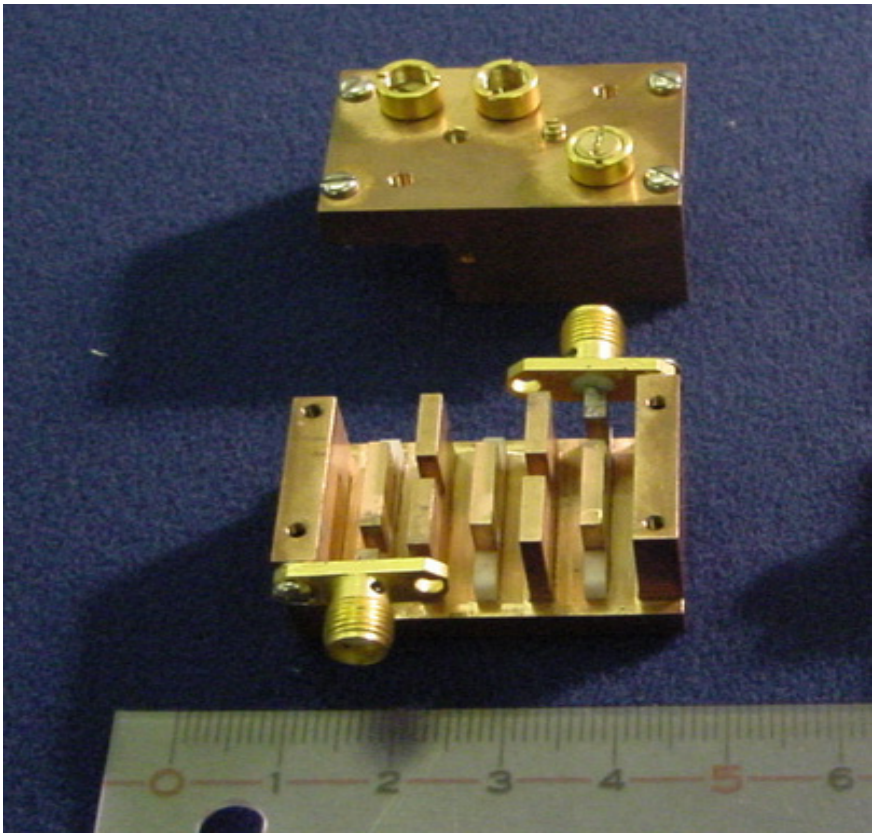

Figure 7-10 Photo of the narrowband X band filter

7.2.5. U-BAND FILTERS

In this section, the simulations of two filters having the structure of Figure 7-5, at higher frequencies will be presented; these filters were designed to operate at 40 GHz and 60 GHz respectively. The problem with these filters is to find the appropriate

dielectric to support the centre conductor; a solution to this problem will be presented in Part II of this chapter, which focuses on self-supported, all-metal structures.

7.2.5.1. TECHNICAL DRAWINGS

The technical drawings for the 40 GHz and 60 GHz filters are shown in Figure 7-11 and Figure 7-12 respectively.

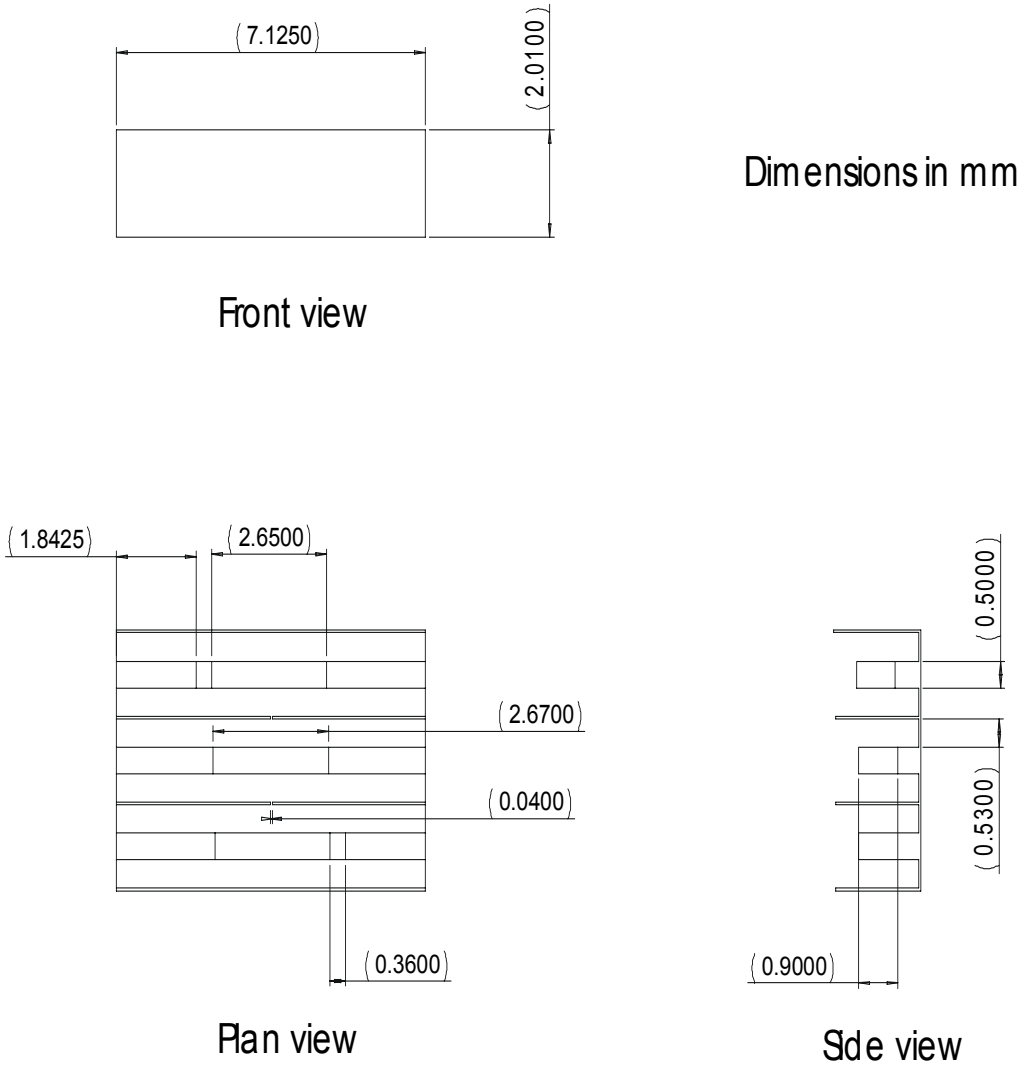

(a)

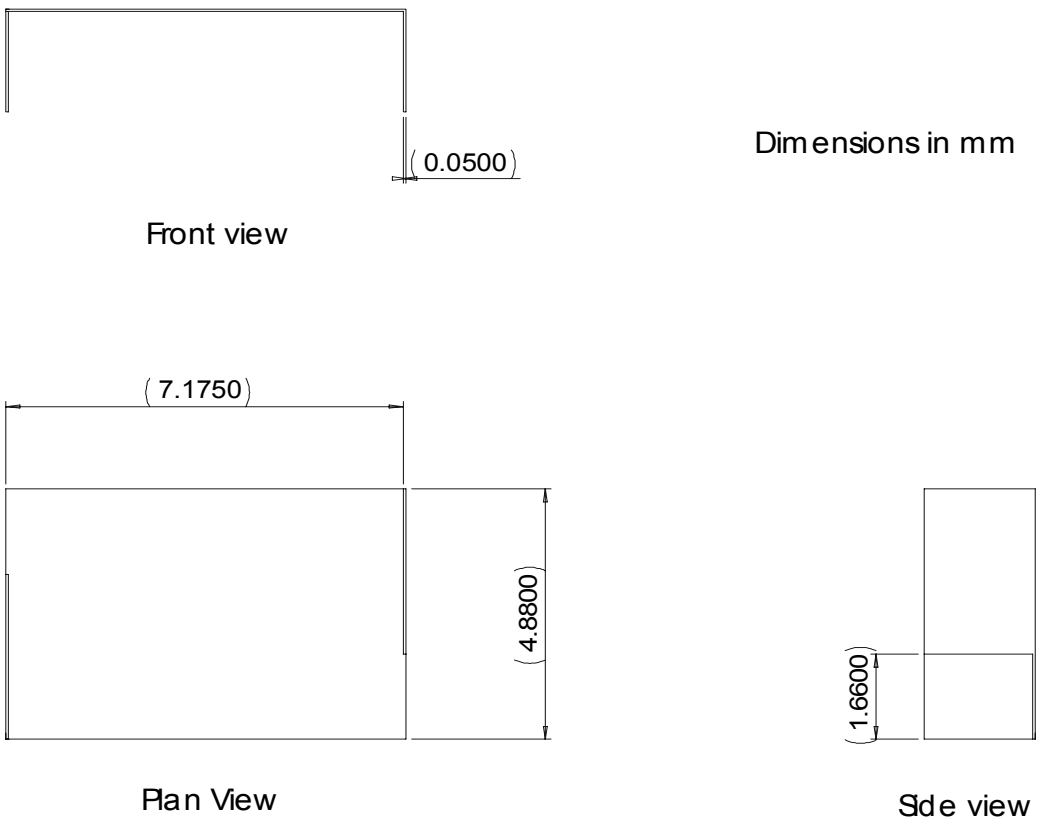

(b)

Figure 7-11 Technical drawings of the narrowband 40 GHz filter
(a) main filter structure (b) lid

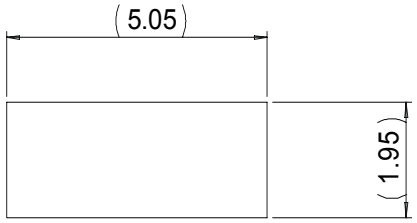

Dimensions in mm

Front view

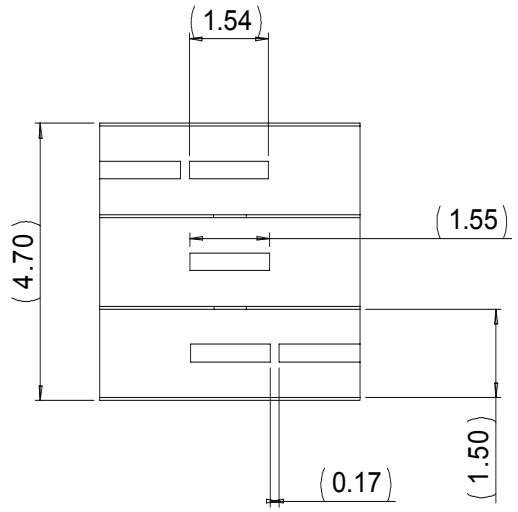

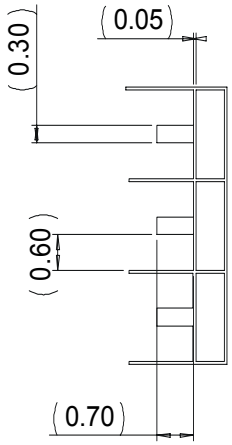

Plan view

Side view

(a)

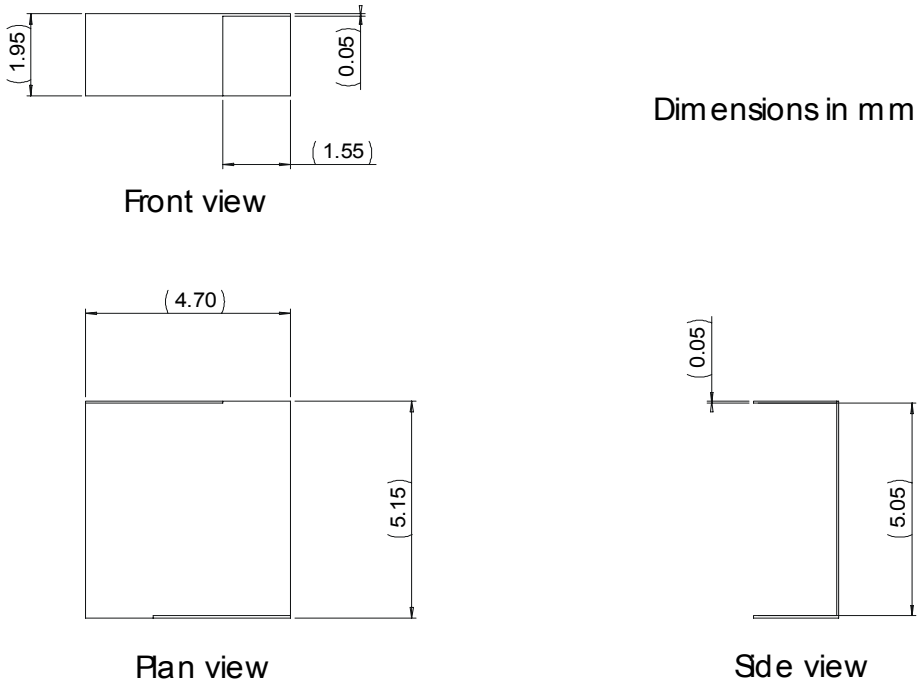

(b)

Figure 7-12 Technical drawings of the narrowband 60 GHz filter
(a) main filter structure (b) lid

7.2.5.2. SIMULATED RESPONSES

The simulated responses for the 40 GHz and 60 GHz filters are shown in Figure 7-13 and Figure 7-14 respectively.

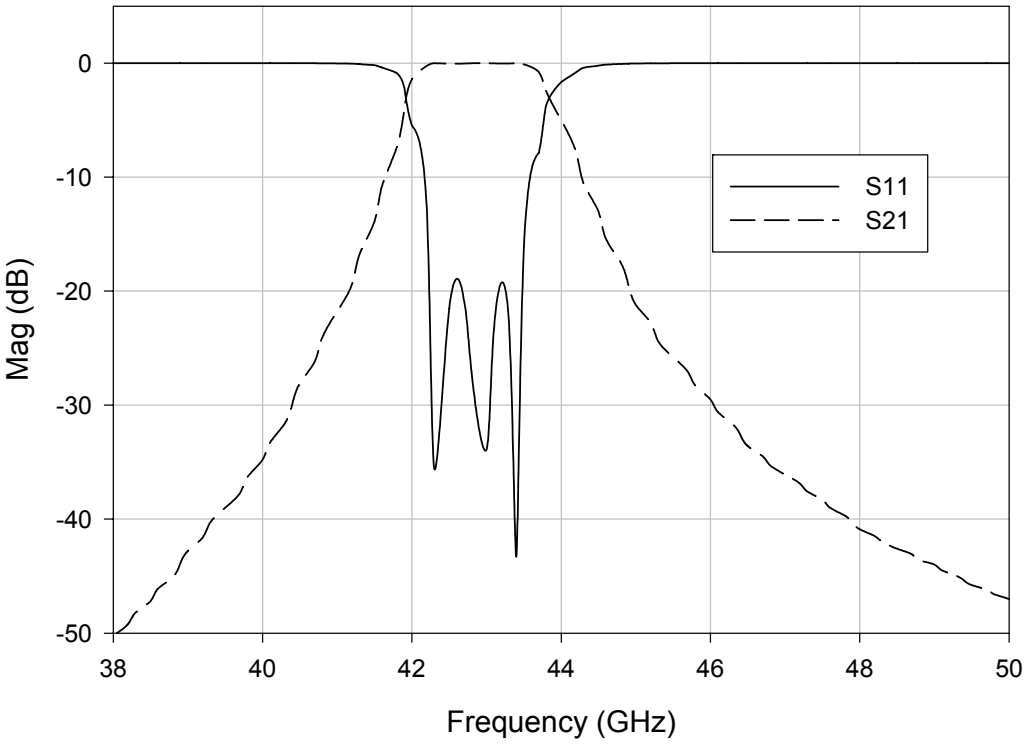

Figure 7-13 Simulated response of the 40 GHz bandpass filter

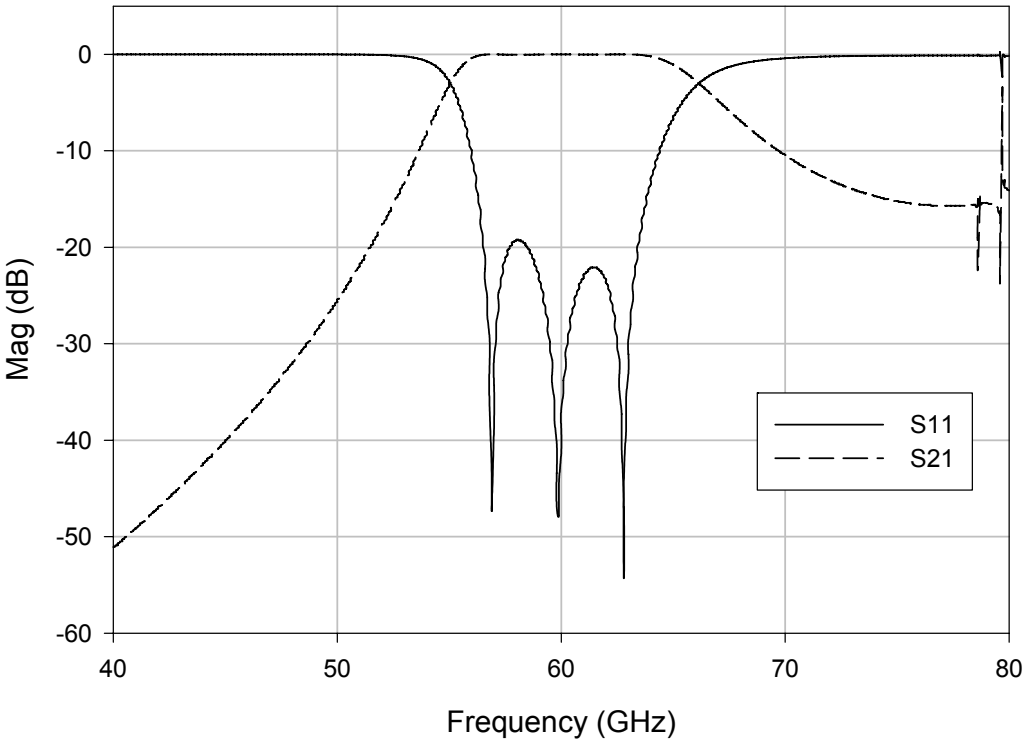

Figure 7-14 Simulated response of the 60 GHz bandpass filter

In Figure 7-14, near the vicinity of 80 GHz, the presence of higher modes distort the out of band response. The filter design can be modified to push these modes further, which will lead to an improved out of passband rejection in this region.

PART II. SELF SUPPORTED FILTERS

7.3. X BAND WIDEBAND FILTER

As seen in the last section, finding an appropriate insulator becomes a problem as the design frequency gets higher. To overcome this problem, self supported metal structures are proposed. The filter discussed in this section was the first step towards

realizing circuits, which consist of stacked copper layers compressed together to form microwave filters.

The filter in this section can be thought of as a transmission line supported by quarter wavelength stubs. Due to its physical nature, it was band limited to a 70% fractional bandwidth filter, with a centre frequency of 9 GHz, with a 0.01 dB band pass ripple. The filter design parameters of this filter are summarized in Table 7-2.

Low pass prototype g values				
g_1= 0.7128	g_2= 1.2003	g_3= 1.3212	g_4= 0.6476	g_5= 1.1007
Characteristic impedances of the shunt stubs				
Z_1= 99.179	Z_2= 50.241	Z_3= 50.24	Z_4= 99.174	
Characteristic impedances of the connecting lines				
Z_{12}= 45.879	Z_{23}= 44.167	Z_{34}= 45.88		

Table 7-2 Design parameters for the wideband X band filter

The design parameters are distributed on the main filter as follows.

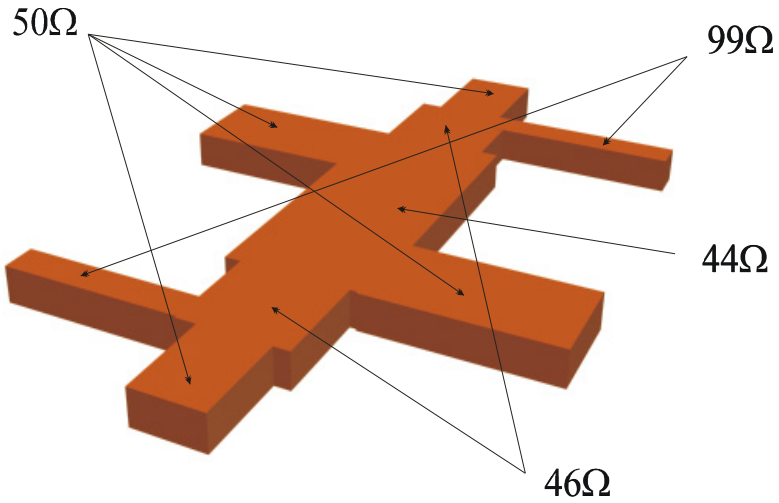

Figure 7-15 Main body of the wideband X band fiter

7.3.1. DESIGN PARAMETERS

The design parameters of the filter were calculated using the design formulae of Chapter 5, section 5.4, and the computed values were adjusted with the aid of a 3D electromagnetic CAD simulator [4-10]. The final coaxial cross-sections for the filter design, which include the cross-sections of the quarter wavelength resonators, and the cross-sections of the quarter wavelength connecting lines between them, are shown in Figure 7-16.

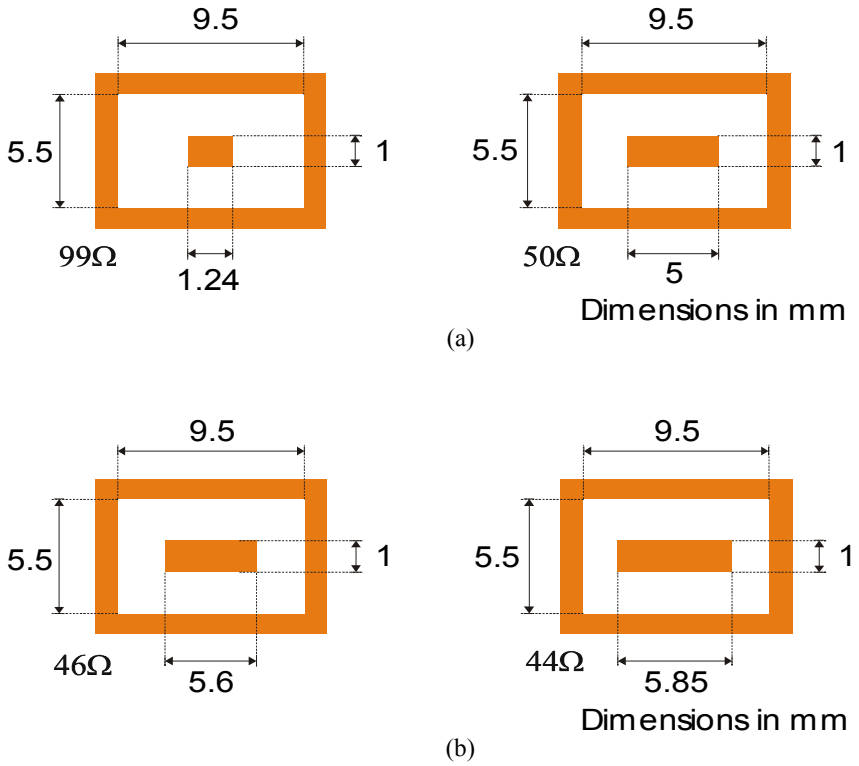

Figure 7-16 Design parameters for the wideband X band filter
(a) shunt stubs (b) connecting lines

7.3.2. FILTER ASSEMBLY AND TECHNICAL DRAWINGS

The filter assembly is shown in Figure 7-17, where five layers of copper were used to form the filter. Layer 3 contains the quarter wavelength supporting stubs and the quarter wavelength connecting lines. Layers 2 and 4 serve to make the coaxial structure, and layers 1 and 5 are plane copper plates that complete the coaxial structure. The five layers are compressed together and aligned with a rod that passes though the alignment holes. Layer 3 is 1 mm thick and layers 2 and 4 are 2.25 mm thick.

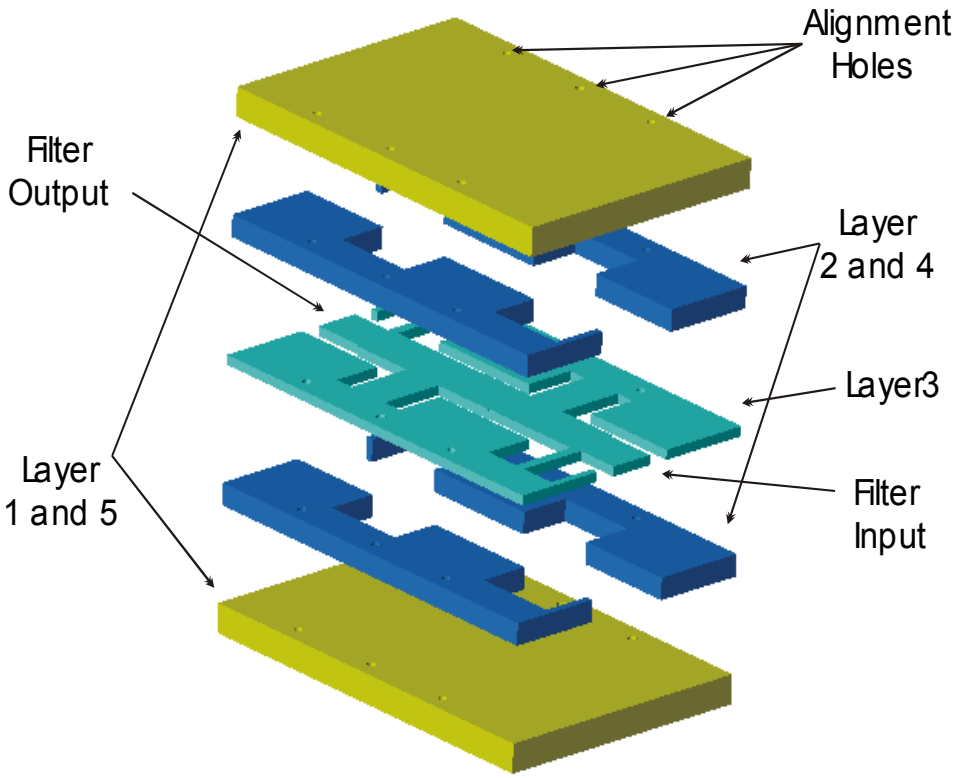

Figure 7-17 Filter assembly for the wideband X band filter

The technical drawings of the five copper layers that compose this filter are shown in Figure 7-18.

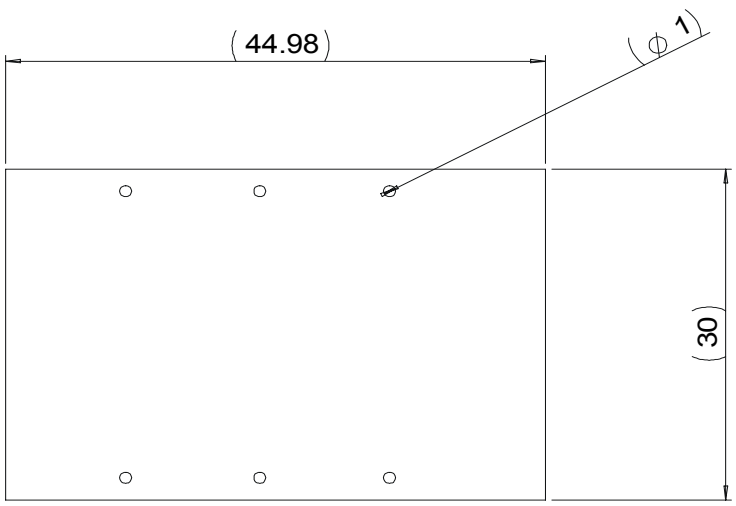

Dimensions in mm

(a)

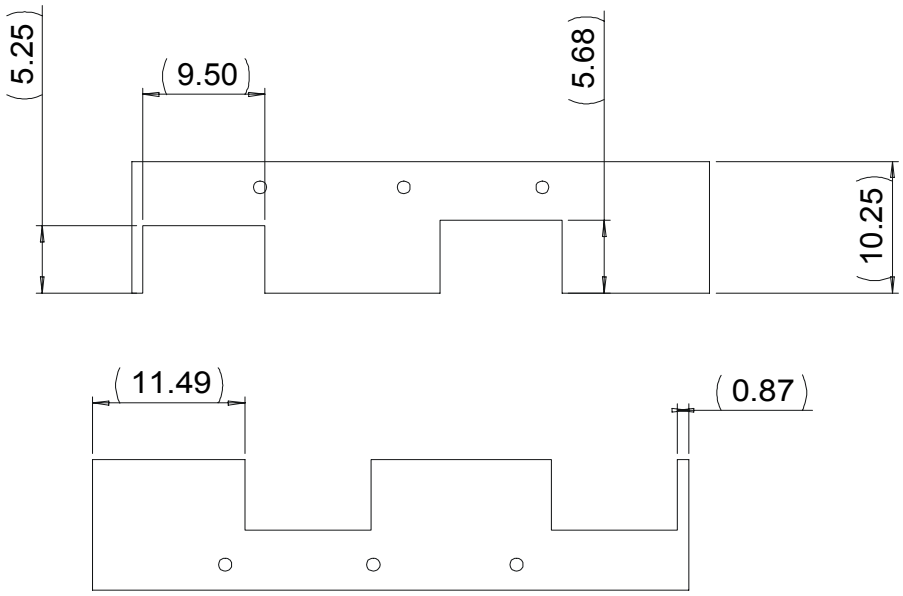

Dimensions in mm

(b)

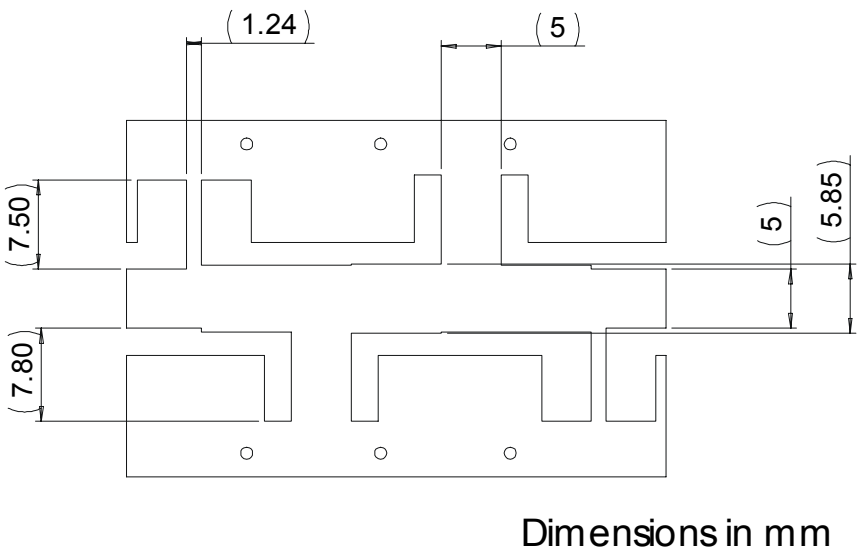

(c)

Figure 7-18 Technical drawings of the wideband X band filter
(a) layers 1 and 5 (b) layers 2 and 4 (c) layer 3

7.3.3. RESPONSE

In this section, the measured and simulated response of the X band wideband filter will be presented.

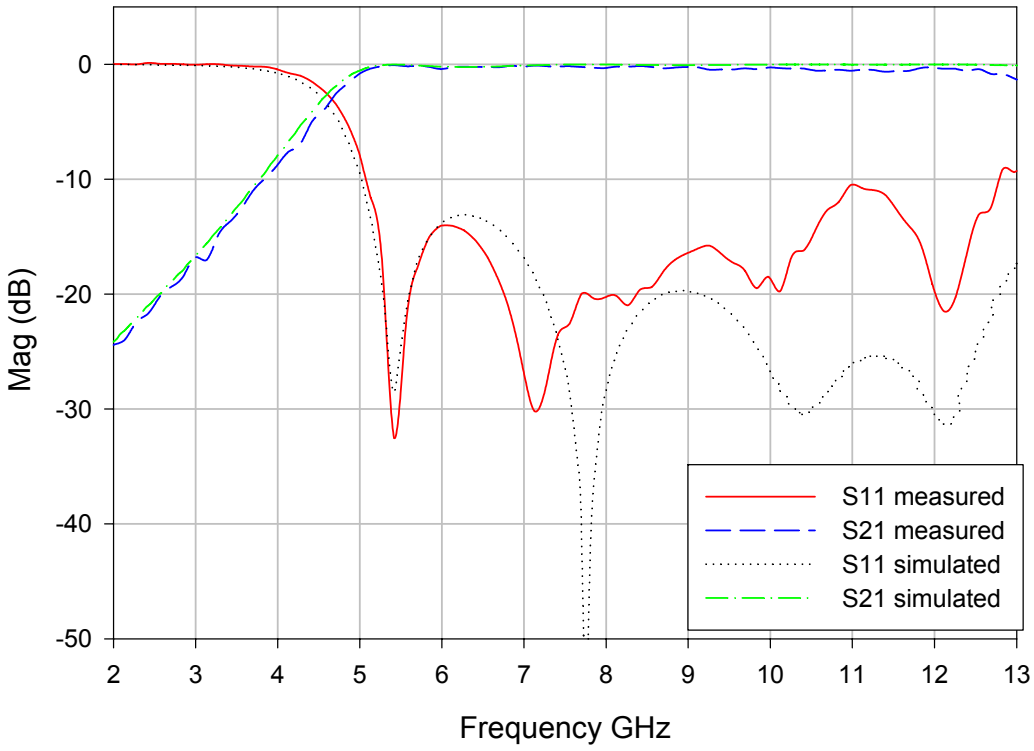

Figure 7-19 Bandpass response of the wideband X band filter

The bandpass response is shown in Figure 7-19, where a good agreement between theory and experiment was obtained. The filter was designed to work up to 13 GHz in a TEM mode; beyond this frequency higher modes propagate through the structure.

The measured insertion loss of the filter was found to be 0.25dB at the centre frequency. The unloaded quality factor for the quarter wavelength resonators was extracted using the method presented in Chapter 5, section 5.5, with the aid of a CAD circuit simulator [7-1], which gave an unloaded quality factor of approximately 150, which is in agreement with the value of 140 obtained using 5-53.

Figure 7-20 shows the photograph of the X band wideband, bandpass filter. In the photograph, the filter is opened to show layer 3, which contains the self-supported

metal structure containing the microwave filter. SMA connectors were used to connect the device.

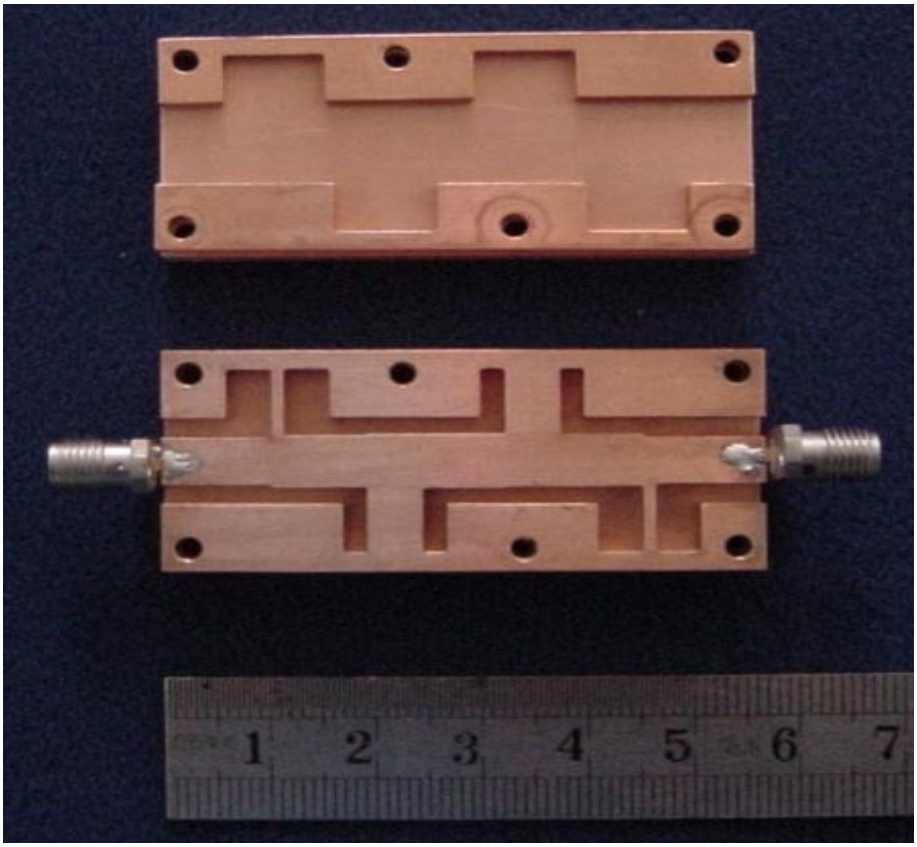

Figure 7-20 Photo of the wideband X band filter

7.4. X BAND DUAL MODE FILTER

After the wideband filter had been designed, the focus of the research changed to demonstrating a narrowband self-supported filter. The final design resulting from this idea was used to make a self-supported dual mode resonator filter. The filter's feed is also a self-supported structure, supported by quarter wavelength stubs. The filter is a 1% fractional bandwidth bandpass filter, with a centre frequency of 9.1 GHz, and a bandpass ripple of 0.01 dB. The filter design parameters are shown in Table 7-3.

g_1= 0.4488	g_2= 0.4077	g_3= 1.1007
$Q_{eA} \approx Q_{eB}$ = 44.88		k_c= 0.023

Table 7-3 Design parameters for the narrow band dual mode filters

7.4.1. THE DUAL MODE RESONATOR

The current flow for the two resonant modes of the dual mode resonator that was used in this filter design is shown in Figure 7-21, where the main current flow on the surface of the dual mode resonator is represented at resonance. One of the resonant modes has its maximum charge distribution following the line approximately across the length of the resonator, as shown in Figure 7-21a, similarly the other resonant mode is represented in Figure 7-21b.

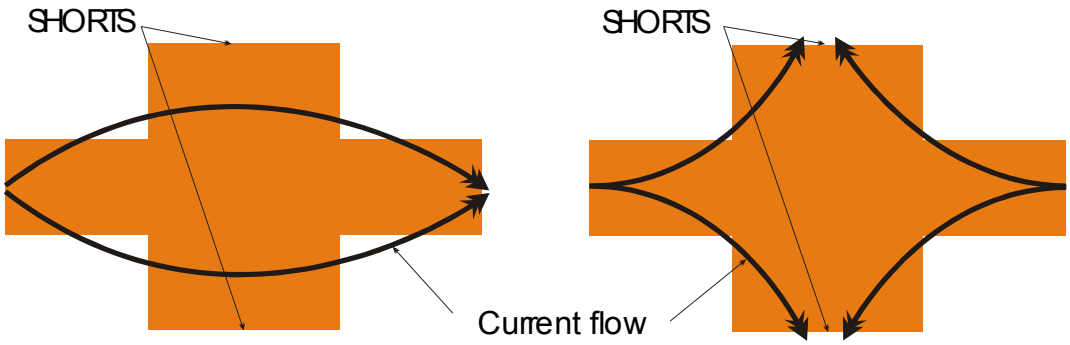

(a) (b)

Figure 7-21 Current flow on the dual mode resonator at resonance

An equivalent circuit of the dual mode resonator is shown in Figure 7-22, the circuit has two LC circuits connected together through an admittance inverter as discussed in section 5.3.2. This equivalent circuit consists of two coupled quarter wavelength resonators.

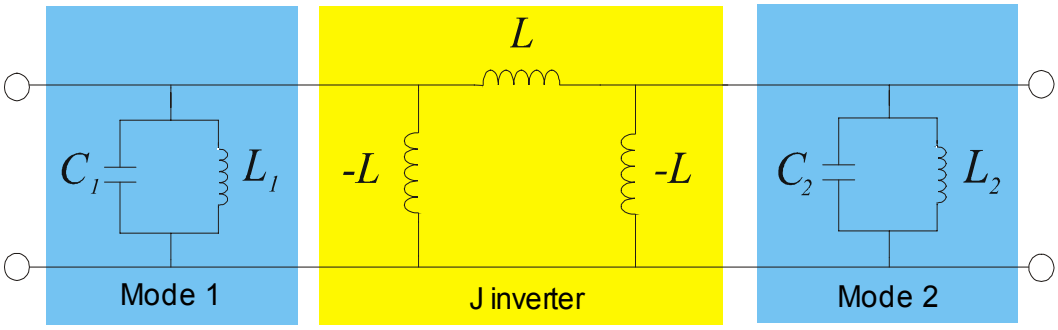

Figure 7-22 Equivalent circuit of the dual mode resonator, modelled as two coupled quarter wavelength resonators

7.4.2. DESIGN PARAMETERS

In this section, the procedure used to get the coupling between the two resonant modes of the dual mode resonator used in this filter, and the filter in section 7.5 will be explained. The couplings were calculated using the theory explained in Chapter 5, section 5.3.4.2, and were set by modifying the dimensions A and B on Figure 7-23.

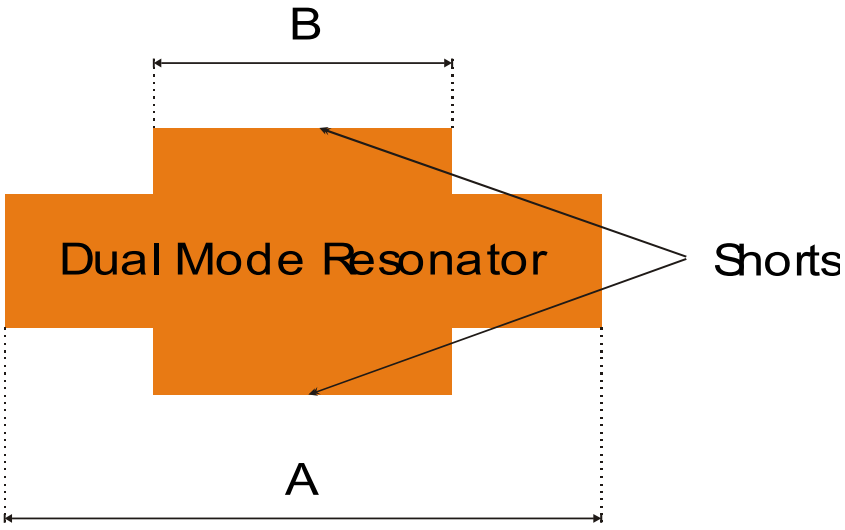

Figure 7-23 Setting the coupling between the two modes of the dual mode resonator

The most important issue to consider here is that when the dimensions of the dual mode filter are altered, the resonant frequency of the final filter response will also be altered. The resonant frequency can be set to be the one which is desired, by synchronically tuning the resonator's dimensions, while obtaining the coupling specified by the design parameters. In other words the final filter response is obtained by changing both dimensions, A and B in Figure 7-23, to satisfy the coupling coefficient as well as the frequency response for the filter.

To set the coupling coefficient, one of the two dimensions in Figure 7-23 is fixed. In Figure 7-24 the coupling coefficient when varying the distance A is plotted, while the distance B is fixed.

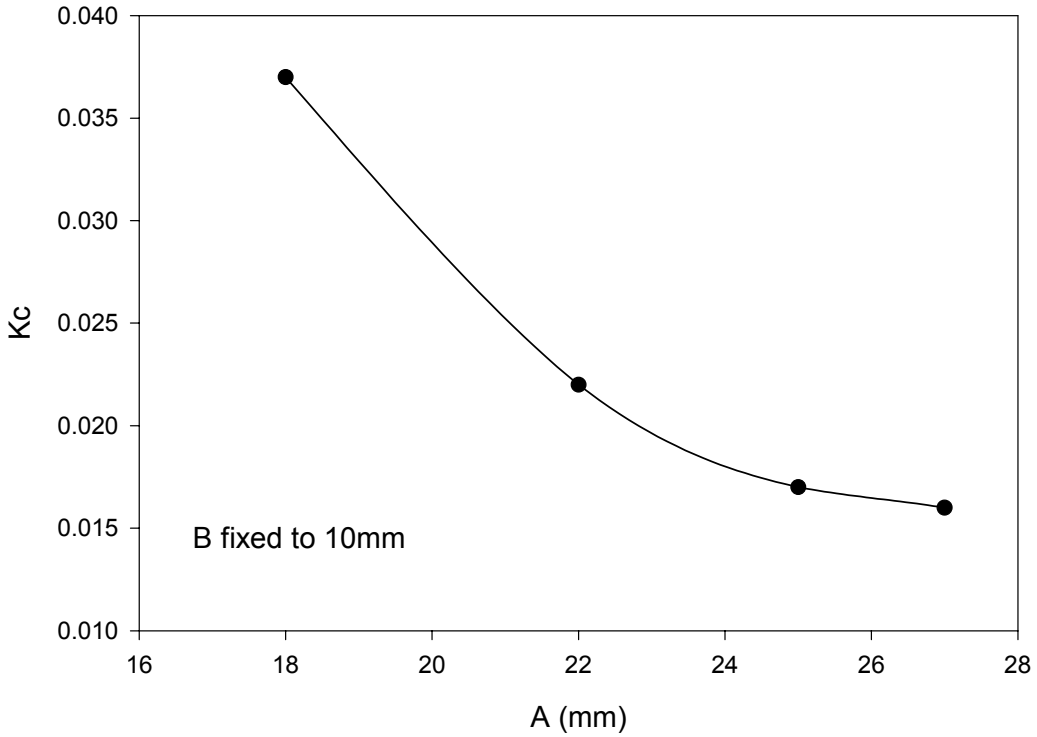

Figure 7-24 Setting the coupling for the dual mode X band resonator with B fixed

Similarly, the coupling coefficient when varying the distance B, is plotted while the distance A is fixed in Figure 7-25.

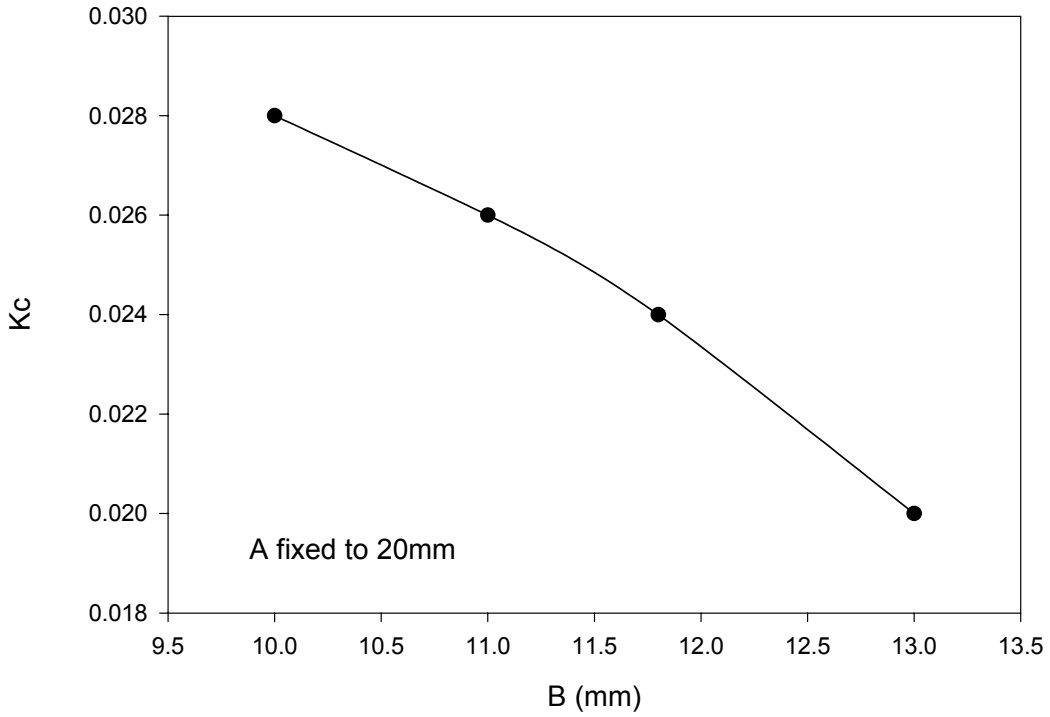

Figure 7-25 Setting the coupling for the dual mode X band resonator with A fixed

The external quality factor was set with the simulator [4-10] to give the desired bandpass response after ensuring the correct coupling between modes. This was done by varying the distance *d* in Figure 7-26, to give the desired final filter response.

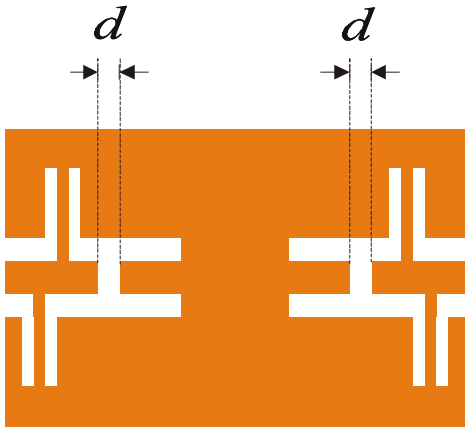

Figure 7-26 Finding Q_e for the dual mode X band filter

7.4.3. THE FEED

To feed the self-supported dual mode resonator, a self-supported feed was designed. The design consists of a 50Ω transmission line, which is supported by quarter wavelength stubs as shown on Figure 7-27.

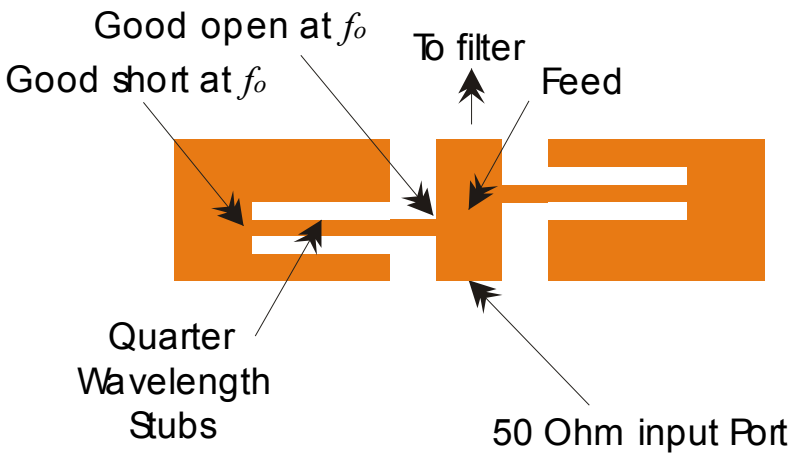

Figure 7-27 Feed of the dual mode filter

The filter's feed was designed and simulated independently, before it was inserted to form the final filter structure; the simulated response of the feed by itself is shown in Figure 7-28.

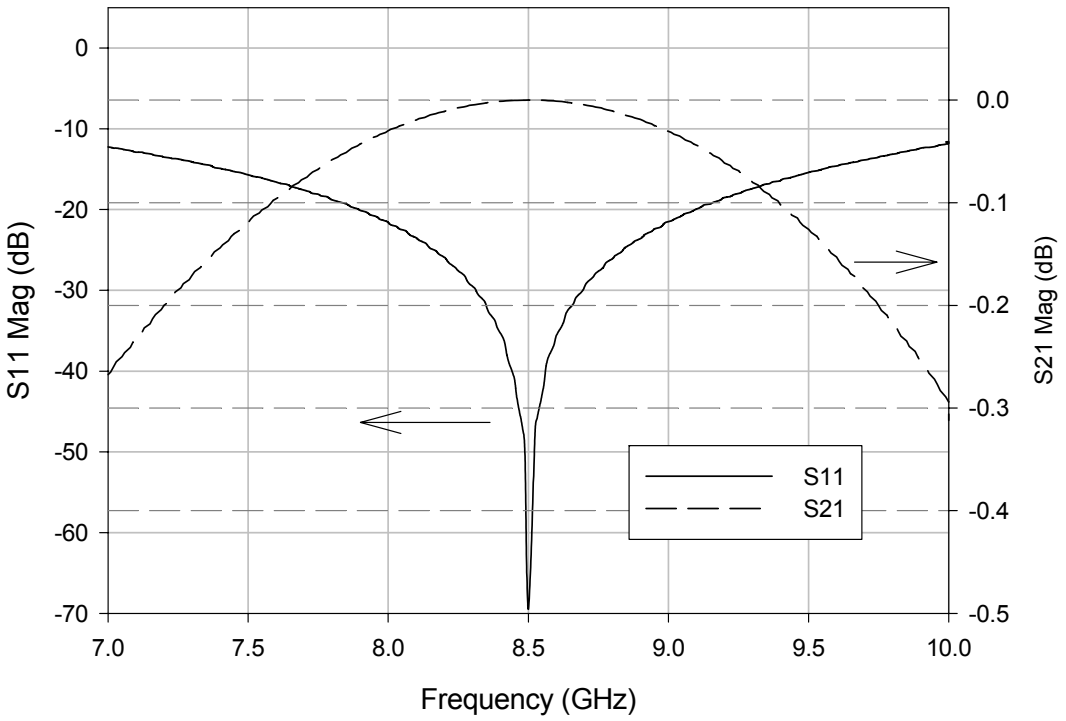

Figure 7-28 Simulated response of the feed for the dual mode X band filter

7.4.4. FILTER ASSEMBLY AND TECHNICAL DRAWINGS

The filter was made from five copper layers as shown in Figure 7-29; layer three contains the dual mode resonator at the centre of the piece, with its respective feed on either side. The five copper layers were compressed together, and aligned with a rod passing through the alignment holes. All layers are 2 mm thick.

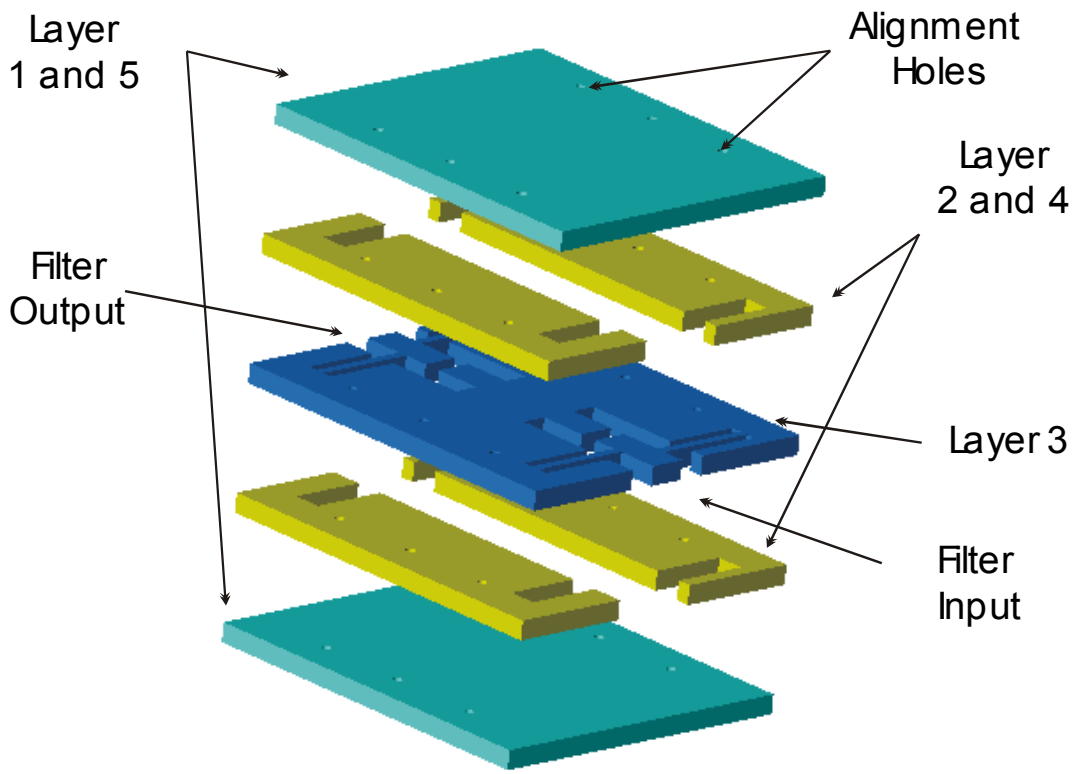

Figure 7-29 Filter assembly of the dual mode X band filter

The technical drawings of the five pieces that compose this filter are shown in Figure 7-30.

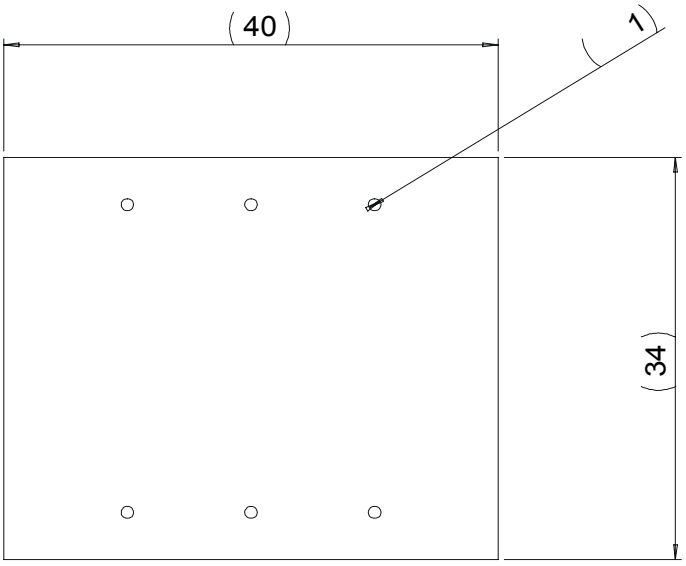
40
1
34
Dimensions in mm

(a)

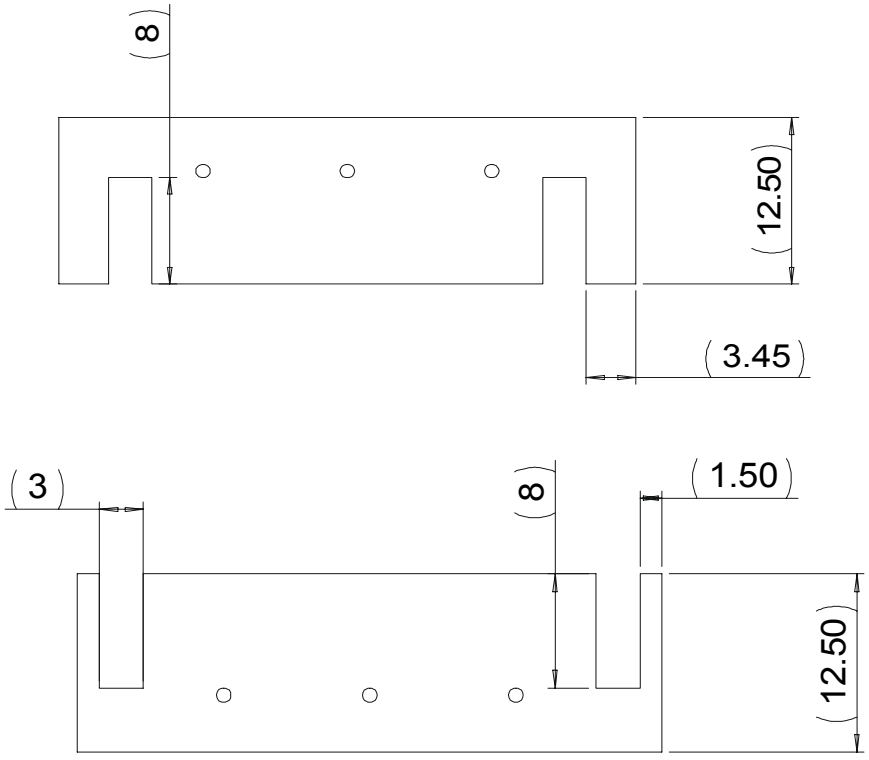
8
12.50
3.45
3
8
1.50
12.50
Dimensions in mm

(b)

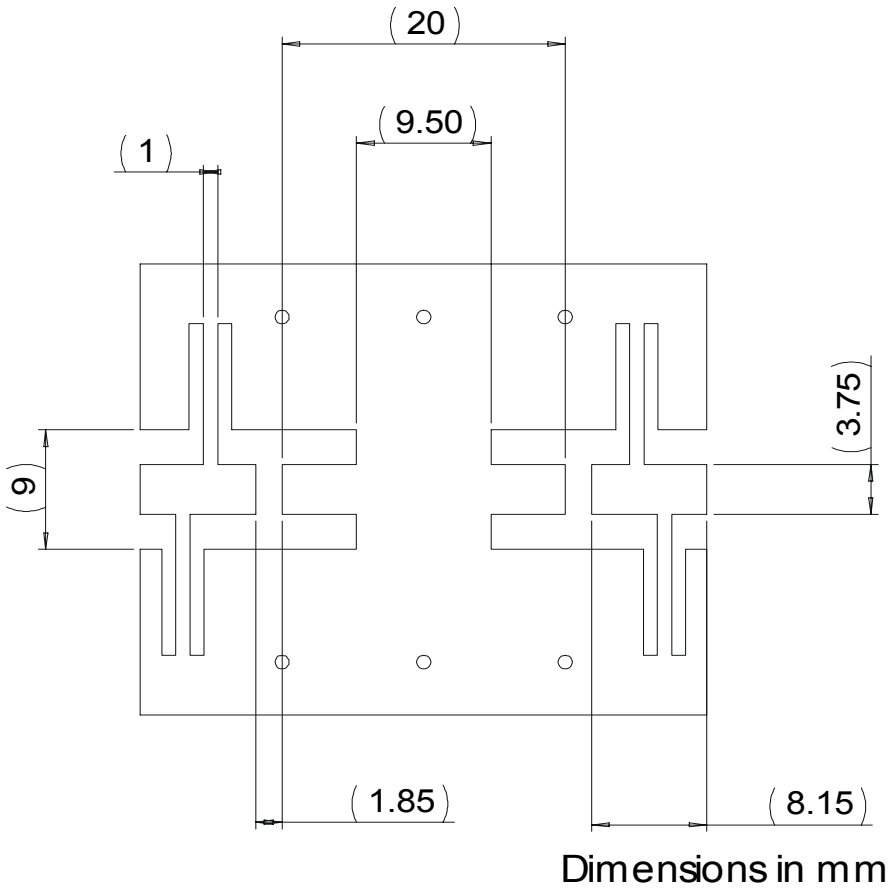

(c)

Figure 7-30 Technical drawings of the dual mode X band filter
(a) layers 1 and 5 (b) layers 2 and 4 (c) layer 3

7.4.5. RESPONSE

In this section, the measured and simulated response of the X band dual mode filter will be presented.

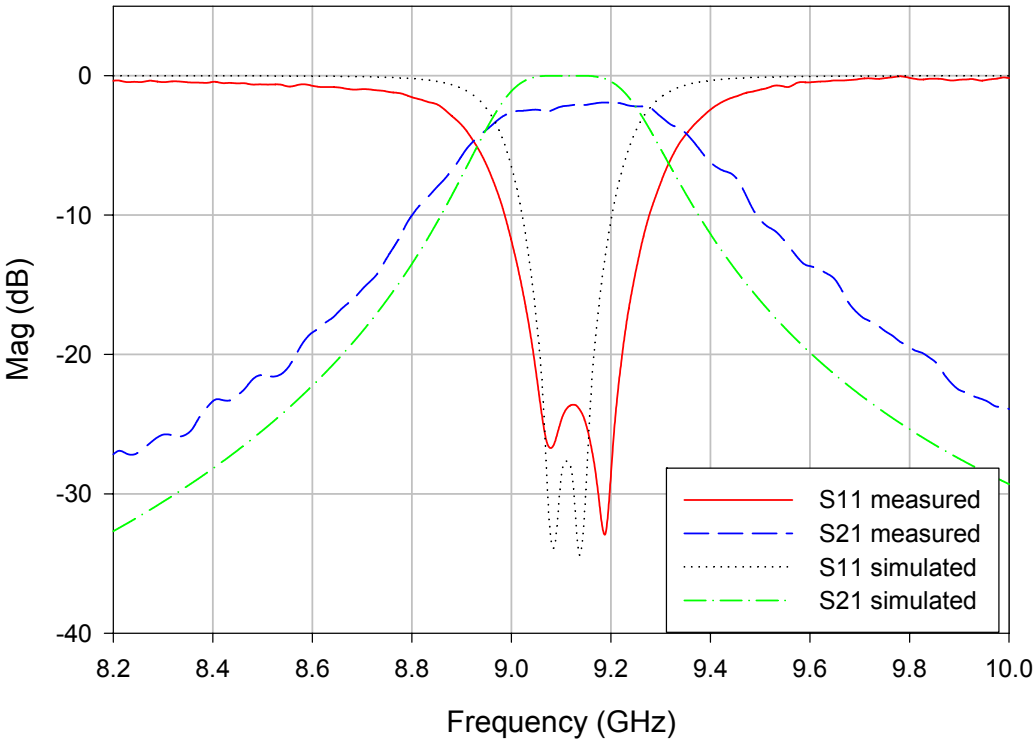

Figure 7-31 Bandpass response of the dual mode X band filter

The bandpass response of the dual mode X-band filter is shown in Figure 7-31, where a good agreement between theory and experiment was obtained. The measured insertion loss of the filter was found to be 2.2dB. From this measurement, the unloaded quality factor for the dual mode resonator was extracted, using the method presented in Chapter 5, section 5.5, with the aid of a CAD circuit simulator [7-1], which gave an unloaded quality factor of approximately 190, which is in agreement with the value of 170 obtained using 5-53. The measured bandwidth increased due to layer misalignment, which changed the coupling between the two modes.

Figure 7-32 shows the photograph of the dual mode X-band bandpass filter; in the photograph, the filter was opened to show layer 3, which contains the self-supported metal structure containing the microwave dual mode resonator, with its self-supported feeds. SMA connectors were used to connect the device.

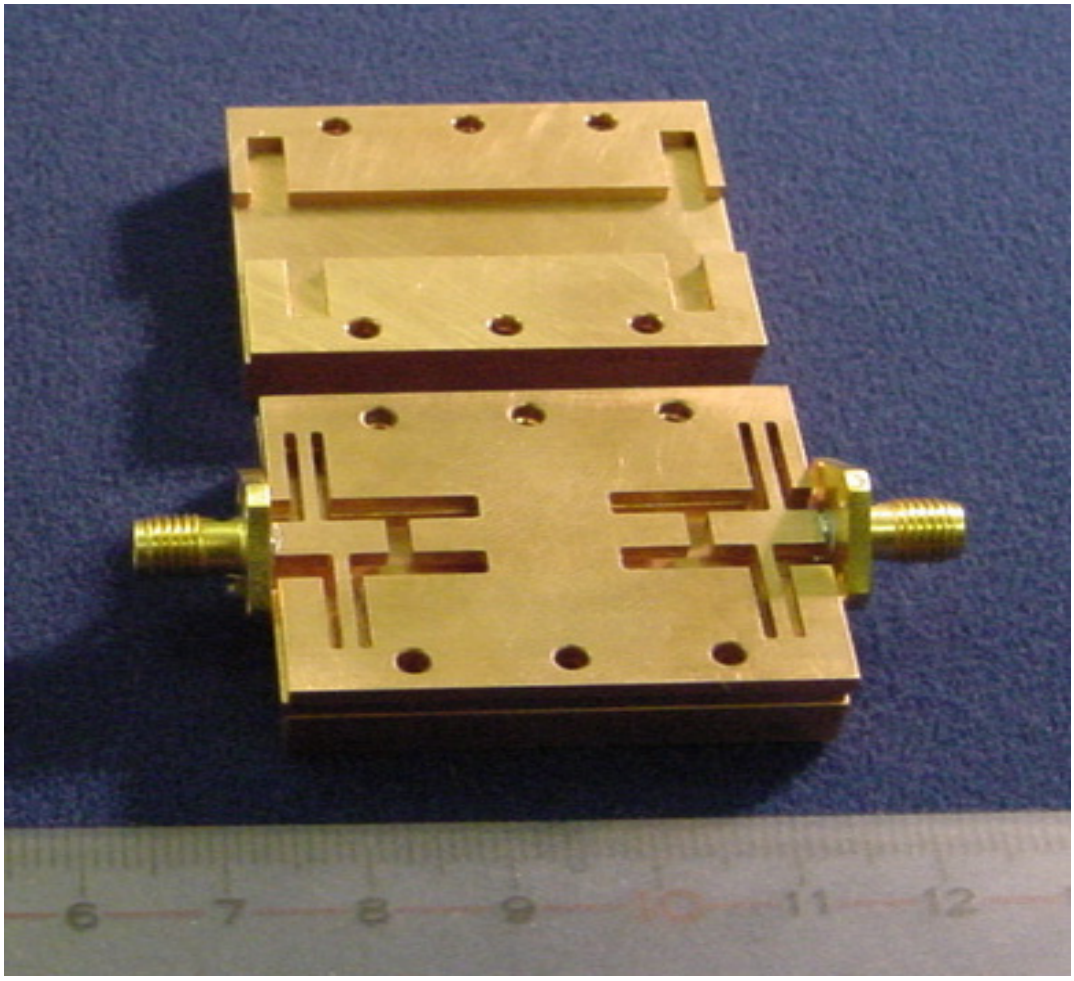

Figure 7-32 Photo of the dual mode X band filter

7.5. KA BAND DUAL MODE MICROMACHINED FILTER

This filter has the same structure as the filter discussed in section 7.4. Here the filter was designed to satisfy the LMDS specification shown in Table 1-2. The filter design parameters are summarized in Table 7-3. The filter is a 1% fractional bandwidth filter, with a centre frequency of 29.75 GHz, and a 0.01dB passband ripple.

7.5.1. DESIGN PARAMETERS

The procedure to obtain the coupling coefficient for this filter was explained in section 7.4.2, referring to Figure 7-23 and the theory described in Chapter 5, section 5.3.3.2. The coupling coefficient when varying the distance A is plotted in Figure 7-33, while the distance B is fixed.

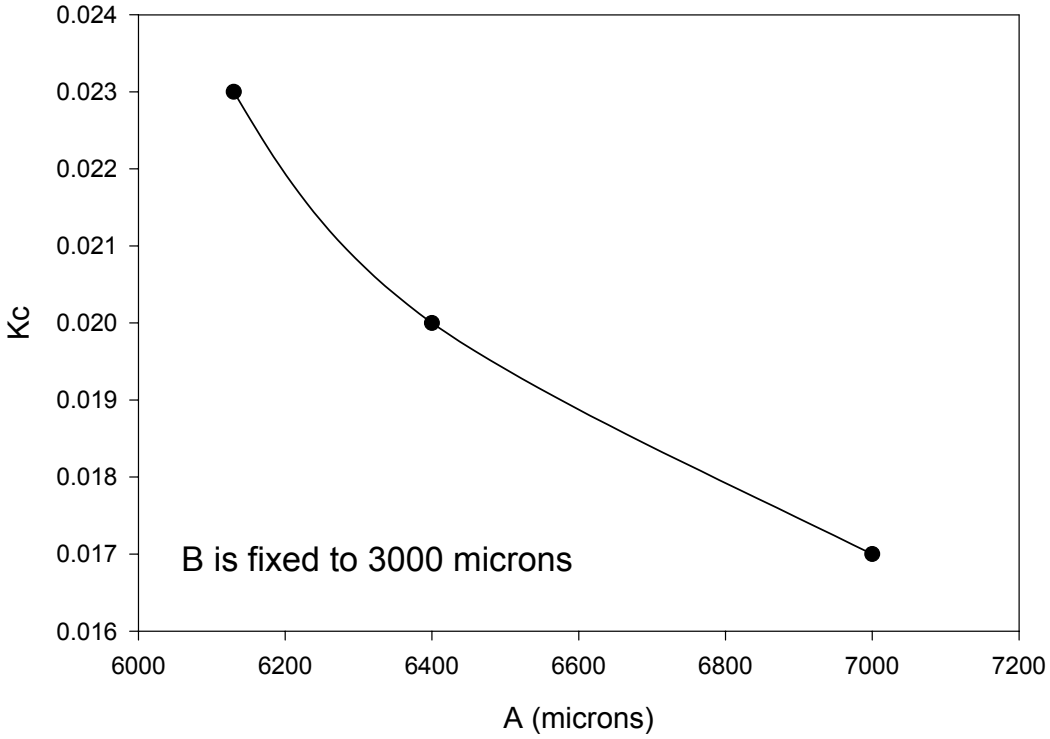

Figure 7-33 Setting the coupling for the dual mode Ka band resonator with B fixed

Similarly, referring to Figure 7-23, the coupling coefficient when varying the distance B is plotted, while the distance A is fixed in Figure 7-34.

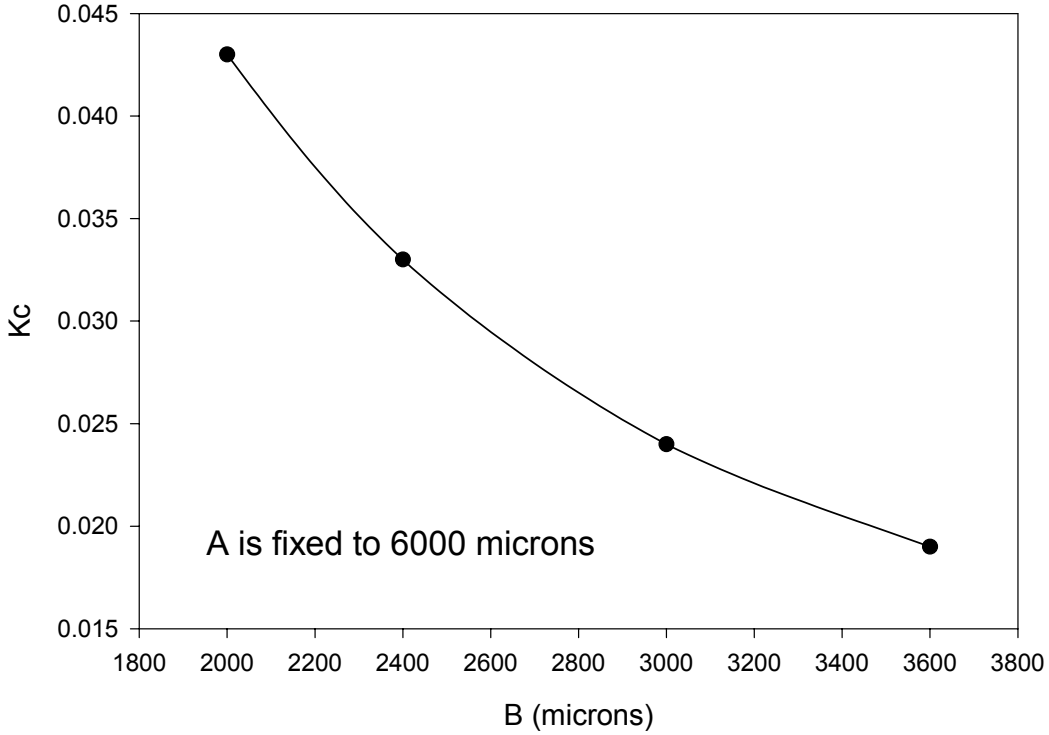

Figure 7-34 Setting the coupling for the dual mode Ka band resonator with A fixed

The external quality factor was set with the simulator [4-10] to give the desired bandpass response after ensuring the correct coupling between modes. The procedure is shown in Figure 7-26, where *d* is adjusted to give the desired filter response.

7.5.2. THE FEED

The feed of this filter was explained in section 7.4.3, and has the form of Figure 7-27. The simulated response for the feed used in the Ka band dual mode filter is shown in Figure 7-35.

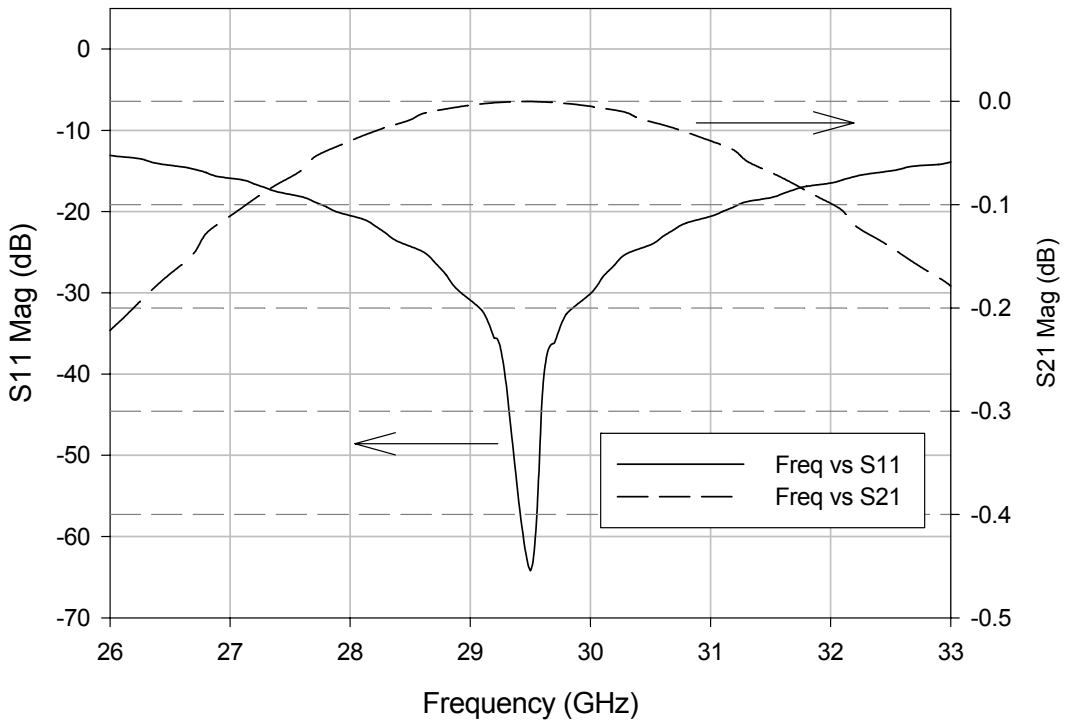

Figure 7-35 Simulated response of the feed for the dual mode Ka band filter

7.5.3. FILTER ASSEMBLY AND TECHNICAL DRAWINGS

The filter was made from five copper layers as shown in Figure 7-37; layer three contains the dual mode resonator at the centre of the piece, with its respective feeds on either side. This layer also contains a mark, which served as a guide for the K connector assembly, defining the centre of the series of holes used to mount the K connector as shown in Figure 7-36, where the holes were drilled once the copper layers were compressed together. The glass bead of the connector was inserted directly into the machined pieces after drilling the holes. The five copper layers were aligned with a 0.5mm stainless steel rod passing through the alignment holes.

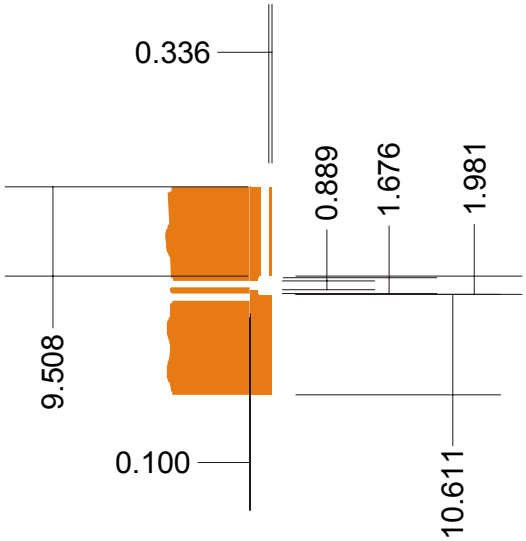

Figure 7-36 K connector assembly for the Ka band dual mode filter (side view)

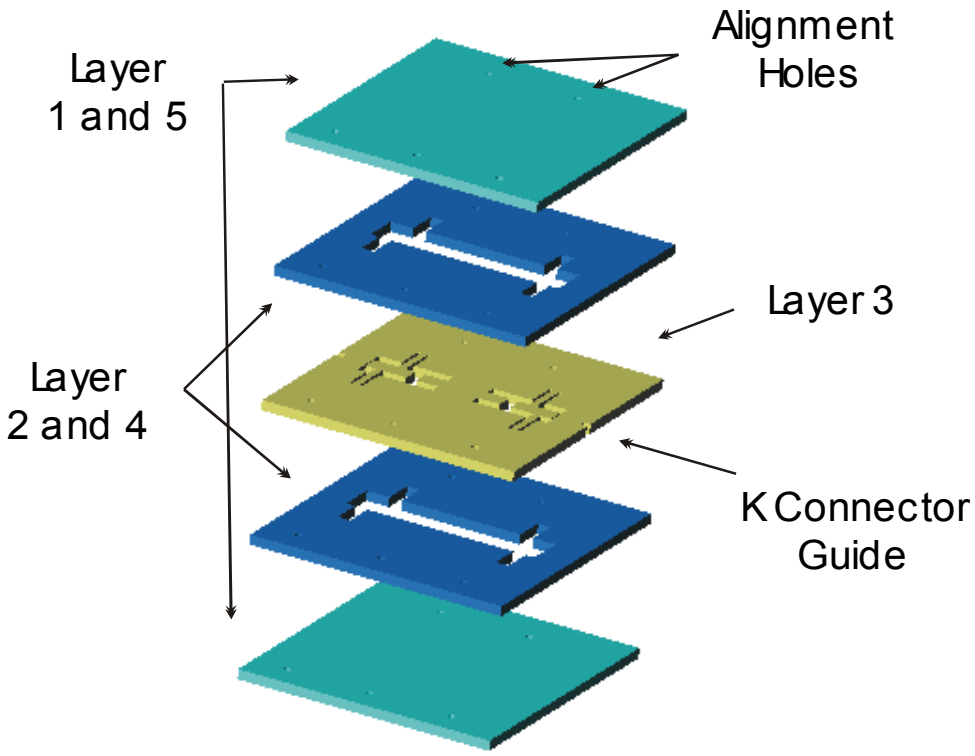

Figure 7-37 Filter assembly of the dual mode Ka band filter

The technical drawings of the five pieces that compose this filter are shown in Figure 7-38

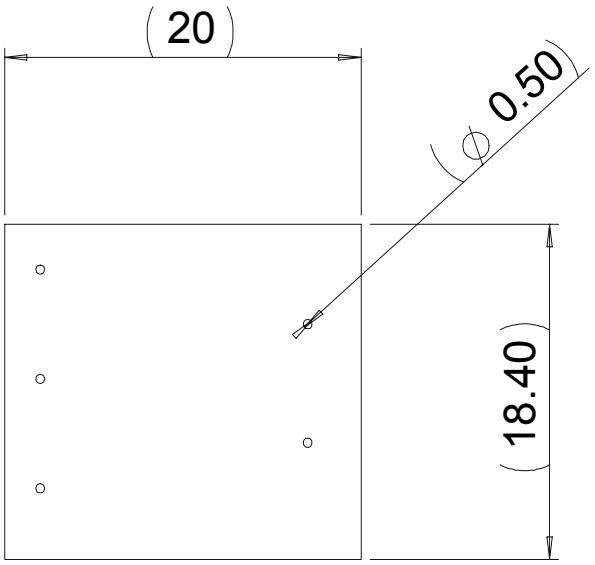
20
ϕ 0.50
18.40
Dimensions in mm

(a)

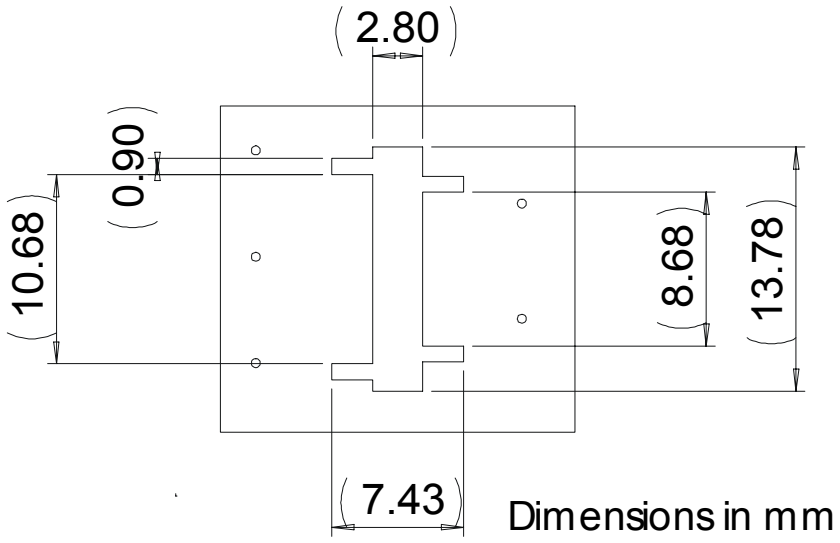
2.80
0.90
10.68
8.68
13.78
7.43
Dimensions in mm

(b)

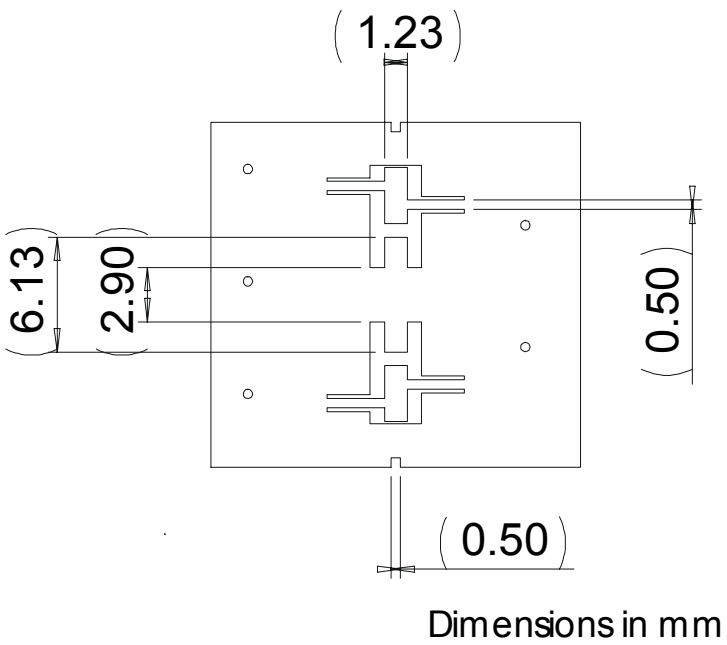

(c)

Figure 7-38 Technical drawings of the dual mode Ka band filter
(a) layers 1 and 5 (b) layers 2 and 4 (c) layer 3

7.5.4. LASER MICROMACHINED FILTER

The Ka band dual mode filter was made out of 700 micron thick copper plates, which were laser micromachined and then stacked and compressed together to form the final filter. The individual pieces that form this filter are shown in Figure 7-39.

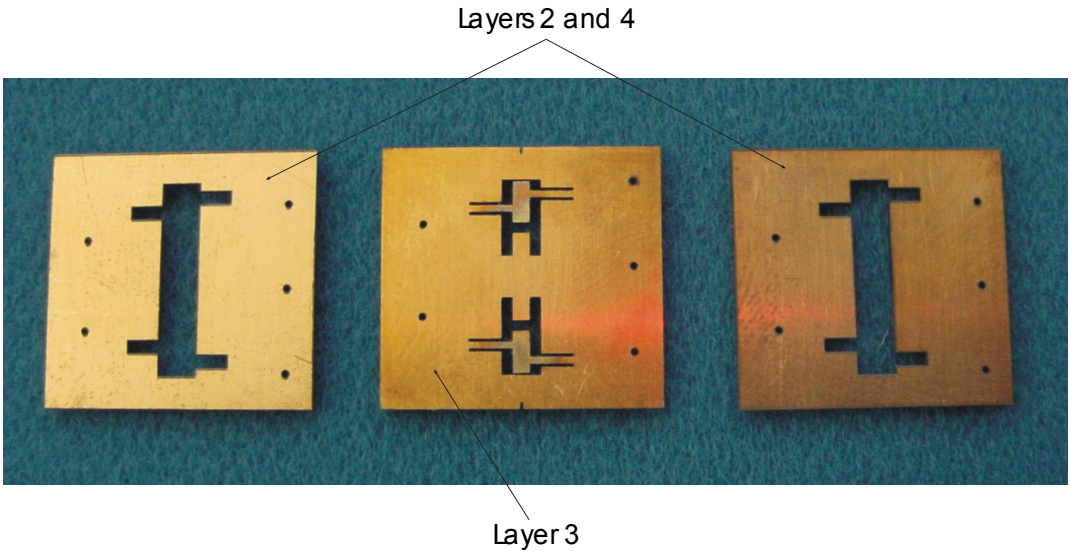

Figure 7-39 Main layers of the Ka band dual mode micromachined filter

The filter was enclosed in a brass box, which holds the complete structure together including the K connectors; the technical drawings for the box are shown in Figure 7-40.

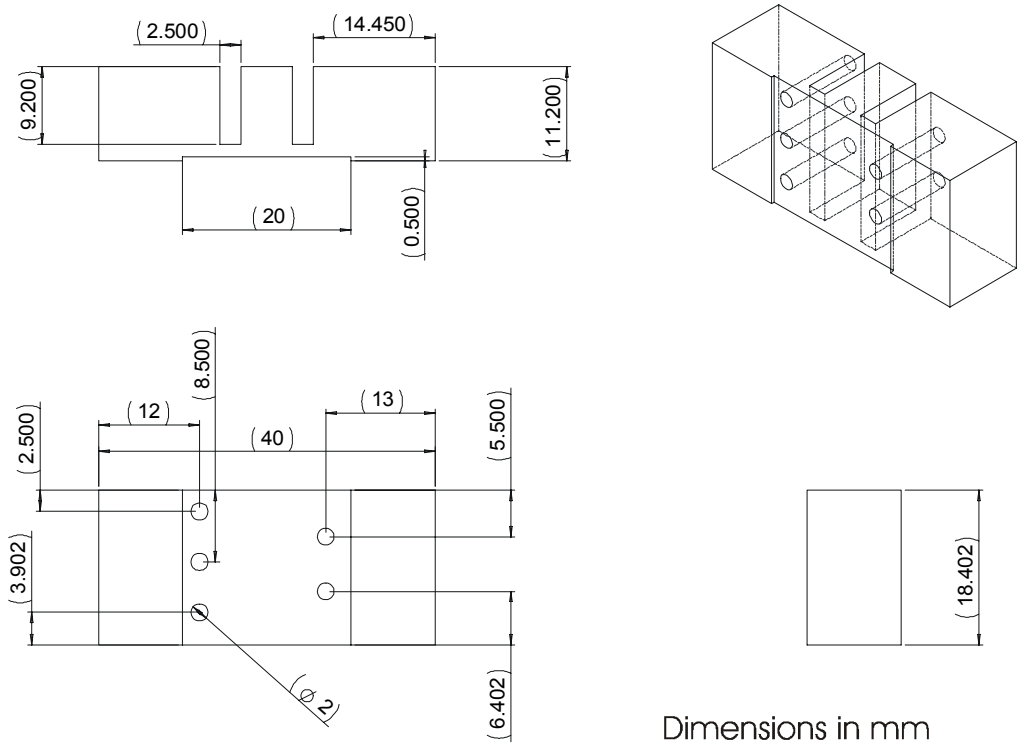

(a)

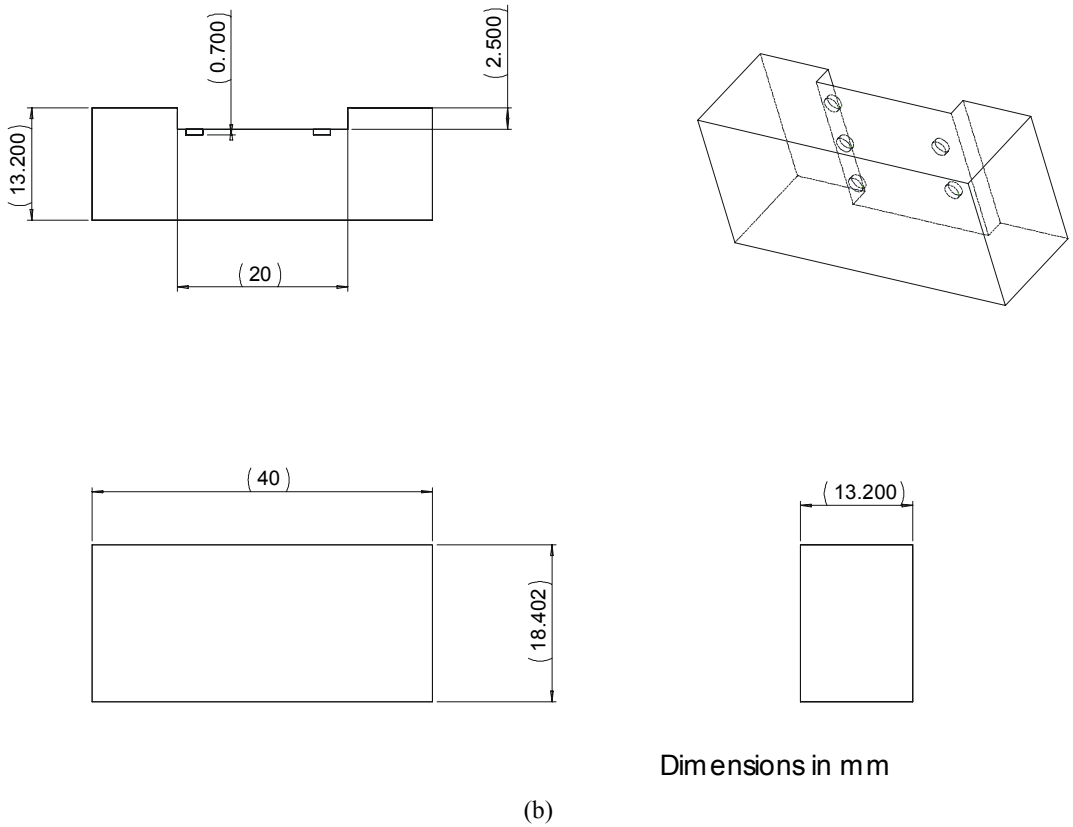

(b)

Figure 7-40 Brass box for the Ka band dual mode filter

The Ka band dual mode filter is shown in Figure 7-41, where the five copper layers form the filter, and the brass box holds the K connectors and compresses the complete filter.

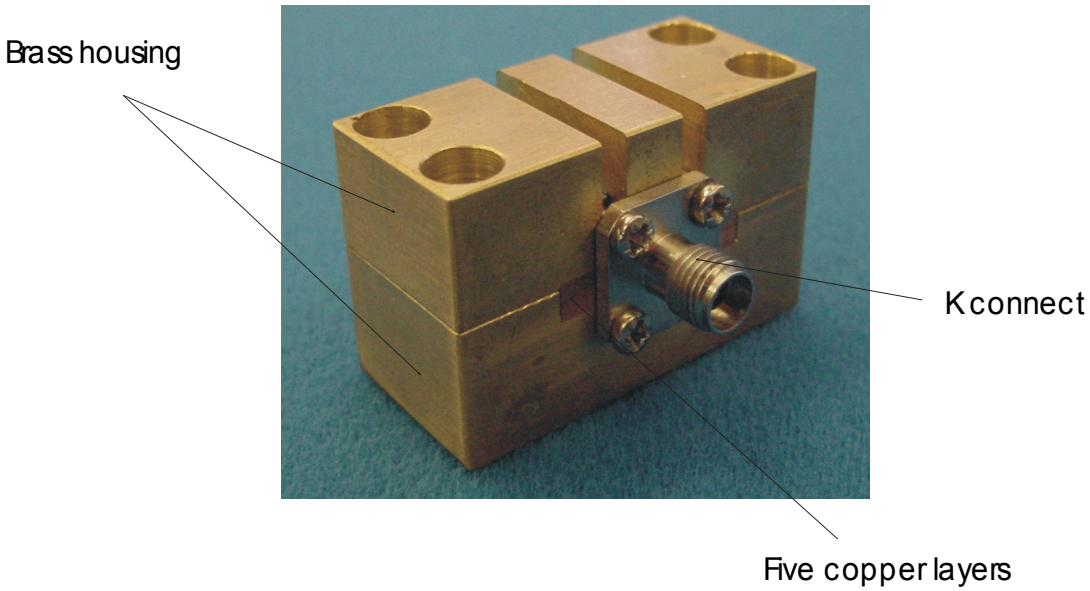

Figure 7-41 Photo of the Ka band dual mode filter

7.5.5 RESPONSE

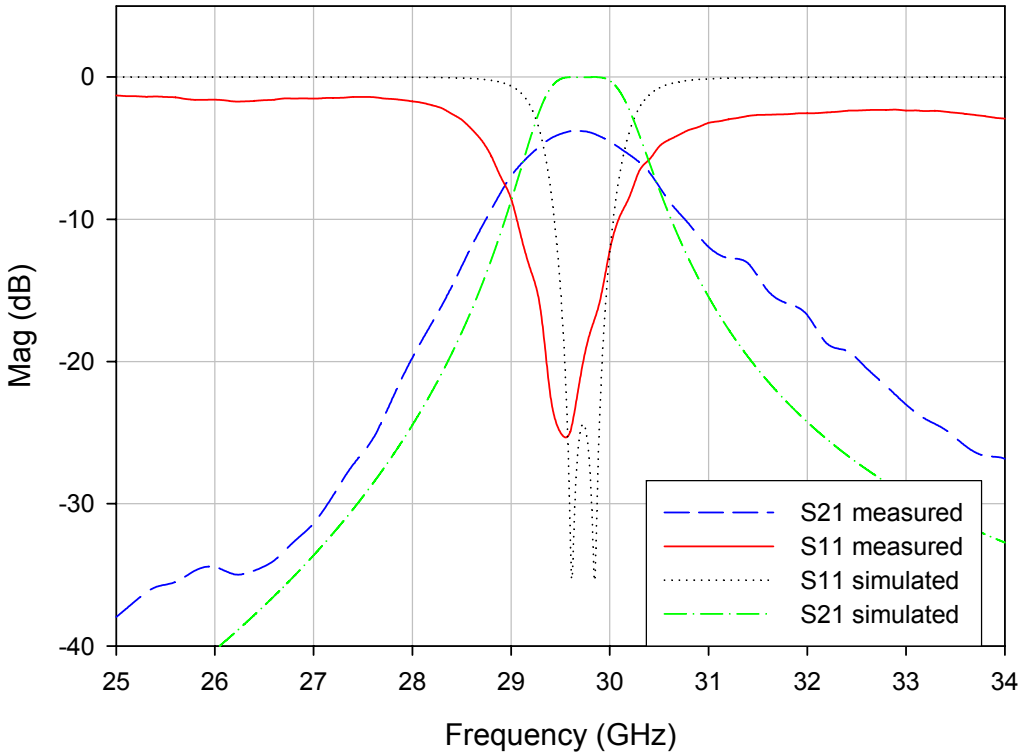

Figure 7-42 Bandpass response of the dual mode Ka band filter

The bandpass response of the dual mode Ka-band filter is shown in Figure 7-42, where a reasonable agreement between theory and experiment was obtained. The return loss was degraded due to layer misalignment, which also changed the coupling between the two modes leading to an increase in bandwidth of the filter. The transition from the connector to the circuit presented a mismatch, which was mainly caused by fabrication tolerances at the time of mounting the connector to the complete layered circuit. The measured insertion loss of the filter was found to be 3.8 dB. From this measurement, the unloaded quality factor for the dual mode resonator was extracted, using the method presented in Chapter 5, section 5.5, with the aid of a CAD circuit simulator [7-1], which gave an unloaded quality factor of approximately 103, which is in agreement with the value of 98 obtained using 5-53.

The simulated loss for this Ka-band filter using [4-10] gave an estimated pass band insertion loss of approximately –0.5 dB, giving a simulated unloaded quality factor of 750, while the X-band dual mode filter presented in section 7.4 presented a simulated insertion loss of -0.3 dB giving a simulated unloaded quality factor of 1200. The increase in the losses in the measured response are believed to be caused by the surface roughness of the copper plates, combined with the trace of the laser cut, which may have changed the conductivity of the copper in the case of the Ka-band filter, and any imperfection in the copper used. These passband simulations do not include connectors and the transitions from these to the circuit, which also contribute to overall measured losses.

7.6. CONCLUSIONS

Dielectric supported coaxial filters were presented at the beginning of this chapter. These presented two challenges, the difficulty to manufacture them, and, as the design frequency gets higher, finding a good dielectric material to support the centre conductor of the coaxial structure became an important issue. Then, the idea of making self-supported coaxial structures was developed and executed with three self-supported square coaxial filters, which presents an interesting and new way of making low loss transmission line structures, which consist only of metal, providing low losses which have the potential for the development of millimetre wave devices.

7.7. REFERENCES

[7-1] *Applied wave research,* Microwave office 2001 V 4.0

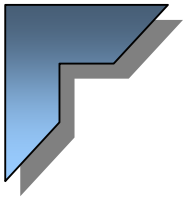

CHAPTER EIGHT
CONCLUSIONS AND FURTHER WORK

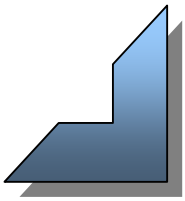

8.1. CONCLUSIONS

The first main objective of this research was to find a low loss transmission line for application in the millimetre wave region. The attempt to do this began with the analysis of the transmission lines and resonators shown in Chapter 6, in which we concluded that the square coaxial transmission line was a compact low loss transmission line suitable to achieve our first main objective.

The second main objective of this research was to find a way of supporting the centre conductor of the square coaxial structure. At low frequencies, the idea of using PTFE to support the centre conductor provided the desired low loss. As frequency got higher, new challenges were presented. The need to find a way of manufacturing a dielectric supported structure like the ones used in the lower frequency range present the problem on which material to use, and the method needed to manufacture the whole

structure. To overcome these challenges, a self-supported layered metal structure was proposed which consists of suspended metal structures having no dielectric, which meets the low loss target necessary at the millimetre wave region.

The third main objective of this research was to develop a way to ensemble a square coaxial transmission line, and the solution found was to stack layers of material which can be coated in metal. For the Ka band dual mode filter, the structure was directly machined in copper layers. In this method, layer alignment can be critical, depending on the overall shape of the microwave circuit.

Despite the fact that the round coaxial transmission line presents better loss characteristics than the square coaxial transmission line, as shown in Figure 6-9 and Figure 6-7. The square coaxial was chosen because it presented the possibility to ensemble the coaxial structure in layers, which allows forming rigid microwave passive devices.

8.2. FURTHER WORK

The parallel plate waveguide and the deep coplanar waveguide presented in Chapter 6 can be refined, considering that they were the first experiments in this thesis, and considering that at the time they were designed, we changed structures, which led to the square coaxial transmission line without giving them more attention. They present possible construction in the millimetre wave region by using LIGA or SU8 micromachining techniques, since these techniques provide the possibility to produce high aspect ratio structures.

In the following paragraphs, proposed further work on the square coaxial all metal structure will be presented. The Ka band, dual mode filter can be fabricated using different micromachining techniques. The technique used for the filter presented in Chapter 7 section 7.5.4 will be addressed here. This filter was fabricated using a 45 Watt copper vapour laser at Oxford Lasers Ltd., with a repetition rate of 10 to 12 KHz,

having a pulse width of 25 ns. The laser has two beams, a green one, with a wavelength of 511 nm and a yellow one having a wavelength of 578 nm. The typical hole diameter of the laser is 1 to 500 microns, and has typical tolerance rates of 1 to 5% depending on the process, namely the number of passes that the laser does on the material and the cut speed. The filter was fabricated on 700 micron copper layers, with a laser cut speed of 5mm/s, and the number of passes per line was 35. The system that was used is shown in Figure 8-1.

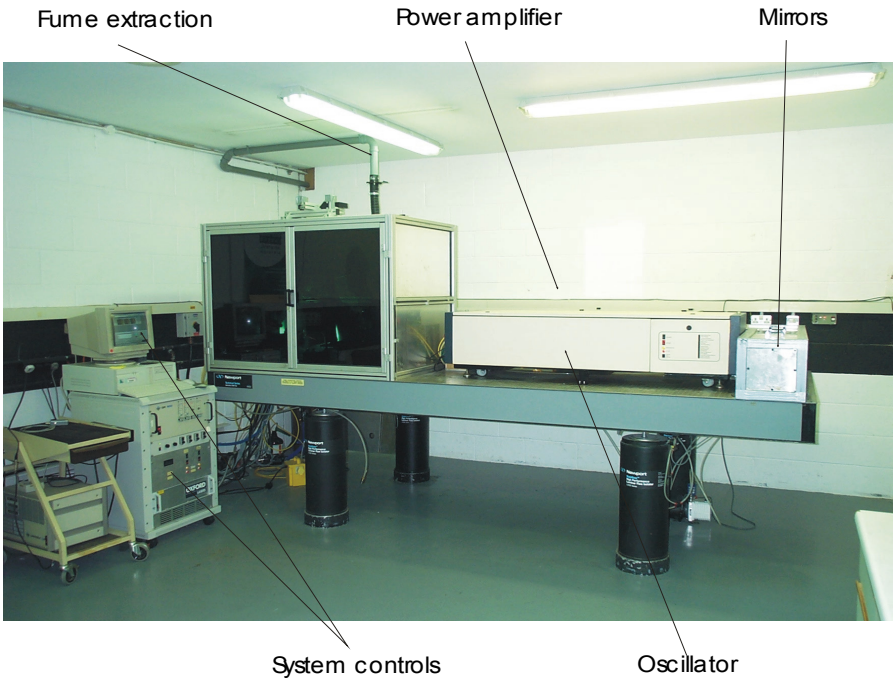

(a)

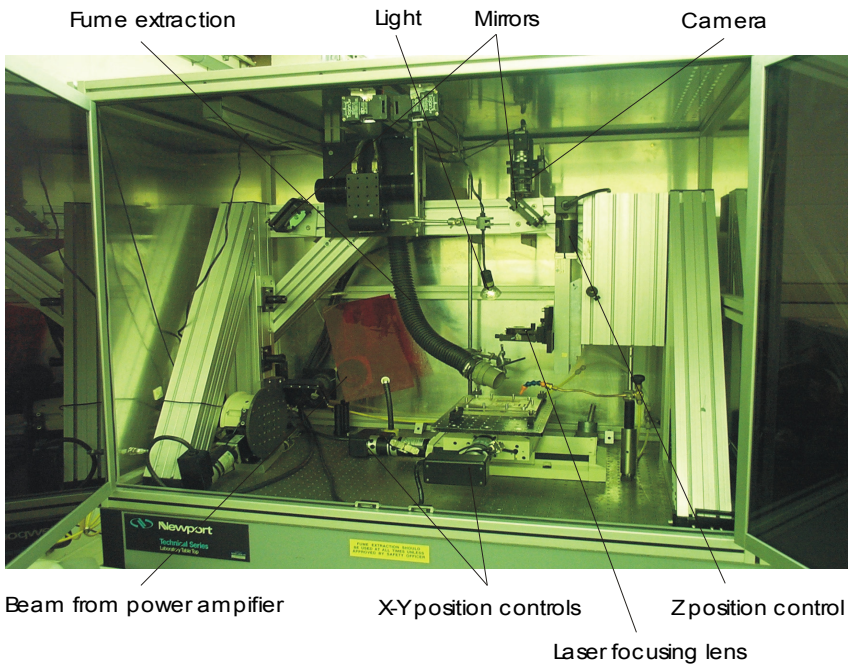

(b)

Figure 8-1 MOPA (Master Oscillator Power Amplifier) system

After the laser machined filter, we focused on considering the possibility of making the filter with other micromachining techniques, and the proposed further work from the research in this thesis is mainly focused on this issue, together with designing new self-supported, all-metal, square coaxial transmission line microwave circuits.

Silicon, SU8 and laser machining are considered as good contenders to make the coaxial structures. In collaboration with the Department of Mechanical Engineering, we have produced the Ka band filter using SU8-50 on silicon, where the silicon is removed after the process. The SU8 on silicon structure bent due to having a large exposed area, which defines the final structure kept after the process, since SU8 is a negative resist. The five layers of the Ka band filter on SU8-50 are shown in Figure 8-2.

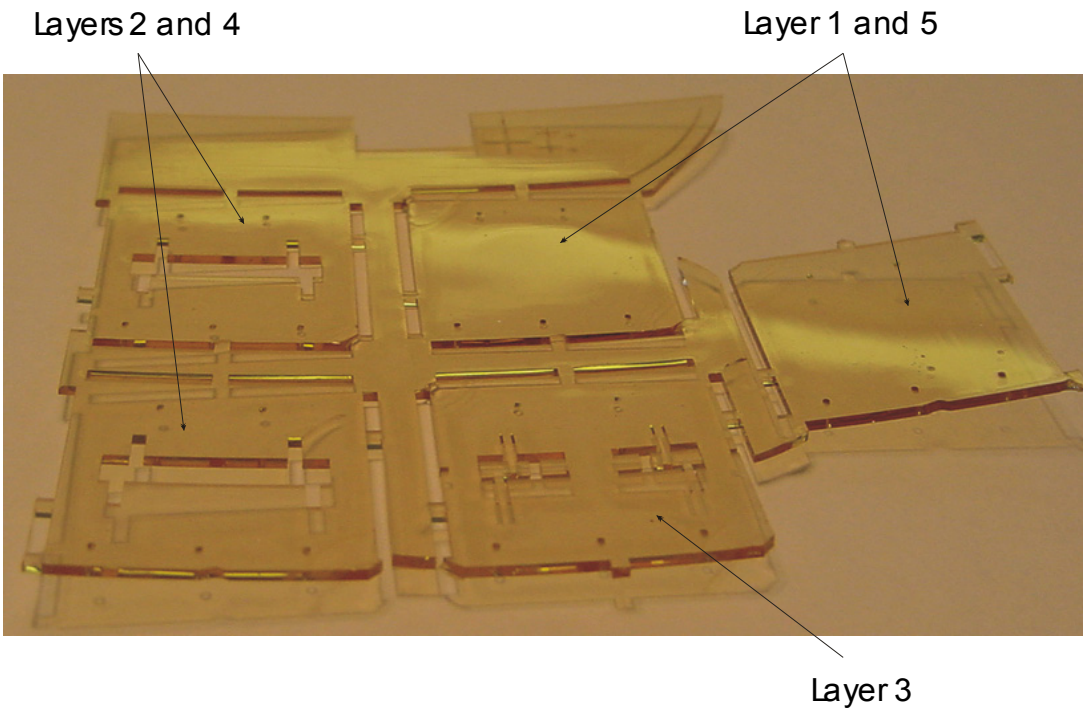

Figure 8-2 SU8 Ka band dual mode filter

To prevent the SU8 from bending, it is possible to reduce the exposed area in the process by either modifying the mask, separating the individual pieces, or by using thinner layers to produce the square coaxial structure.

The biggest challenge presented by the SU8 filter was how to coat the structure with metal. The structure will need to be coated in a three-dimensional way. The temperature of the coating process is also an important issue, since the SU8 may deform depending on the temperature used in the process.

The SU8 can also be used as a mould, and then the metallic pieces can be made by electroforming technology, followed by the removal of the mould and substrate, as illustrated in Figure 8-3. Here the biggest challenge is the SU8 removal since it is a hard material to remove.

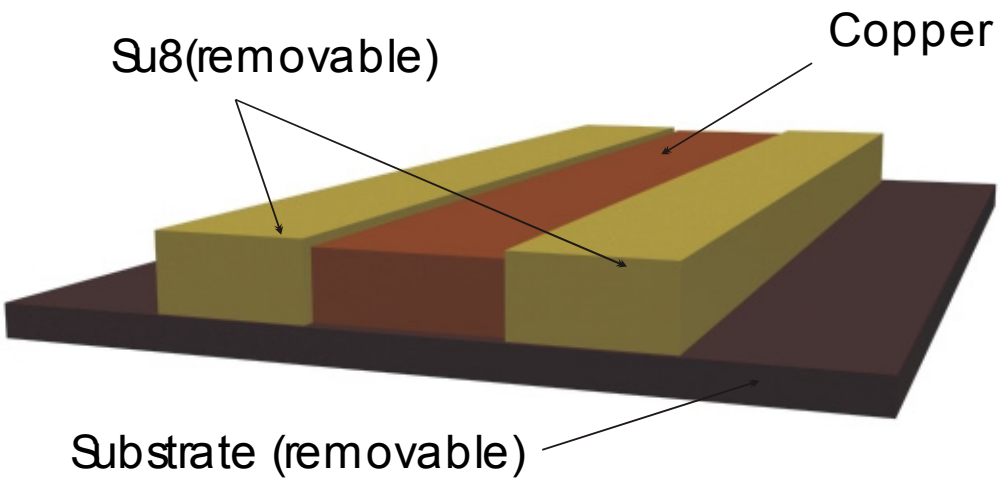

Figure 8-3 SU8 used as a mould to produce the circuit layers

It is also important to consider designing new microwave circuits with micromachining techniques, regardless of their shape, with the objective of having low loss and low dispersion for the millimetre wave region.

APENDIX
PUBLICATION LIST

Journal papers

- K. Jiang, M.J Lancaster, I. Llamas-Garro and P. Jin, "SU-8 Ka-band filter and its microfabrication", Journal of Micromechanics and Microengineering, Vol 15, No. 8, August 2005, pp 1522-1526.
- I.Llamas-Garro, M.J.Lancaster, and P.S.Hall, "Air filled square coaxial transmission line and its use in microwave filters", *IEE proc. on microwaves antennas and propagation,* Vol. 152, No. 3, June 2005, pp. 155-159.
- I.Llamas-Garro, M.J.Lancaster, and P.S.Hall, "Erratum to: A low loss wideband suspended coaxial transmission line", *Microwave and optical technology letters,* Vol. 43, No. 6, 2004, pp 543.
- I.Llamas-Garro, M.J.Lancaster, and P.S.Hall, "A low loss wideband suspended coaxial transmission line", *Microwave and optical technology letters,* Vol. 43, No. 2, 2004, pp 93-95.

Conference papers

- I.Llamas-Garro, K.Jiang, P.Jin, and M.J.Lancaster, "SU-8 Microfabrication for a Ka-Band filter" *MEMSWAVE, 4th Workshop on MEMS for millimeter wave communications*, LAAS-CNRS, Toulouse, France, 2nd – 4th of July 2003. pp F55-F58.
- I.Llamas-Garro, M.J.Lancaster, and P.S.Hall, "A high Q, X-band square coaxial resonator and filter design", *EPSRC PREP 2002 conference*, University of Nottingham, United Kingdom, 17th-19th April 2002, pp 1-2.